03-06

The Flemish Ministery
Department of Environment and Infrastructure
Waterways and Marine Affairs Administration
Flanders Hydraulics Research

MODEL 678/1

ALTERNATIVE DUMPING STRATEGY

WALSOORDEN

RESULTS PHYSICAL & NUMERICAL MODELLING

Final report

to

PROSES

November 2003

CONTENTS

contents i
1 INTRODUCTION 1
1.1 General 1
1.2 Methodology of the research program 3
1.3 Nomenclatura for the research area 3
2 HYDRODYNAMIC TESTS IN THE SCALE MODEL 4
2.1 General description of the physical model 4
2.1.1 Scales 4
2.1.2 Bathymetry 4
2.2 Results 5
3 HYDRODYNAMIC NUMERICAL MODELLING 6
3.1 Introduction 6
3.2 2Dh model of the whole Scheldt Estuary 6
3.3 Detailed 2Dh and 3D model of the research area 9
3.4 Analysis of the flow fields 10
4 COMPARISON HYDRODYNAMIC SIMULATIONS WITH MEASUREMENTS 11
4.1 Introduction 11
4.2 Drifter measurements 11
4.3 Field campaign 12/06/2002 13
4.4 Field campaign 03/06/2003 14
5 ARTIFICIAL SEDIMENTS IN THE SCALE MODEL 15
5.1 General 15
5.2 Analysis of the experimental results 16
5.2.1 Dumping location P1 17
5.2.2 Dumping location M2 17
5.2.3 Dumping location M3 and M4 18
5.2.4 Dumping location L2 18
5.2.5 Dumping location between R2-R3 18
5.2.6 Dumping location as before 1995 19
6 EFFECTS OF THE ALTERNATIVE DUMPING STRATEGY 20
6.1 Future morphology of the Walsoorden Sandbar 20
6.2 Possible effects of the future morphology 20
6.3 Conclusion 21
7 CONCLUSIONS AND RECOMMENDATIONS 22
7.1 Conclusions 22
7.2 Recommendations 27
8 APPENDIX A 30
8.1 Validation of the tidal propagation 30

8.1.1 Boundary conditions 30
8.1.2 Roughness elements 30
8.2 Measuring velocities and flow patterns in the scale model 31
8.2.1 Eulerian velocity vectors 31
8.2.2 Visualisation of tje flow pattern 31
8.3 Comparison of Eulerian velocity with DGPS-measurements.....
8.3.1 General.....32
8.3.2 Analysis 33
8.4 Comparison of flow pathways with DGPS-measurements 36
8.4.1 General 36
8.4.2 Analysis.....37
8.5 Conclusion 39
9 APPENDIX B 40
9.1 Description of the detailed 2D and 3D numerical model.....40
9.2 Comparison of current pattern computed with the 2D-model and the 3D-model..40
9.2.1 General 40
9.2.2 Analysis 41
9.3 Comparison with DGPS drifter measurements for variating horizontal eddy viscosity and numbers of vertical layers.....43
9.3.1 General 43
9.3.2 General Analysis.....43
9.4 Comparison of numerical model results with scale model tests 46
9.4.1 General 46
9.4.2 Analysis.....46
9.5 Comparison with velocity profiles along transect 48
9.5.1 General 48
9.5.2 Analysis.....50
9.6 Comparison of salinity with field data.....52
9.6.1 General 52
9.6.2 Analysis.....53
9.7 Comparison of velocity profiles with field data measured on 03/06/03 56
9.7.1 General 56
9.7.2 Analysis.....58
9.8 Influence of grid refinement in M- and N-direction 62
9.8.1 General 62
9.8.2 Analysis.....63
9.9 Conclusions 64
10 APPENDIX C 65
10.1 Use of artificial sediments in the physical model 65
10.2 Physical model laws 66
10.2.1 Scaling laws for water motion 66
10.2.2 Scaling laws for sediment motion.....67
SEDIMENT TRANSPORT MODELLING ACCORDING TO THE IDEAL VELOCITY SCALE 70

10.2.3 Relaxation of the scaling law conditions.....71
10.3 Additional scaling laws.....73
11 LITERATURE 75
FIGURES 77

1 INTRODUCTION

1.1 General

Within the framework of the Long Term Vision Scheldt Estuary, Flanders Hydraulics Research was asked to conduct a study concerning the feasibility of an alternative dumping strategy for dredged sediments near the Walsoorden location in the Western Scheldt (letter with reference C.15.2-16EA-U-02-1408, dated May 27th 2002 from director-general Jan Strubbe).

As requested in this letter, a research program was proposed to 'Projectdirectie Ontwikkelingsschets Schelde-estuarium' or PROSES, in which all activities were included that could be carried out by Flanders Hydraulics within the period of 1 year ending in the summer of 2003. The research program had to be carried out in close coöperation with the Port of Antwerp Expert Team (PAET) who proposed the idea for the alternative dumping strategy.

Within a period of six months several meetings took place to define a general agreed research program with which the feasibility of this alternative strategy could be investigated (July 4th 2002, December 13th 2002). During that period already important activities took place to prepare the research program. Among these are the DGPS-drifter field campaign (from September 23th to October 9th 2002, carried out by Institut für Wasserbau - Bremen) to assess the overall flow field around the Platen of Valkenisse and the (positive) evaluation of the availabe fixed bottom scale model of the Scheldt Estuary at Flanders Hydraulics for use with artificial sediments.

A final research program was proposed to PROSES on December 20th 2002 (letter with reference 16EB-U-02-0718) which was awarded on May 7th 2003 (letter with reference Proses/BM 00006651). In this program focus was given to the numerical modelling and the physical modelling that could be carried out in the short period from January to July 2003 by Flanders Hydraulics Research itself.

Although the PAET recommended to have sediment transport measurements, numerical sediment transport modelling and even a real-life test included in the research program as the only final way to confirm or contradict the new dumping strategy, this was not proposed to PROSES because of budgetary and logistic uncertainties and the limited time given to conduct the research. However, a limited one day field campaign for measuring sediment transport in the Walsoorden area could be carried out on June 3th 2003. This field campaign was financed by Flanders Hydraulic Research and could be carried out with the help of Meetinformatiedienst Vlissingen (Rijkswaterstaat) and Maritime Access Division (Flemish Ministery).

The results of the numerical and physical modelling carried out at Flanders Hydraulics Research in the first half of 2003 were communicated with the PAET, which led to to their first note concerning the feasibility of the dumping strategy handed over to PROSES on July 15th 2003. The results of the physical modelling with artificial sediments was not included in that note because the appropriate material could not be obtained before the summer of 2003 as originally foreseen.

During the discussion between the PAET and Flanders Hydraulic Research in preparation of the note of July 15, it was agreed among each other to go deeper into the hydrodynamic numerical modelling. This was needed to be absolutely sure that all deviations between the simulations and the measurements only could be blamed to the inability of science to find mathematical formulations that represent the real physics of nature.

In the period July to October 2003 this further numerical modelling and the experiments with artificial sediments, finally delivered in August 2003, could proceed. By doing so the total originally foreseen research program could be finalised.

This report describes the whole of the results obtained between January and October 2003. The contents of the chapters are as follows:

Chapter 2: results of the hydrodynamic flow fields and flow pathways in the physical model.

Chapter 3: results of the hydrodynamic flow fields and flow pathways in the best suited numerical model.

Chapter 4: results of the validation of the physical and numerical model against the available hydrodynamic measurements.

Chapter 5: results of the experiments with the artificial sediments in the physical model.

Chapter 6: effects of a possible evolution of the Walsoorden sandbar when maintaining the dumping strategy during a certain period.

Chapter 7: conclusions and recommendations.

Chapter 8: appendix A regarding the comparison of the hydrodynamic results of the physical model with the measurements.

Chapter 9: appendix B regarding the comparison of the hydrodynamic results of the physical model with the measurements.

Chapter 10: appendix C regarding the experiments with artificial sediments in the Western Scheldt scale model.

1.2 Methodology of the research program

The original goal of this research program was to assess the feasibility of the alternative dumping strategy with a limited amount of research tools. If with these tools a first estimate of feasibility could be proven, then further research could be carried out which would allow to give final prove of the feasibility and to investigate what would be the impact of this dumping strategy on the maintenance dredging works, the flow distribution in the ebb and flood channels and on the development of the sand bar of Walsoorden and the Platen of Valkenisse.

With further research was then meant to carry out in situ dumping of dredged material to get detailed insight in the sediment dynamics in the area, to prove actually the feasibility of the dumping strategy and to collect information that would help validate numerical modelling of morphology which is very valuable (if validation is successful) to predict the impact of the dumping strategy on longer terms as it is also impossible to obtain this information out of the in situ dumping test.

The various aspects of the methodology are explained in chapter 7 ‘conclusions’ and are not repeated here again.

1.3 Nomenclatura for the research area

In figure 2 an overview of the research area is shown in which the characteristic regions are given a unique name. There will always be referred to these names in the whole of the report to identify where certain phenomena occur.

- MEC: Main ebb channel (Zuidergat)
- MFC: Main flood channel (Schaar van Valkenisse)
- WSB: Walsoorden sandbar
- ETW: Eroded tip of Walsoorden sandbar (seaward tip)
- SSS: Southern sand spit
- NSS: Northern sand spit
- MSF: Minor Southern flood
- MNF: Minor Northern flood

REMARK

Many figures in this report show a geographic coördinate system and a contour plot of the bathymetry in the research area as a background. Unless described otherwise in the figure itself the shown coördinate system is always the Dutch ‘Rijksdriehoek’ system or RD Paris of geoïde ED50 and the bathymetry is always referenced to the Belgian averaged low low sea level TAW.

2 HYDRODYNAMIC TESTS IN THE SCALE MODEL

2.1 General description of the physical model

2.1.1 Scales

The scale model used for the physical modelling is built in 1990 and covers the Scheldt estuary from Baarland/Ossenisse up to Antwerp, using the in 1992 most recent available depth charts of the area. Except for the area of the Verdronken land van Saeftinge that is reconstructed from an aerial photo of 1979, the bathymetry for the whole area is constructed with data measured in 1989 and 1990. The remaining part of the tidal area is schematised as a labyrinth. The horizontal and vertical scale of the model is respectively 1/400 and 1/100. An overview of the most important model-scales is given in the table below.

HORIZONTAL SCALE	1/400
Vertical scale	1/100
Velocity scale	1/10
Time scale	1/40
Discharge scale	1/400.000

Scales of the Western Scheldt scale model

In figure 3 the main features of the scale model are shown with clearly the representation of the downstream boundary towards the sea side, and the labyrinth needed for a correct representation of the stored volumes of water each tidal cycle in the Scheldt estuary upstream of

2.1.2 Bathymetry

Between 1990 and 2002, some major morphological changes appeared. A short discussion about these changes will be given here. Figure 4 compares the bathymetry of 1990 with the bathymetric data (2001) available during this research program

An important bathymetric change is situated at the downstream end of the Main Flood Channel MFC. In this area the channel deepened out from 7.5m to 10m and even 12.5m TAW. The main reason for the deepening of this region is that the dumping of sediment in this part of the flood channel (the Schaar van Waarde) has stopped between 1990 and 1996. For this reason the river Scheldt started to erode this region and consequently the Geul van Zimmerman, situated more upstream in the flood channel became deeper and the tip of the “Platen van Valkenisse” at the upstream end of the main flood channel MFC has slightly eroded.

A second important difference between the two bathymetries is situated at the upstream end of the main flood channel MFC. The upstream tip of the “Platen van Valkenisse” has completely eroded, resulting into a diminished corner between ebb and flood channel in this area. Consequently the water flow from the flood channel in the present situation will

easily flow into the ebb channel during flood and will easily enter the flood channel during the ebb tidal phase. In the middle of the flood channel, the region where MNF enters the MFC, a certain amount of sedimentation took place, resulting in a reduced depth.

Concerning the tip of the plate, the southern side of the Walsoorden Sand Bar WSB near the Minor Southerly Flood channel MSF has partly eroded. More northerly, sedimentation took place and made the Northerly Sand Spit NSS become longer in the downstream direction.

2.2 Results

In figures 5 tot 10 for each hour of a mean spring tide the results of the physical model are presented by means of a contour plot of the velocity magnitude. In appendix A it is explained how these results have been obtained.

An analysis of these results is made in chapter 7 and in appendix A and is not repeated here. In appendix A much attention is given to the validation of the physical model on basis of the field measurements with DGPS drifters during autumn of 2002.

3 HYDRODYNAMIC NUMERICAL MODELLING

3.1 Introduction

Within the limited time available for conducting this research program, the numerical modelling was only focused on representing as accurate as possible the hydrodynamics in the Walsoorden area.

The goals of the numerical modelling are as follows:

- Collecting more data about the flow patterns and flow velocities than possible with the field campaign (see chapter 4). Analysis of this information gives insight in the sediment transport pathways. It can show where possible dumping locations (where flow velocities are most of the tide rather low) can be found

- Assess the effect of a possible evolution of the Walsoorden Sandbar on the flow patterns and velocity magnitudes around the sandbar in general and above the sill of Walsoorden in particular.

- Preparing the numerical models that will be used to simulate sediment transport and morphology in a later stage of further research.

In the paragraphs below the results will be shown of the different parts of the numerical modelling. These parts are distinguished as follows:

- 2Dh modelling of the whole tidal influenced zone of the Scheldt

- 2Dh detailed modelling of the area of interest around Walsoorden

- 3D detailed modelling of the area of interest around Walsoorden

The first part of this numerical modelling aims at representing the tidal propagation and horizontal salinity gradient. When succesful, this global area model can generate boundary conditions for any kind of detailed model.

The second and third part of the numerical modelling aims at investigating the flow fields around the sandbar of Walsoorden. It is only with these models that the goals of the numerical modelling can be achieved.

3.2 2Dh model of the whole Scheldt Estuary

To run a numerical model, always boundary conditions are needed. These conditions most of the time have to be derived from measurements. For numerical models in which tidal propagation will be simulated, these boundary conditions will exist in a combination of tidal waves at the downstream side and discharges at the upstream side. As the locations where discharges are accurately measured in the Scheldt are situated at least 100 kilo-

meters upstream of Walsoorden, a large global area model starting from the sea and ending at the upstream freshwater discharge locations is needed to represent accurately the tidal propagation and the salinity intrusion around Walsoorden.

To establish this global area model, Flanders Hydraulics Research has relied on the existing numerical 2D global area models from Rijkswaterstaat which have been developed the last ten years en for which many calibration has been carried out. An overview of this numerical model train for tidal propagation form the North Sea into the Dutch estuaries, rivers and waterways, including the Western Scheldt is given in figure 11. This numerical model train exists of several successive 2Dh models in which one model receives boundary conditions from another model, except one model which is the engine of the whole model train. Starting from the “engine” model we have:

Continental Shelf model CSM: the engine model in which boundary conditions consist of astronomic water levels at locations near the Atlantic Ocean and wind and pressure fields above the surface of the North Sea. The model is based on a rectangular grid with spherical coördinates.

Southern North Sea Model ZUNO: a model that covers a smaller part of the North Sea but with a higher resolution. Receives boundary conditions from the CSM model. This model is based on a curvilinear grid with cartesian coördinates.

Coast Region model: a model that covers a stretch of 70 kilometers along the whole Dutch-Belgian Coast again with a higher resolution than the ZUNO model form which it receives its boundary conditions. This model is also based on a curvilinear grid with cartesian coördinates.

The resolution of the ZUNO model is three times higher than the CSM model and the resolution of the Coast Region model is three times higher than the ZUNO model. The Coast Region model is the model that supplies boundary conditions to several models that cover the different estuaries along the Dutch Coast. For each estuary model also boundary conditions are needed for the upstream boundaries which always consist of measured or predicted discharge time series.

In figure 11 it can be seen that also an estuary model called SCALWEST (part of RAND-DELTA III) exists for the Western Scheldt, which is also shown in detail in figure 12. The numerical grid of that model covers almost entirely the tidal influence zone of the Scheldt (only the tributaries Kleine Nete and Grote Nete are not included). It can be seen that the Belgian part of the Scheldt is roughly schematised. This is probably the reason why tidal propagation is not so well simulated with this model upstream of Bath according to Dutch reports about the calibration of that model.

This whole series of models are run with Rijkswaterstaats own hydrodynamic software called SIMONA. This software became available to Flanders Hydraulics Research in January 2003. However, the models were only delivered as standalone models en all the scripts and programs to make the models run automatically were not available.

Because it means a lot of work to develop all these scripts and programs and because the performance of the SCALWEST model is not so good upstream of Bath, it was decided to make modifications to the SCALWEST model in the interest of this project. These enhanced the following:

- Strip of the coast region part of the SCALWEST model up to locations where continuous measurements of the tide take place (in casu Westkapelle and Zeebrugge). By doing so the SCALWEST model could be run as a standalone model for which boundary conditions at the downstream side can be generated based on these measured tidal levels.

- Refine the numerical grid in the Belgian part of the Scheldt and update the bathymetry (according to Dutch reports the bathymetry was based on very old measurements upstream of Rupelmonde) and also add the missing region of the tidal influenced zone of the Scheldt. By doing so it became possible to define discharge boundaries at the upstream locations where in reality discharges are measured.

The results of these modifications on the numerical grid are shown in figure 13.

This 'new' model was NOT calibrated. All values for bottom roughness, eddy viscosity and diffusivity known from the SCALWEST model for the Dutch part of the Western Scheldt were simply taken over(cf. Rijkswaterstaat-RIKZ, 2002). For the Belgian part of the Scheldt the same was applied, but in this case the information came out of older studies in which a 1-dimensional model of the Belgian Scheldt was calibrated.

To validate the performance of this model on the tidal propagation and horizontal salinity intrusion over the whole Scheldt Estuary, all measurements during the period 1st of June up to 13th of June 2002 were gathered. This period was chosen because during that period special field campaigns took place during which a lot of measurements were carried out between Waarde and Schelle to collect detailed information about the salinity intrusion in the Scheldt.

The results of this validation run of almost two weeks are presented in figures 14 to 16 for what tidal propagation is concerned and in figure 17 for what the salinity intrusion is concerned. It can be seen that the modified SCALWEST model simulates rather accurately the tidal propagation even far upstream of Antwerp. After one week of simulation, also the salinity intrusion starts to be simulated rather well.

It can therefore be concluded that the modified SCALWEST model is very well suited for generating boundary conditions for detailed numerical models of the research area. Within the simulated validation period, boundary conditions can be selected within the period of June 6th up to June 13th 2002.

3.3 Detailed 2Dh and 3D model of the research area

To be able to analyse the flow fields around the tip of the sand bar of Walsoorden en to study the influence of the numerical parameters in the numerical model on these flow fields, a part of the numerical grid of the SCALWEST model was separated. This part is shown in figure 18.

By doing so a new model was made with which it is possible to make much faster calculations en to extract much more data for processing flow fields. The global area 2Dh model is not well suited to generate these data as calculation time is high (the model is only 3 à 4 times faster than real time) and as the produced data from such a large model always come to a huge amount for only short time series which makes it practically impossible to process the data.

The 2Dh global area model of the Western Scheldt has been run with the Rijkswaterstaat SIMONA software, while the detailed 2Dh and 3D model is run with the DELFT3D software. Both softwares are highly compatible (in fact the “mathematical heart” is almost the same as development of both softwares was carried out by the same persons) and both use curvilinear numerical grids.

With the 2Dh global area model boundary conditions and initial condition values have been generated within the above mentioned validation period starting on June 11th to June 13th. During that calculation period mean spring tides occurred with a comparable tidal range as the cyclic tide used in the physical model.

In appendix B an extensive study has been carried out concerning the different parameters that could influence the results of the numerical modelling. The need to study these parameters can be argued as follows:

- The bifurcation between ebb channel and flood channel produces secondary currents which only can be modelled correctly by 3D models. Also saline intrusion in the Scheldt can introduce 3D phenomena. For this reason at least the difference between 2D and 3D modelling has to be investigated.

- The sensitivity of the number of vertical layers in the 3D model on the flow patterns has to be investigated.

- The sensitivity of both the 2D and 3D model has to be investigated in view of the horizontal turbulence. The mathematical formulation of this physical phenomena is not well understood yet and is build in the software by means of the constant horizontal eddy viscosity. This parameter can influence the bifurcation of the flow around the sand bar and has therefore to be investigated.

- The resolution of the numerical grid is also an important parameter. As the grid resolution of the SCALWEST model is on average 40 by 100 m, then it is easily understood that the bathymetric representation of the sand spits and minor flood channels around the sand bar of Walsoorden can be improved. The

question then rises if a higher resolution is necessary for simulating accurately the flow patterns.

Another reason for introducing a higher resolution is the fact that the sand bar of Walsoorden is a large area in which drying and flooding of the river bed occurs. This physical phenomena is also build in the software with a simple mathematical formulation that does not represent reality. This formulation often easily leads to numerical oscillations and therefore numerical algorithms (that involve neighbour numerical cells of the cell in which drying and flooding occurs) have been added to damp these oscillations and to keep the calculations stable. The question here rises how far the influence is of these numerical algorithms on the flow velocities calculated in the neighbour numerical cells.

CONCLUSION

The results shown in the appendix B allow to conclude that use of a 3D model with at least 10 vertical layers is best suited to produce the most reliable flow fields, although still non neglectable differences are found both for flow pathways as for velocity magnitudes.

It has to be emphasized that the numerical grid of this model has exactly the same grid schematisation as the global 2Dh model SCALWEST for the whole Western Scheldt. To this model will be referred from now on as the basic 3D model. The bathymetry of this model is based on the surveys of 2000-2001 and is shown in figure 19.

3.4 Analysis of the flow fields

In the figures 20 to 43 the results are shown of the basic 3D model for every hour of the tidal wave measured on June 12th 2002. The plots for velocity magnitude (surface and bottom layer) and velocity direction (red: bottom velocity; black: surface velocity) are presented for each successive hour of the tidal wave and are always referred to the moment of high water.

4 COMPARISON HYDRODYNAMIC SIMULATIONS WITH MEASUREMENTS

4.1 Introduction

To assess the accuracy of the hydrodynamic simulations both for the physical model and the numerical models, several field campaigns with measurements of the flow velocities and flow pathways were available.

The first field campaign was carried out in the framework of the research program 'Study of density currents in the Lower Sea Scheldt' (cf. general tender request on European level, reference 16EB/2001/01) and was financed by Maritime Access Division from the Flemish Ministery. These measurements were conducted with ADCP and CTD and give mainly information about the flow in a vertical transect during one single specific tide. The results of this field campaign are useful for comparison with results of the 3D numerical models. They are less useful for the physical model or 2D numerical models.

The second field campaign was carried out especially for the research of the alternative dumping strategy and especially for the validation of the physical model, and was financed by PROSES. These measurements were conducted with DGPS drifters. The results of this field campaign are useful for comparison with all kinds of numerical models and the physical model.

It has to be emphasized that the measurements during both the field campaigns were carried out during tides which are not always reproduced exactly in the physical model or the numerical models.

For the ADCP measurements, the tidal range and the water levels (corresponding with average spring tide) match very well with the cyclic tide used in the physical model, while the numerical models reproduce exactly the tide measured during the ADCP measurements.

The drifter measurements were carried out during several successive tides. Only few of these tides have a comparable tidal range as the tide used in the physical model and numerical models. Therefore only a part of the drifter measurement results could be used for comparison with the simulation results as described in appendix A and B

4.2 Drifter measurements

From 23th of September 2002 until 8th of October 2002, field measurements were carried around the Walsoorden Sandbar and the Platen van Valkenisse by the "Institut für Wasserbau" of the University of Applied Sciences, Bremen.

The measurements were carried out using a drifter measuring system with DGPS. The drifters are buoys with drogues consisting of crossed sheet metal plates. The buoy is a cylinder with a diameter of 50 centimetres and a height of 12 centimetres, which contains a

data logger/GPS receiver and an electric power supply. The drogues are connected to the buoys with a steel rope with a varying length (cf. figure 44).

The buoys, at a certain moment thrown into the water, can receive signals from up to 6 satellites. From these 6 signals the four signals with the best results are used to compute the position of the buoy. To obtain a high accuracy, the technique of Differential GPS is used. At a certain location on land a GPS receiver is positioned. Because the coördinates of this position are known, the error between this position and the position computed out of satellite signals give an idea about the errors from receiver clocks, satellite clocks, the satellites position, Selective Ability, or from ionospheric or atmospheric nature. This error is also send to the drifter buoys to correct its positions computed from the satellite signals and is stored in the drifter buoys. With this method an accuracy of better than one meter can be achieved, while the accuracy of normal GPS is approximately 100 meter.

The measurements in the region of the plate of Walsoorden were carried out at three different depths: 0.8 meter, 2.0 meter and 5.0 meter water depth. The drifter buoys receive data from the different satellites every 20 seconds. For every day that current measurements were carried out, the depth of the drifter, starting and ending time for each track are given. Because these numerical data are given each 20s, the instantaneous measured velocity magnitude is also known.

A general overview of all measured float tracks is given in figure 45 for ebb period and flood period separately.

The results of an analysis on the float tracks are:

a. During the initial phase of the ebb, the near surface and the near-bottom floats in the MFC follow the thalweg's direction, except for the near-surface ones along the NSS, which have the tendency to cross it towards the MNF. Floats in the MEC released along the WSB cross the SSS, following the general direction of the axis between left bank and WSB high bank. Floats released on the higher part of ETW tend to join the MSF.

b. During the initial phase of the ebb, the general trend seen during the beginning of ebb remains. Floats released in the MFC along the sandbar maintain the same tendency, with flow "spilling" from the MFC over the NSS towards the MNF.

c. During the end of the ebb phase, the flow in the MFC is following the thalweg, with the near-bottom flow slowed down because of the density stratification. At slack low water, near-surface currents are deviated towards the North, except for those following the edge of NSS, some "spilling" over the spit or moving around it towards the South. The floats released along the southern bank of the Walsoorden sandbar follow the same trend as for the previous phase of the ebb, but at about slack low water, the floats at the ETW return along the same path, while those ending at the seaward end of MNF turn North towards the MFC. The situation with low tidal amplitude needs more analysis, because it shows that flow coming at the end of the ebb from MFC and MNF join the flow of the MEC.

d. During the first phase of the flood, a peculiar situation occurs in the region downstream of the ETW, where the flow heads northwards before entering into the MFC, more the near-surface flow than the lower one. After this initial situation, the flow in the MFC follows roughly the overall direction of that channel, except that the flow closest to the NSS seem to spread over the edge at the landwards part, where it connects to the Walsoorden sandbar. The flow in the MSF passes transversally over the SSS.

e. In the middle of the flood phase, before the highest flood velocities, it seems that the zone of the MNF, between NSS and ETW, acts like a dead zone, so that the flow divides between the MFC and MEC+MSF, spilling over the SSS.

f. With the highest flood velocities, the “dead zone” effect in the MNF reduces and the flow is divided by the ETW. Flow in the MNF spills over the NSS towards the MFC, mainly in the area where it connects to the Walsoorden sandbar. The effect of density stratification is visible, mainly in the MFC.

g. At the end of the flood phase, some flow is oriented towards the ETW, flowing over the WSB. The flow in the MFC has similar direction as during the previous phase of the flood, and so is the case for the flow in the MEC+MSF, spilling over the SSS.

4.3 Field campaign 12/06/2002

Within the frame work of the research project “Density currents on the river Scheldt”, on June 12th 2002 ADCP-current and CTD-measurements were carried out on a transect near Waarde (IMDC, 2002).

During the field campaign 14 ADCP-measurements were carried out along a transect from Perkpolder to Waarde. The average starting and ending coördinates of the sailed transects are displayed in the table below. During the field campaign the vertical velocity profile is measured while sailing along the transect with an average direction of 216 degrees.

	STARTING POINT	ENDING POINT
X [m RD-Paris]	59924	62463
Y [m RD-Paris]	379609	381666

Coördinates of starting and ending points of the transect

When returning to the starting point of the transect the salinity profile was measured in 5 points located on the transect. The table below gives the average position of the CTD-measurements. Figure 46 gives an overview of the location of the transect and the points where the salinity profile is measured.

	X [RD-PARIS]	Y [RD-PARIS]
WC1N	60429	380033
WC2N	61218	380656

WC3N	61983	381283
WC4N	62372	381598
WC5N	60758	380290

Average coördinates of the CTD-measurement points

The measurements carried out on the 12th of June 2002 give valuable information about the vertical profiles of the flow patterns near the research area. It can reveal the existence of secondary currents (which is the case) and the possible influence of the horizontal saline intrusion in the Western Scheldt on the flow patterns (for which no indication is found). However the information on this transect is only related to the deeper parts of the research area.

4.4 Field campaign 03/06/2003

To assess the feasibility of the alternative dumping strategy with only the tools available in this research program, PAET stipulated that it was absolutely necessary to have at least a minimum of bedload sediment transport measurements available.

Despite the financial and logistic difficulties to organise this in a very short time, a limited program of such kind of measurements could be carried out on June 3th 2003. In figure 47 the locations are shown where during a full tidal cycle from three anchored ships sediment transport measurements above the river bed were carried out (cf. PAET, 2003c) in combination with vertical velocity profile measurements.

Both kind of data were very valuable because:

- On the level of hydrodynamics vertical profile flow velocity measurements became available in the undeeper parts of the research area on different locations on exactly the same moment of the tide.

- With the bedload measurements unique information became available concerning the sediment dynamics on top of the Walsoorden sandbar. <u>This information showed that for the tidal conditions observed, sediment is moving predominantly to the sandbar during the flood, while ebb transport is very weak.</u>

5 ARTIFICIAL SEDIMENTS IN THE SCALE MODEL

5.1 General

In appendix C a detailed analysis is given of the scaling laws that have to be applied for simulating sediment transport in the Western Scheldt scale model. This thorough analysis was necessary because the scale model was never designed to carry out experiments with artificial sediments. Oriëntating tests with the available kinds of artificial sediment at Flanders Hydraulics Research showed immediately that none of these materials was mobile enough to respect the scaling parameters defining incipiënt motion of sediment transport.

Therefore new kinds of material were looked for, and finally the problem of simulating bedload transport in the Western Scheldt scale model could be solved with the use of lightweight polystyrene but with a very fine average grain size diameter d_{50} of 450 µm.

Because of the occupation of the flume facilities at Flanders Hydraulics Research with which it would have been possible to analyse the real experimental behaviour of this new material under conditions of incipiënt motion (the analysis of the scaling laws in appendix C proves the theoretical similarity of the material for incipiënt motion, but practical values can sometimes deviate from this), oriëntating tests showed that sediment transport in the corresponding locations in the scale model where measurements had been carried out on the 3th of June 2003 was increasing rapidly on the same moments of the tide. It could be concluded that the material now behaved only little too mobile which is a safer approach for the experiments because it would underestimate the capacity of the real sediment in nature to stay in place after being dumped. Moreover, the spreading of the artificial sediments in the scale model also showed a predominant transport during the flood from the deeper parts in the Walsoorden Sandbar area towards the tip of the sandbar.

The dumping sites in the area of Walsoorden are exploited in such a way that each tidal cycle approximately one dredging ship dumps its whole carriage capacity. This means that approximately 5000 m³ of dredged material is dumped every tide. This dumping lasts about 2 to 3 weeks for one dredging-dumping campaign. As dumping 5000 m³ each tide of a cycle of 28 tides on a scaled basis in the physical model represents a very small amount of artificial sediments (according to the scale laws explained in appendix C this would correspond with only 5.25 kg of dry artificial sediment) and as simulating 28 successive tides as a representable dumping-dredging campaign is very time consuming (each tidal cycle last 20 minutes), a practical approach is chosen to visualise the sediment behaviour in the physical model.

As the artificial sediment polystyrene has a bright white colour and as the physical model is painted in bright red, green and blue, it was easy to take images in colour (with Hasselblad camera's) above the physical model in which the modifications of the dumped artificial sediment could be very well visualised during the succession of the tides. The only thing to be taken care of was to dump enough artificial sediment in the physical model. Therefore an amount of 40 kilograms dry material for each separate experiment has been chosen.

The sediment was dumped in five times during five successive tides (tide 0 to 4). The first image with he camera was taken at the end of the fifth tide (tide 4) an taken again every 3 tides up to the end of the day which is always tide 16. This means that the alterations of the dumped material were monitored during 12 tides. This corresponds with a morphological predicted period of almost 8 years.

The experiments consisted out of dumping a fixed amount of artificial sediments in a certain location of the scale model (around 40 kg). Because of the light hydrofobic property of the material, this amount was mixed with a chemical substance that made it easy to sink in the scale model. This substance had no influence on the transport properties of the artificial sediment but was only needed to overwin the surface tension of water. A remaining scale effect of the material was that portions of the material thrown on places in the scale model where drying and wetting occurs, again started to float on the water surface and were carried away upstream in the scale model. This did not allow to carry out experiments that lasted for more than 24 hours (according to the theoretical morphological time scale this corresponds with a prediction over 25 years).

With this type of experiments in a fixed bed model it is possible to study the stability of the dumped sediments against erosion, to visualise where sedimentation of the transported material will occur and best of all it gives detailed insight in the sediment transport pathways. It is more difficult with these experiments to analyse on what time level these events will occur in reality. For this comparative tests are needed with morphological events that have been measured and which are repeated in the scale model.

5.2 Analysis of the experimental results

In the figure below the possible dumping locations are shown for which it was assumed to carry out experiments. However the dumping locations E2, E3, L1, L3, R1 and M1 were not carried out because orientating tests immediately showed that these were not realistic dumping locations. A dumping location P1 was added which is situated northwest of location R1.

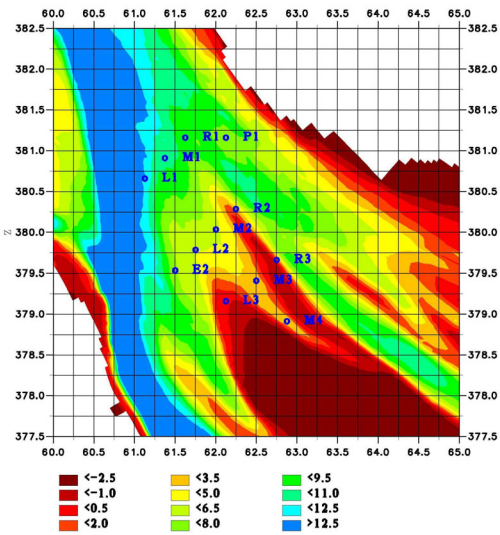

5.2.1 Dumping location P1

This was the first test to be carried out. On basis of the main flood flow direction, it was hoped that the residual transport would result in a transport direction towards the tip of the sand bar.

However the largest part of the material is directed straight into the main flood channel, where it stays in place. Only a small part of what comes into the main flood channel goes trough to the Overloop of Valkenisse. Because of the wide spreading of the material also a part is directed to the northerly minor flood channel where it also stays in place. There is no loss of material towards the main ebb channel.

Conclusion

This dumping location is not suited to start the alternative dumping strategy.

5.2.2 Dumping location M2

Out of the test with dumping location P1 it became clear that the alternative dumping strategy in an initial phase should start rather close to the intertidal areas of the tip of the sand bar. Therefore the M2 location was chosen as next dumping location while the L1, M1 and R1 locations already could be excluded as valid dumping locations.

The results show that a large part of the material stays in place even after a long series of tides. More or less equal amounts of sediment are bifurcated around the tip of the sand bar and are directed towards the northerly minor flood channel and southerly minor flood channel. However the material transported towards the southerly minor flood channel accumulates at the edge of the southerly sand spit from where it is taken by the ebb flow towards the sill of Waarde. It can nicely be seen that the sediments cross the main ebb channel from the Platen van Valkenisse to the Platen van Ossenisse just above the sill of Waarde. This accumulation of sediments above the sill of Waarde already occurs only after 7 tides. Sediments that have reached the ebb channel stay there in place especially near the sill. This suggests that the sediment transport dynamics is represented rather well in the physical model as in nature the sill are the favourable sedimentation locations.

Conclusion:

This dumping locations seems to be suited for the alternative dumping strategy as a lot of material remains in place just in front of the tip of the sand bar even after a long series of tides. Also the filling up of the northerly minor flood channel is achieved. However there is a danger that rather quickly a substantial part of the sediments will reach the sill of Waarde, suggesting that the frequency of maintenance dredging near the sill will be increased.

Therefore this dumping location is not recommended.

5.2.3 Dumping location M3 and M4

As the northerly minor flood channel did not exist in the past, one of the goals of reshaping the sand bar of Walsoorden is to fill up this minor flood channel and then to extend the sand bar towards Hansweert. With the dumping location M3 it is attempted to fill up the minor flood channel by dumping at the mouth of the channel and then hoping that the spreading of the material goes in the desired direction.

The results show that this is not completely the case. Starting from dumping location M3, the flood channel is not so easily filled up. A possible reason for this could be the fact that by dumping a high amount of artificial sediment, the flow in the northerly minor flood channel is blocked, which is an exaggeration of reality. Also an important amount of the sediment is transported across the tip of the intertidal area (painted in green on the physical model) of the sand bar of Walsoorden. But this could also be caused by the too extensive height of the experimental dumping in the physical model. Denote also that because of the hydrofobic properties of the polystyrene, the sediments that have settled on the green area of the physical model have drifted away on the water surface in much larger quantities. This is the main reason why this material is not found back in the main ebb channel as was the case with the dumping location M2.

For the dumping location M4 the same scale effects concerning the behaviour of the polystyrene above the intertidal area play a role. But it can be seen that even after many tides the majority of the dumped material stays in place.

<u>Conclusion:</u>

Dumping locations M4 and M3 can be recommended for the alternative dumping strategy. It is clear that first the upstream part of the northerly minor flood channel should be filled up before extending the dumping towards Hansweert.

5.2.4 Dumping location L2

To check the sensitivity of dumping near the mouth of the northerly minor flood channel, also the dumping location L2 has been chosen. It becomes immediately clear that dumping material just south of this minor flood channel absolutely has to be avoided. If dumped in such area's large amounts of the sediments are transported directly towards the main ebb channel and will afterwards will be transported towards the sill of Waarde.

<u>Conclusion:</u>

The dumping locations L and E have to be avoided.

5.2.5 Dumping location between R2-R3

We have seen that the northerly minor flood channel could be filled up by dumping in successively in locations M4 and M3. After the filling up of the channel the only possibility to dump further near the tip of sand bar is in locations M2 and the R2 and R3 locations. From the test with M2 is has also been noticed that a part of the sediment is directed towards the main ebb channel within a succession of only seven tides.

With the middle of the R2-R3 location it is attempted to see if transport of material towards the main ebb channel can be avoided. The exact location of the R3 location has not been chosen because this is situated in the intertidal area of the northerly sand spit.

The results show that after several tides large amounts of sediment have stayed in place an that the sediments that have moved followed smoothly the northerly and southerly banks of the northerly sand spit. A very low quantity of sediment seems to reach the main ebb channel and is then only after 16 tides transported towards the sill of Waarde. A minor part is also spreaded into the main flood channel but remains more or less close to the sand bar of Walsoorden because of the ebb currents that take the material in the direction of Hansweert. It can be noticed that a large part of the sediments moves towards the northerly minor flood channel and slowly fills it up.

Conclusion:

The dumping location close to the tip of the northerly sand spit is recommended as a dumping location for the alternative dumping strategy once the northerly minor flood channel has been filled up by careful dumping in location M3 and M4. There is a possibility that only dumping in this location could satisfy to fill up the minor flood channel.

5.2.6 Dumping location as before 1995

In the paragraphs above it has been mentioned that some quantities of the sediment are transported towards the main ebb channel by the flood currents and are then successively transported towards the sill of Waarde by the ebb currents. Depending on the chosen dumping location sedimentation of the sediments on the sill occurs after 7 tides or only after 16 tides.

It has been mentioned that if this sedimentation occurs already after 7 tides (meaning a morphological time horizon of almost 5 years), this probably would lead to an increase of the frequency of maintenance dredging on the sill of Waarde.

Of course this is speculative because the artificial sediments are scaled according to the similarity of incipient motion but not according to the similarity of the length of sediment transport within a given time period. It is this last kind of similarity which is deterministic for the number of tides after which sediments reach the sill of Waarde.

The only way to evaluate if the similarity of length of sediment transport is reached in a physical model is to perform a historical test which allows to determine experimentally the morphological time scale

6 EFFECTS OF THE ALTERNATIVE DUMPING STRATEGY

6.1 Future morphology of the Walsoorden Sandbar

In order to asses the effect on the current pattern of the morphology obtained by executing the alternative dumping strategy for the plate of Walsoorden, the PAET proposed the most likely evolution of the Walsoorden Sandbar by means of a drawing with contour lines of equal depth.

With the use of Delft3D these contour lines are converted into a bathymetric grid. This grid is then fitted into the existing grid of the bathymetric surveys of 2000-2001. By use of triangular interpolation this new set of bathymetric data is then transformed into a new bottom of the numerical model. Figure 68 shows this new situation for the Walsoorden Sandbar.

In figure 69 the difference in depths between the new situation and the present situation is shown. It can be calculated that the stored volumes of wet sand to obtain this morphological development, within the assumption that all dumped material remains in place (which will certainly not be the case), correspond with a total volume of 4.5 million m³. It has to be noticed that the biggest part is stored in the Minor Northerly Flood channel MNF and near the tip of the Northerly Sand Spit NSS, according to the findings of the tests with artificial sediment.

6.2 Possible effects of the future morphology

To estimate the effect of the morphology obtained by reshaping the tip of the Walsoorden, numerical computation have been repeated with this new bathymetry. To analyse the influence, 4 different transects and 4 monitoring stations around the Walsoorden Sandbar are defined.

- Transect “Schaar van Waarde” and “Zuidergat” cross the sandbar at the downstream tip and are chosen to visualise the changed discharge distribution between main ebb and flood channel
- Transect “Schaar van Waarde 2” and “Zuidergat 2” are located more upstream at a location where the bathymetry has not changed compared with the present situation.
- The monitoring stations are chosen to analyse the effect on velocity magnitudes in the middle of main flood and ebb channel. A increase of discharge in a

transect does not necessarily mean that this is due to increased velocities because the cross-sectional area of that transect could have been increased also.

The “Walsoorden” and “Waarde” stations have been selected particularly because they are located in the middle of the present dumping and dredging areas.

The differences in discharge are presented in figures 71 to 74. The differences in velocity magnitude are presented in figures 75 tot 78. In all these figures a black line represents the future situation and the red line the present situation.

Transect “Schaar van Waarde” – Monitoring station “Waarde”

A small decrease of the discharge is noticed both for ebb and flood period, but this corresponds with a significant increase of the flow velocities of up to more than 0.1 m/s (an increase of approximately 10% on the depth averaged flow velocity).

Transect “Zuidergat” – Monitoring station “Walsoorden”

A small increase of the discharge is noticed both for ebb and flood period and this corresponds with a slight increase of the flow velocities of up to a maximum of 0.05 m/s (an increase of less than 5% on the depth averaged flow velocity).

Transect “Schaar van Waarde 2” – Monitoring station “Valkenisse”

The small decrease of the discharge in “Schaar van Waarde” is also noticed here both for ebb and flood period, but this corresponds now with a slight decrease of the flow velocities of up to 0.05 m/s (a decrease of less than 5% on the depth averaged flow velocity).

Transect “Zuidergat 2” – Monitoring station “Baalhoek”

A small increase of the discharge is noticed both for ebb and flood period and this corresponds with a slight increase of the flow velocities of up to a maximum of 0.05 m/s (an increase of less than 5% on the depth averaged flow velocity).

6.3 Conclusion

The effects of the reshaped Walsoorden Sandbar seems to generate favourable effects. There is a significant increase of flow velocities in the area where now dumping of maintenance dredging material is licensed. This offers a good perspective for the stability of the Main Flood Channel MFC, even if the amounts of dumped material would be raised.

Even in the vicinity of the sill of Waarde an increase of velocities is noticed which could lead to a new equilibrium for the depths on top of the sill.

It has to be remarked that in the upstream end (or delta) of the Main Flood Channel MFC velocities apparently will decrease slightly. It is not clear what effect this could have on the longer term.

7 CONCLUSIONS AND RECOMMENDATIONS

7.1 Conclusions

Research methodology

Within the scope of this research program and the limited time given, use of several research tools was available to assess the feasibility of the alternative dumping strategy on the tip of the sand bar of Walsoorden. The chosen research methodology consisted out of the following succession of tasks.

Several field campaigns carried out in 2002 and 2003 gave to a certain degree insight in the hydrodynamics of the research area, especially the field campaign with DGPS drifters carried out by 'Institute für Wasserbau-Bremen" (IWA, 2003). In figure 45 it can be seen that the flood flow is attacking rather heavily the Walsoorden Sand Bar WSB and that only a small zone near the Northerly Sand Spit NSS and the Minor Northerly Flood channel MNF is characterised by low flow intensities. The main purpose of the field campaigns however is to supply enough data to validate the several models.

The use of the Western Scheldt scale model aimed primarely at simulating sediment transport with artificial sediments knowing that complex 3D phenomena in the flow and large scale turbulence are easily represented well in a scale model in which distortion of the horizontal and vertical scale is limited (which is the case). As these phenomena are not automatically represented well in numerical flow models, use of the scale model with artificial sediments and a fixed bed was in this stage of the research program more favourable to get qualitative insight in the sediment transport pathways and the stability of the sediment regarding erosion on different locations in the wider area of the Walsoorden Sand Bar then using non validated numerical morphological models.

The use of a numerical flow model on the other hand was chosen because it is an easy tool to study the effect of a reshaped sand bar on the flow patterns. This is needed to evaluate if flow intensities would rise in the Main Flood Channel MFC as it was hoped that this could be an additional effect of the alternative dumping strategy.

An outcome of this research methodology is that both the scale model and the numerical model simulate the flow patterns in the research area and can be compared with the results of the several field campaigns (cf. appendix A and B).

Main results hydrodynamical modelling

The main results of the simulated flow patterns are presented for each hour of the tidal cycle (mean spring tide) in figures 5 to 10 for the physical model and 20 to 43 for a 3D numerical model with 10 vertical layers.

It can be seen that during that the largest part of the flood period the velocity magnitudes on top of the Eroded Tip of the Walsoorden sandbar ETW are quite high and velocity directions are mainly directed towards the Main Ebb Channel MEC. This is not the case on top of the Northerly Sand Spit NSS and in the Minor Northerly Flood channel MNF. In that location only during maximum flood the flow intensity rises and the flow direction is directed towards the upstream end of the Main Flood Channel MFC.

During the whole ebb period all these previous locations including the Eroded Tip of the Walsoorden sandbar ETW can be situated in the shadow zone of the Sand Bar of Walsoorden in which flow intensities are always low.

The hydrodynamic results suggest that the alternative dumping strategy on the tip of the Walsoorden sand bar would not mean dumping in the location of the eroded tip of the Walsoorden sand bar ETW, but dumping near the Northerly Sand Spit NSS and in the Minor Northerly Flood channel MNF. This knowledge of flow velocities and flow directions defines these regions as locations where dumped sediments have a higher chance of remaining in place with large enough quantities of sediment. The amounts of sediment that would not remain in place will be carried away mainly in the direction of the Main Flood Channel MFC or on top of the Walsoorden sandbar.

Validation of the hydrodynamical modelling

In appendix A and B a detailed overview is given of the comparison of the results of physical and numerical modelling with results of various field campaigns. The latter include information regarding velocity patterns in plane view as also information regarding vertical velocity distributions.

In general it can be concluded that flow directions and velocity magnitudes are predicted very well in the Main Flood Channel MFC and the Main Ebb Channel MEC both in the numerical model(s) and the physical model. There seems to be only one phase of the tide (the first hour of the flood period) where there is a

clear deviation in the flow directions: in nature the DGPS drifters tend to cross the Main Flood Channel MFC which is not found back in both type of models. Also during the slack water periods important deviations are found, but this is not unexpected as it is known that during such kind of period the water is “wandering” around.

For the numerical models in the undeeper parts of the research area (depths above 10 m TAW), nor the flow directions nor the velocity magnitudes are simulated satisfactory. The vertical velocity distributions show deviations in the velocity magnitude of a factor of sometimes 2 or -2 (depending on the moment of the tide) when following a line from the sill of Waarde up to the Minor Northerly Flood channel MNF. In this whole undeeper area including the edges of the Main Flood Channel MFC important differences in the flow pattern are found, no matter the chosen values of the few numerical parameters. There is only one undeeper location where the prediction remains good and that is the area between the Eroded Tip of the Walsoorden sandbar ETW and the Main Ebb Channel, especially when flow velocities increase.

For the physical model comparison with vertical velocity distributions is senseless as this can only be measured on two points in the vertical. Therefore only comparison with the DGPS drifters is possible, from which it is possible to extract Lagrangian flow pathways as Eulerian velocity vectors. From the latter it is however difficult to find many vectors covering the whole research area within a short period of the tide which makes it in return hard to estimate the accuracy of the physical model on the level of velocity magnitude.

The results of physical and numerical modelling regarding the undeeper parts of the research area though suggest that the prediction of the velocity magnitude is only slightly overestimated in the physical model while in the numerical model there seems to be an underestimation of up to 5 à 10%. Filtering the effect of the bathymetric differences in the physical model caused by the used bathymetric surveys of 1989-1990 with which the physical model was constructed, the flow pathways in the physical model simulate in general the DGPS drifter results rather well. In the numerical model important deviations are found. <u>In spite of these differences in flow pathways or velocity magnitudes in the undeeper parts of the research area, which cannot be explained so far, the main features of the bifurcating flow and the phases when these features appear in the physical and numerical model are qualitatively comparable with what was measured in nature.</u>

With respect to the numerical modelling it must be further emphasized that 3D modelling is absolutely necessary because in the whole research area during important moments of the tide, strong secondary currents occur. These have been measured during the several field campaigns and have been clearly noticed in the physical model (although it is not visualised in the figures of this report as this is almost impossible). These currents show the complex 3D aspect of the bifurcating flow around the Walsoorden sandbar and are very important for the sediment transport direction.

Results experiments with artificial sediments

In appendix C an overview is given of the selection method for finding the appropriate artificial sediment to carry out experiments for sediment transport on a fixed bed within the available Western Scheldt scale model. Although the scales for the horizontal and vertical dimensions originally were not designed for carrying out such kind of experiments with the artificial material available at Flanders Hydraulics Research at the beginning of this research project, new material could be found (lightweight polystyrene with grain size diameter d_{50} of 550 µm) with which it was possible to respect the scaling laws for the incipient motion of sediment particles. Although it was not possible to obtain the experimental values of the artificial sediment parameters for incipiënt motion by tests in a flow flume, oriëntating tests in the Western Scheldt scale model revealed that the behaviour of the artificial sediment corresponded rather well with the bedload sediment transport measurements that ware carried out on the 3d of June 2003 (cf. PAET, 2003c and 2003d) showing that only maximum flood period of the tide induces significant sediment transport on the Walsoorden sandbar location.

Although the artificial sediment was very well suited to be used as a perfect sediment tracer and as a material that could show where sedimentation occurs, the use of a fixed bed scale model does not allow to define the time rate within which this sedimentation will occur. This is due to the fact that only mobile bed experiments allow to perform a historical test that enables to deduct the morphological time scale of the artificial sediment. To get round this, an experiment was carried out in which the dumping strategy for the Walsoorden region until 1995 was applied. The number of tides after which sedimentation occurred on the Sill of Waarde was then considered as a criterium that allowed to check if a dumping location would induce faster or slower sedimentation rates on this sill and therefore would have a positive or negative effect on the maintenance dredging on that sill.

In figures 48 to 67 the results of dumping on different locations are presented. Within the limitations of this kind of experiments (cf. paragraph 7.2) it can be concluded that the alternative dumping strategy is feasible. All locations in the Minor Northerly Flood channel MNF and close to the tip of Northerly Sand Spit NSS (locations M3, M4 and between R2 and R3) are capable of maintaining large amounts of sediment in place even after many tides. The results show also that dumping on top of the Eroded Tip of the Walsoorden sandbar has to be avoided, even after the Minor Northerly Flood channel MNF would completely be filled up with sediments. If this stage of the alternative dumping strategy would be reached, it is recommended to apply dumping always on the tip of Northerly Sand Spit NSS which will extend in the direction of Hansweert.

Comparison with the experiment in which dumping was carried out in the middle of the Main Flood Channel suggests that the alternative dumping strategy will not increase the maintenance dredging on the sill of Waarde or on the south side of the Southerly Sand Spit SSS where now intensive sand mining takes place. The figures show that for the best suited dumping locations only after the same number of tides sedimentation of the artificial sediment in these area's occurs.

Effect of the alternative dumping strategy

In figures 68 to 78 the possible effect of the alternative dumping strategy is analysed when assuming the Walsoorden sandbar would develop to the shape as shown in figure 68. In this configuration 4.5 million m³ of wet sand is stored (specific density of 2400 kg/m³).

These results show that although there is not always an increase of the discharge depending on the transect chosen (figure 70), there is clearly an increase of the velocity in all locations upstream of the sill of Waarde. This increase is the strongest during flood period and in the Main Flood Channel MFC. Depth averaged velocity magnitude reaches values which have increased more than 0.1 m/s. Even during ebb period and in the Main Ebb Channel depth averaged velocity magnitude has increased with values up to 0.05 m/s.

This effect in the Main Flood Channel MFC stresses the importance for research regarding the opportunity to dump higher amounts of maintenance dredging sediments. The effect in the Main Ebb Channel MEC on the other hand suggests that there is a possibility that a new equilibrium depth of the sill of Waarde could develop with higher depths for the navigational channel on top of the sill.

7.2 Recommendations

Why the need for an in situ test?

The results of this research program have shown that the alternative dumping strategy should be feasible.

Proof of this feasibility relies dominantly on the experiments with artificial sediments. Although the indications are that large parts of dumped sediments will remain in place at locations which are favourable for the alternative dumping strategy and that no increase of the maintenance dredging works around the sandbar should be expected, still significant simplifications of the processes in nature during the experiments stress the need of an in situ test to give final proof of the alternative dumping strategy.

The most important simplifications of the experiments are:

- the uniform grain size diameter d_{50} with which the experiments have been carried out while in nature there exists a grain size distribution; this made it impossible to assess the role the finer grain fraction plays, especially if it could remain in place on top of the sandbar or not

- the scale effect induced by the hydrofobic properties of the used artificial sediment; this made it impossible to simulate the behaviour of sediment transport in the intertidal areas (artificial sediments thrown on top of these areas started to float on the water surface; the more tides were run in the scale model, the more material had drifted away)

Apart from the final proof of the feasibility of the alternative dumping strategy, there is also another need for the in situ test, given by the fact that it would be very useful to predict the morphological development of Walsoorden sandbar if the alternative dumping strategy would carried out for a longer period.

As this kind of morphological predictions cannot be carried out in the available Western Scheldt scalemodel with mobile bed experiments (due to a too high distortion of the horizontal and vertical scale values and of the too close seaward boundary to the research area), the only remaining research tool at this moment would be a numerical morphological model.

The hydrodynamical modelling in this research program however has shown that evaluation of the simulated flow patterns and velocity magnitudes in the undeeper parts (i.e. above 10M TAW) of the research area is extremely difficult. Although the aspect of the numerical hydrodynamical simulations seems comparable with

what has been measured in nature, big differences occur and cannot be explained straightforward.

This allows to conclude that morphological predictions with numerical models is very uncertain. The way morphological features of the Walsoorden sandbar like the Northerly and Southerly Sand Spit have developed during the years can depend strongly on the near field flow patterns in this area. For this reason the in situ test could supply extremely valuable data to validate numerical morphological models.

Approach for the in situ test

The in situ test is allowed to be carried out in the licensed dumping zone as shown in figure 79. It can be seen that this zone covers only partly the locations which have been found suited for the alternative dumping strategy. When the alternative dumping strategy would be carried out, it is desired to start with filling up the Minor Northerly Flood channel MNF from upstream tot downstream. As this cannot be done, figure 80 shows the location where it is recommended to carry out the in situ test. From the experiments with artificial sediment it can be expected that this minor flood channel will fill up by the spreading of the dumped sediments which is always dominantly upstream, but the possibility exists that the dumped material blocks the flow in the minor flood channel, therefore reducing the spreading of sediments and after all leaving a hole in the most upstream part of the minor flood channel.

Another important aspect to consider for the in situ test is dumping a high enough amount of sediments to create enough ‘visuable’ effect. In figure 69 it can be seen that the estimated morphological evolution is in fact already very limited (in the sense that only the minor flood channel and tip of the sand spit has been suppleted, but the whole area of the eroded tip of the Walsoorden sandbar ETW has not been restored) and already the stored volumes reach values of more than 4 million m³ wet sand. An amount of dumping 500000 m³ wet sand for the in situ test should therefore be considered as a strict minimum.

Desired evolution of the Walsoorden sandbar

The possible morphological evolution of the Walsoorden sandbar as presented in figure 68 is only an answer to the amounts of sediments that could be stored when applying the alternative dumping strategy in a restricted way.

When applying the alternative dumping strategy in a broader perspective of “morphological dredging and dumping” (cf. PAET, 2003d), this shape is not a final stage of dumping sediments. The effects on the flow in the main flood and ebb channel suggest that increase of the flow on top of the sill of Waarde can be enforced if

the growth of the sandbar goes further and further in the direction of Hansweert. The way this desired morphological evolution could develop is schematised in figure 81 (full black line). It is very well possible that a new equilibrium depth for the sill of Waarde is created with higher depths. However this needs further research in which also the negative effects of the eroding forces, which have caused the eroded tip of the Walsoorden sandbar ETW, have to be involved. The experiments with artificial sediment also suggest that to obtain such an evolution only dumping in the vicinity of the Northerly Sand Spit NSS is allowed once the Minor Flood Channel MFC would be filled up.

Another aspect to be considered within this concept of morphological dredging and dumping, is that the morphological freedom in the whole area has been diminishing the last two decades (cf. Rijkswaterstaat-RIKZ, 2001). When we look at the bathymetry of the Walsoorden sandbar and the Platen van Valkenisse, we see that up to 1974-1975 still undeep secondary channels existed between the Main Flood Channel MFC and the Main Ebb Channel while the undeep water zone above 10 m TAW around the tip of the Walsoorden was much more extended towards Hansweert (see striped line in figure 81). Within five years after starting to dump dredged material in the Main Flood Channel, these secondary channels have been filled up (a situation which apparently seems to have stabilised nowadays, while before that moment the location of the different secondary channels was very mobile during a long period) and also the area between the Walsoorden sandbar and Hansweert west of the navigational channel has been progressively eroding and deepening.

It would therefore be worthwhile to investigate if also morphological dredging as suggested by the dotted line in figure 81 could mean a benefit for the alternative dumping strategy in particular and the management in general of the navigational depth above the sill of Waarde and elsewhere in the area around the Walsoorden sandbar.

Flanders Hydraulics Research,

November 2003

Youri Meersschaut Kristof Verelst

8 APPENDIX A

VALIDATION OF THE PHYSICAL MODEL FOR HYDRODYNAMICS

8.1 Validation of the tidal propagation

8.1.1 Boundary conditions

During the scale model tests, the boundary condition applied at the downstream boundary located near Baarland and Ossenisse is a repetition of a mean spring tide. The tide used for the calibration of the model (FHR, 1994) is measured on June 29th 1992 with high water in Antwerp equal to 5.32m TAW and low water in Antwerp equal to 0.21m TAW. During the field campaign, tidal gauges were located in Ossenisse, Hansweert, Schaar van de Noord, Bath, Prosperpolder, Liefkenshoek, Schelle en Dendermonde.

Figure 82 and 83 compare the tide measured on June 29th 1992 with the water level measured in the scale model for the tidal gauges located at the downstream boundary and for the tidal gauges near the research area. The tidal curve measured in the scale model at Hansweert, Baarland, Ossenisse and Bath show a good representation of the field data. The high water measured at the different locations in the scale model is slightly overestimating the high water of the field data. The explanation for the oscillations of the tidal curve for Baarland and Ossenisse in the scale model can be found in the steering of the valves. The position of the valves at the downstream boundary is calculated from the difference between the measured and desired water level at Baarland and Ossenisse.

8.1.2 Roughness elements

Due to the difference in horizontal (1/400) and the vertical scale (1/100), the scale model is distorted with a factor 4. To obtain a correct tidal propagation in the whole model roughness elements were added. As roughness elements triangular concrete prisms are used whit the point of the prisms pointed in the downstream direction when influencing the ebb phase and in the upstream direction when influencing the flood phase. Originally the area around the Walsoorden sandbar contained 7 prisms/m² pointed upstream and 5 prisms/m² pointed downstream (FHR, 1994).

With lower water depths vortices are formed when a current from the point of the prism towards the other end is present. These vortices in combination with the upper side of the prisms falling dry with lower water depth influence the flow pathways and the sediment transport. Therefore all the roughness elements around the Walsoorden sandbar are removed during the scale model tests. Figure 84 and 85 display the influence of the local removal of the roughness elements on the tidal propagation. These figures show a not significantly different water level for the tidal gauges at Hansweert, Schaar van de Noord, and Bath. Only at location Waarde in the MFC a slightly lower water level is measured af-

ter the removal of the roughness elements. Especially the falling dry of the roughness elements with lower water depths provides a little damming of the water in the MFC.

8.2 Measuring velocities and flow patterns in the scale model

8.2.1 Eulerian velocity vectors

The instantaneous surface velocity in the scale model is measured using 4 digital cameras positioned above the model. The area of the scale model covered by each camera is approximately 2 by 3 meters. Consequently 4 different positions are needed to cover the whole area around the Walsoorden sandbar. An overview of the positions of the 4 digital cameras is displayed in figure 86.

During the whole tidal cycle little drifters are spread out in the area covered by these 4 cameras. With the program WBKL.EXE a PC processes the images taken during 4.64s by each camera. This program computes the length and the direction of each vector out of the difference in grey-value between the image and the reference situation (an image without any drifters). Finally the program visualises the vectors computed out of the images of the digital cameras on the screen of the PC. Figure 87 displays a screen dump after the visualisation of the vectors. A point indicating the ending point of the vector gives an indication about the heading direction of the vector.

8.2.2 Visualisation of flow pattern

The flow pathways in the scale model are visualised using Hasselblad cameras, covering an area of 6 by 6 meter of the scale model. Consequently only 2 cameras are needed to cover the whole area around the Walsoorden sandbar. The area covered by both cameras is represented in figure 88.

For visualising the flow pathways drifters were spread out in the scale model and images are taken with a long opening time of the lens of the camera. To have an idea about the heading direction of the float track in the scale model, the lens at first is opened during a short time, then closed during a short time and opened again during a longer time. Figure 89 displays an image of the Hasselblad camera. A short and a long white line on the image represent each flow pathway.

Concerning the dropping of the drifters in the scale model, two different methods are used. The first method consists of spreading out the drifters over the whole area of interest. With the Hasselblad camera an images is taken with 20s as the opening time of the lens of the camera. Using the model scales of the physical model, 20s is equivalent with 800s or 13 minutes in nature. Afterward these pictured are converted into digital format. Using this method for visualising the flow pathways an overview of the current pattern for the whole research area is obtained. In the following paragraphs this method will be referred to as 'method 1'.

The second method for visualising the flow pathways in the scale model consists out of throwing the drifters into the water at almost the same location as during the field cam-

paign and at the equivalent starting time of the scale model. Due to the selection of the starting points and computation of the starting times in the scale model, this method is only carried out for the flow pathways measured on October 4th and 7th during the flood tidal phase around the tip of the Walsoorden Sandbar. Out of a careful study of the starting points of the flow pathways measured on these 2 days follows that during the field campaign mainly 3 transects were used for dropping the drifters into the water. The distance between the starting points was approximately equal to 50 meter. For the execution of this second method for visualising the flow pathways, always 11 drifters equally spaced along the transect (with a distance of 12.5cm between them, equivalent with 50 meter in nature) were dropped into the water. Afterwards 2 images are taken with the Hasselblad camera with an opening time of the lens of 20s. Consequently the drifters are followed during a period of 40s, corresponding with 1600s in nature (26 minutes). In order to compare the flow pathways with the field data, these images of the cameras are converted into digital format. This method will be referred to as 'method 2'.

8.3 Comparison of Eulerian velocity with DGPS-measurements

8.3.1 General

This paragraph discusses the comparison of the instantaneous velocity measured in the scale model with the instantaneous velocity measured during the drifter measurements carried out from September 23rd 2002 until October 8th 2002. Because only one tidal cycle as boundary condition is used for the scale model tests, it is needed to select from this period the days on which the tidal range is almost the same as the tidal range in the scale model. Using this selection method September 24th, October 4th, 7th and 8th are selected. Because on the selected days no drifter measurements were carried out during the ebb tidal phase, also September 26th and 27th are selected to compare with the scale model tests during the ebb phase. Figure 90 displays the water level measured at Hansweert during the period the field measurements were carried out. The selected tidal curves for the comparison with the scale model tests are indicated in red.

Figures 91 to 123 display for each hour of the tidal cycle the current pattern measured during the scale model tests (displayed with blue vectors) together with the instantaneous velocities of the drifters measured on the selected days during the field campaign (red vectors). The current pattern of the scale model is computed out of the images of the digital cameras. Concerning the field data, drifter measurements were carried out at 0.8, 2.0 and 5.0 meter water depth. For the comparison with the scale model tests, the drifters measured at 0.8 and 2.0 meter water depth are displayed in the figures, without making any distinction between the water depths. During the field campaign the drifter positions were recorded every 20s. The files received by IWA contain also the instantaneous velocity at each recorded position computed out the coördinates of 2 consecutive positions. It should be noticed that out of the files with numerical data for the different float tracks, the data of the column with header ‘average of 6 values’ is used. The plotted magnitude of the velocity is the average of 2 time steps before and 4 time steps after the indicated moment. The background of each figure displays the contour lines of the bathymetry of 2001 (as used in the numerical model). The different colours indicated the depth in meter TAW.

Together with the vectors, the current velocity is printed in the figures. For a better reading of the figures, both for the scale model tests as for the field data a selection of the vectors is carried out. From the vectors displaying the instantaneous velocities measured during the field campaign only these vectors with a minimum distance of 150 meter between the starting points are selected. The vectors of the flow pathways measured at 0.8 meter and 2.0 meter water depth are displayed together, keeping in mind that the minimum distance between the starting points of two vectors should be more then 150 meter. Concerning the current pattern measured in the scale model, every second vector and the vectors with a minimum distance of 150 meter between the starting points are displayed in the figures.

In order to have an indication about the heading direction of the float track, which was measured during the field campaign, the vectors of the flow pathway measured during the field campaign is displayed using a time window of 30 minutes. Referring to the moment of the field data, which is equivalent with the moment of the tidal cycle in the scale model, the vectors are displayed 15 minutes before and 15 minutes after this moment. Especially for the current velocity, this means that the velocity of the vector in the middle of a series gives an indication of the velocity at the specified moment. It is also possible that one or two vectors belonging to the beginning and the end of the time window are plotted.

8.3.2 Analysis

Before starting with the analysis of figure 91 to 122 displaying the comparison of the instantaneous velocity measured in the scale model with the velocity out of the drifter measurements, some general remarks about the current pattern measured in the scale model are given.

A first remark concerns the current pattern at the end of the ebb tidal phase (at HW+5h and HW+6h, figure 118 to 122). With low water depths at the ETW, WSB and MNF, an area with low velocities exists over there. Into such an area with low velocities some vortices are created, due to the contact of this area with the moving water in the MEC. Also in the MSF, vortices are formed around the SSS during this period.

Secondly, the current pattern in the scale model at HW+1h (figure 113) show that the current coming from the MNF seems to cross the MEC and seems to enter the Schaar van Ossenisse. Checking this current pattern visually in the physical model learnt that a drifter starting at slack high water in the MFC, enters the MNF, is then crosses the ETW or the WSB and is even crossing a part of the MEC. At the thalweg of the MEC, the drifter continues following the MEC into a downstream direction.

Comparing the current pattern measured in the scale model with the instantaneous velocities of the flow pathways of the field campaign provides the following conclusions.

Concerning the direction of the current pattern measured during the flood phase (from HW-5h until HW), out of the comparison of figures 91 to 112 follows the general conclusion that especially for the MFC and the MSF the direction of the instantaneous velocity measured in the scale model is almost the same as the direction measured during the field campaign. A little different direction is measured in the scale model at the WSB and at HW-5h at the ETW.

On September 24th the most flow pathways were measured in the MFC during the flood tidal phase. The direction of the instantaneous velocity measured in the scale model at HW-5h (figure 91), HW-4h (figure 95), HW-2h (figure 103), HW-1h (figure 107) and HW (figure 111) is the same as the direction measured during the field campaign. Concerning the comparison of the velocity with the field data, lower velocities are measured during the scale model tests in the downstream end of the MFC at HW-5h (figure 91). The velocity measured in the scale model is 0.3 m/s, while during the field campaign velocities of 0.6 were measured. Contrary at HW-2h and HW (figures 103 and 111) 0.1-0.2 m/s higher velocities are measured in the physical model. These differences in velocity can be explained by the changes in the bathymetry at the downstream end of the MFC during the last 10 years. The diminished dumping of dredged material at this location after 1996 resulted into a deepening of the downstream end of the MFC. It should be noticed that out of figure 99 (HW-4h) follows that the bifurcation between the MFC and the MSF at the downstream end of the NSS is rather good represented in the physical model. As well as the direction as the velocity of the current in the scale model turning into the MFC and into the MSF is almost the same as measured during the field campaign.

In the middle of the MFC, where the MNF enters the MFC, 0.3 m/s higher velocities are measured in the scale model at HW-1h (figure 107). The vectors of the flow pathway measured at HW-4h in this area are situated within an area with rather high bottom slopes. Consequently rather high differences in velocity exist in a rather small area in the physical model, which makes it difficult to compare the velocity of the physical model with the field data.

Also in the MSF, a rather good correspondence is found between the directions of the instantaneous velocity measured in the scale model and during the field campaign. Due to the steep bottom gradients near the WSB at HW-5h (figure 94) significantly higher velocities of 0.7 m/s are measured in the scale model near the WSB then in the MSF and above the SSS (0.4-0.5 m/s). This provides difficulties in comparing the velocity measured in the scale model with the field data. At HW-4h (figure 98), HW-3h (figure 102), HW-1h (figure 110), the scale model provides velocities in the MSF, which are 0.1-0.2m/s higher then measured during the drifter measurements. Only at HW-2h (figure 106) up to 0.2 m/s lower velocities are measured in the scale model. At this moment, in the scale model a velocity of 0.8-1.0 m/s is measured, while the field data show a velocity of 1.0-1.2 m/s.

A significant difference in direction between the field data and the velocity measured in the scale model is noticed at the ETW at HW-5h (figure 92) The drifters starting at the ETW cross the NSS and a part of the MFC before turning into it. This phenomenon is not noticed during the scale model tests. The current in the scale model turns almost immediately into the MFC. Along the report of the field campaign (*IWA 2003*) this effect takes place during the first two hours after each low water. Looking at the annexes of the report with drawings of the float tracks at the beginning of the flood phase, this effect is not only recognised on October 4th but also on September 25th. The report provides the next possible explanation. At the beginning of the flood tidal phase, the current coming from the Schaar van Ossenisse crosses the ebb channel and even crosses a part of the flood channel before turning into it. Trying to force the appearance of this phenomenon in the scale model by adding roughness elements or by changing the boundary conditions of the

physical model did not have any effect. The downstream boundary of the scale model being that close to the research area is a possible explanation for the current at the beginning of the flood tidal phase crossing the NSS and a part of the MFC is not appearing in the physical model.

Smaller differences in direction between the current measured during the drifter measurements and the current measured in the scale model are noticed at the ETW and the WSB. The direction of the vectors of the field campaign at HW-5h (figure 93) and HW-4h (figure 96-97) is almost the same as the direction of the current measured in the physical model. The float tracks measured at these moments during the field campaign are located in an area where not that many drifters were recorded during the scale model tests, because of the drying of the WSB. This makes it difficult to compare the velocities.

During the period from HW-3h until HW (figures 100-101, 104-105, 108-109 and 112), a little different direction between the current pattern measured in the scale model and during the field campaign is found. The current measured in the scale model at the ETW is turning earlier into the MSF then measured during the field campaign. This can be explained by the changes in bathymetry during the last 10 years. Due to the erosion of the southern side of the WSB, the WSB is oriented more northern. Consequently, with higher water levels during the maximum flood phase the turning of the water into the MSF in the present situation is appearing more upstream then in 1990. Out of figure 97, 101, 108-109 and 112 follows that around the WSB the splitting of the current in the MSF and the MNF is correctly modelled. Vectors of a float track that during the field campaign was heading into the MSF or MNF are noticed at a location where the current in the scale model is also heading into the MSF or MNF.

Concerning the velocity measured from HW-3h until HW, a velocity of 0.6 m/s is measured at HW-3h (figure 100) in the physical model, while the field data show velocities of 0.7 m/s. Studying figure 101 (HW-3h), 104-105 (HW-2h), 109 (HW-1h) and 112 (HW) provides the conclusion that at these moments the velocities measured in the scale model rather good predict the velocity measured during the drifter measurements. The difference in velocity between scale model and field data at these moments is lower then 0.1m/s. Only at HW-1h (figure 108) a velocity of 1.2 m/s is measured in the scale model being 0.1-0.3 m/s higher then the field data (0.8-0.9 m/s). It should be noticed that due to the flooding of the WSB during the flood phase, the changes in bathymetry at the southern side of the WSB (the erosion of the WSB near the MSF during the last 10 years) and the water level in the scale model being not exactly the same as the water level during the field campaign can explain some of these differences in velocity between scale model results and field data.

During the field campaign insufficient measurements were carried out to check if the current at HW+1h coming from the MNF really is crossing the ETW before entering the MEC almost perpendicular to the thalweg of it. The vectors belonging to the float track measured at October 4th at the WSB (figure 113) give a little indication that the current from the MNF is crossing the ETW.

On the days selected to compare the instantaneous velocity measured during the ebb tidal phase in the scale model with the field data most of the drifter measurements were carried

out in the MFC. The direction of the currents measured at HW+2h and HW+3h (figures 114, 115 and 116) in the scale model in the area of the MFC with strong ebb flow (the area where the MNF enters the MFC), is the same as measured during the DGPS-measurements. Also the current in the scale model the current spilling over the NSS has the same direction as the current of the field data. In this area rather high differences in velocity exist between field data and the velocity measured in the scale model. During the scale model tests a velocity of 1.2-1.4 m/s is measured at HW+2h (figure 114) and 1.1-1.3 m/s at HW+3h (figure 115-116). The field data show s at these moments velocities of 0.8-1.0 m/s. Remarkable is the high velocity of 1.3 m/s at HW+2h and 1.5 m/s at HW+3h measured in the scale model when the current of the MFC is spilling over the NSS. During the field campaign velocities of 0.8 m/s were measured (figure 114 and 116).

Higher differences in direction between the current measured in the scale model and the field data are noticed at HW+4h and HW+5h in the downstream end of the MFC (figure 117 and 118). The current measured during the field campaign, especially for the area of the MFC near the downstream end of the NSS (figure 117), is entering the MEC almost perpendicular to the thalweg of it. The current in the scale model is flowing into the MEC with a direction, which is almost parallel to the MEC. In the middle of the MFC this difference in direction is less present (figure 118). The velocity measured in this area of the scale model is 0.8-0.9 m/s, while the field data show a velocity of 0.7 m/s at HW+4h and 0.5 m/s at HW+5h. The higher velocity in the scale model can be explained by the MFC in 1990 being less deep then in the present situation.

As mentioned above, at HW+5h and HW+6h (figure 119 to 122) an area around the WSB exists in the scale model with low velocities. In this area, consisting out of the ETW, MSF and the MNF vortices appear. Due to this vortices, which are less or not present in the river Scheldt, the direction and also the velocity of the current measured in the scale model is different from the direction and velocity measured during the DGPS-measurements. With higher water depths closer to the MEC, the current in the scale model has the same direction as measured during the field campaign. The velocity in this deeper area of the ETW measured in the scale model differs +/- 0.1 m/s from the field data.

8.4 Comparison of flow pathways with DGPS-measurements

8.4.1 General

Figure 123 to 139 display the flow pathways measured in the scale model compared with the float tracks measured during the field campaign. This comparison is only carried out for the flood phase of the tidal cycle (from HW-5h until HW).

Each figure with the compared flow pathways covers the Walsoorden Sandbar (WSB), the seaward tip of the sandbar (ETW), the Minor Northern and Southern Flood channels (MNF and MSF), the Northern and Southern Sand Spits (NSS and SSS) and the Main Ebb and Flood channels (MEC and MFC). The flow pathways measured during the scale model tests are displayed in blue, the float tracks measured during the field campaign in red. The contour lines in the background display the bathymetry of 2001 (which is used in the numerical model) together with the labels indicating the depth in meter TAW. The name of

the displayed float tracks (as provided in the files from IWA, 2003), is displayed together with information about the scale model test in the title of the plot. During the field campaign the drifter measurements were carried out with drifters at 0.8, 2.0 and 5.0 m below the surface. For the comparison with the scale model tests, the flow pathways of the drifters at a depth of 0.8 and 2.0 m below the surface are selected and plotted without making any distinction between both water depths.

As mentioned in paragraph 8.2.2 the flow pathways are visualised using two different techniques. For the comparison with the field data, the flow pathways visualised using these both techniques are used. An indication about the method used for the visualisation is displayed in the title of the figure (The indication 'method1' or 'method 2' when referring to the scale model tests). The float tracks measured in the scale model using 'method 1' are compared with the flow pathways measured during the field campaign on the same days as selected for the comparison of instantaneous velocities (September 24th, October 4th, 7th and 8th). Due to the selection of the starting points and starting times for the second method for visualising the flow pathways in the scale model, this comparison is only carried out for October 4th and 7th. On these days the flow pathways were measured at the ETW.

Concerning the figures displaying the comparison of the flow pathways resulting out of these two methods with the field data, the following remarks should be made. Using the first method to visualise the flow pathways in the scale model, the images are taken with a Hasselblad camera with an opening time of 20s. The float tracks measured during the field campaign compared with the scale model tests are displayed starting from the equivalent starting time and ending 800s later (the time in nature equivalent with 20s in the scale model). Figure 137, 138 and 139 provide for the different hours of the flood phase an overview of compared flow pathways. For a certain hour of the flood phase, these last figure contain the flow pathways measured in the scale model at this moment together with all float tracks of the field campaign compared with.

For the comparison with the flow pathways visualised in the scale model using 'method 2', the same technique is used to define the length of the displayed float tracks of the field campaign. Because for each test during 2 x 20s an images is taken with the Hasselblad camera and because the moment of taking the images is the equivalent with the moment of dropping the drifter into the water during the field campaign, the ending point of the float track measured during the field campaign is situated 2 x 20s x40=1600s later.

8.4.2 Analysis

The comparison of the flow pathways measured in the scale model with the float tracks measured during the DGPS-measurements (Figure 123 to 139) is only carried out for the flood tidal phase (from HW-5h until HW). Figure 137, 138 and 139 provide for each hour of the flood phase an overview of figure 124 to 136.

During slack low water and at the beginning of the flood phase (at HW-5h, figure 123 and HW-4h figure 126) a significant difference exists between the flow pathways measured with 'method 2' in the scale model and the float tracks measured on October 4th and 7th. It should be noticed that on October 4th and 7th rather strong southern winds were present

(+/- 6m/s on October 7th). The flow pathways measured during the field campaign at a depth of 0.8 meter crossing those measured at 2.0 meter depth can be explained by this wind drift (*IWA 2003*). Concerning the length of the flow pathways, the float tracks heading in the scale model into the MNF have almost the same length as measured during the field campaign. Due to the changes in bathymetry at the southern side of the WSB, higher velocities exist over there, resulting into longer flow pathways measured in the scale model.

The direction of the flow pathways measured at HW-4h in the scale model with 'method 1' at the ETW and above the SSS is the same as the direction of the float tracks measured with DGPS (figure 124). The current in the scale model at the WSB turning earlier into the MSF as followed out of the analysis of the comparison of the instantaneous velocities is also noticed in figure 125. Comparing the length of the float tracks measured in the scale model of figure 124 and 125 with the length of the flow pathways measured during the field campaign provides also the conclusion that at the ETW slightly longer float tracks are measured in the scale model. The flow pathways in the scale model starting at the MSF and flowing over the SSS into the MEC (figure 125) have almost the same length and direction as the float tracks measured during the field campaign.

With the rising water levels from HW-3h until HW, the flow pathways at the WSB in the scale model earlier turning into the MSF is more clearly noticed (HW-2h: figure 130, HW-1h: figure 134 and HW: figure 136). Comparing the field data with the flow pathways of the scale model visualised using 'method 2' in figure 129 (HW-3h), 132 (HW-2h) and 135 (HW-1h) makes clear that the division of the current at the ETW into a current through the MNF and the MSF is correctly modelled. The flow pathways that during the field campaign were flowing into the MSF/MNF in the scale model also are flowing into the MSF/MNF. This is also the fact for the bifurcation of the current around the NSS in a current into the MFC and a current into the MSF and even the MEC (figure 128). Out of the figures 129, 132 and 135 and figures 128, 131 and 133 follows also that near the starting points the flow pathways measured during the field campaign and in the scale model have the same direction. The effect of the earlier turning of the current into the MSF is only noticed near the tip of the WSB. Also the flow pathways, which during the field campaign were heading into the MNF are correctly represented by the physical model (figure 132, 134, and 135). Concerning the length of the flow pathways out of a study of figure 127 to 136 follows that especially for the flow pathways heading during the field campaign into the MSF, the scale model provides flow pathways longer then the ones measured during the field campaign. The length of the float tracks heading in the scale model into the MNF is almost the same as measured with DGPS.

At HW-3h (figure 127) the flow pathways measured in the scale model with starting points in the MSF and crossing the SSS before entering the MEC have the same length and direction as the field data. With higher water depths at HW-2h and HW-1h (figure 130 and 133), the direction of the flow pathways of the scale model and field data keeps the same, but the scale model is providing longer float tracks, due to higher the higher velocity in the scale model. Concerning the flow pathways at the downstream end of the MFC, out of figure 131 follows that the direction of the flow pathways measured at HW-2h in the scale model is the same as the direction of the float tracks measured during the field campaign. Due to the difference in bathymetry, longer float tracks are measured in the scale model.

8.5 Conclusion

Out of the comparison of the flow pathways measured in the scale model with the DGPS-measurements follows that in general the direction of the flow pathways is well simulated in the scale model. Due to differences in bathymetry the current at the tip of the WSB in the scale model is turning earlier into the MSF then measured during the field campaign. The bifurcating current around the Walsoorden sandbar is well represented, as well as for the splitting of the current into MEC and MFC as for splitting of the current at the ETW into the MSF and MNF.

The locations where the differences in the length of the flow pathways are significant correspond with the Main Flood Channel MFC and the upstream part of it. This seems logic as in this area the bathymetry of the scale model is undeeper than during the DGPS drifter measurements resulting in higher velocities. Generally the flow pathways in the scale model starting at the ETW heading into the MNF and starting in the MSF and crossing the SSS have the same length as the field data or slightly overestimate them.

Although it is extremely difficult to gather space varied velocity vectors over a large area at the same moment of the tide out of the DGPS drifter measurements, the general impression is that there is a slight overestimation of the velocity magnitude, especially in the undeeper parts of the research area.

9 APPENDIX B

VALIDATION OF THE NUMERICAL MODELS FOR HYDRODYNAMICS

9.1 Description of the detailed 2D and 3D numerical model

In figures 140 to 153 an overview is given of the most important aspects regarding the approach for numerical modelling starting from the global area 2Dh model up to the 2D and 3D model characteristics of the detailed model.

Figures 140 to 142 show the modifications made to the SCALWEST model tot obtain a better schematisation of the numerical grid in the Belgian part of the Scheldt estuary. Figures 143 and 144 give the difference in performance of simulating the tidal propagation, showing that the modified SCALWEST model is capable of simulating rather accurately the tides both in phase and amplitude far upstream of Antwerp.

The following figures represent the main characteristics of the detailed model which are all the same whether the model is run in 2D mode or in 3D mode as long as there are no changes made to the numerical grid between them: the used bottom roughness coëfficiënt (according to Manning) which is taken over from the SCALWEST model without further calibration, the grid sizes and smoothnesses in N and M direction, the orthogonality of the curvilinear grid and the Courant number according to different numerical time steps.

It can be seen that the numerical grid of the model has a grid size along the longitudinal axis (N-direction) of the Scheldt of on average 100 m and along the transversal axis of the Scheldt (M-direction) of on average 40 m. It is also denoted that according to the Courant-Levy criterium for numerical stability of the ADI numerical scheme the model has to be run with a numerical time step of not bigger than 0.25 minutes (Courant number should be below 10-15).

9.2 Comparison of current pattern computed with the 2D-model and the 3D-model

9.2.1 General

This paragraph compares the current pattern around the tip of the Plate of Walsoorden computed with a 2D hydrodynamic model and with a 3D-model. For this comparison the area around the tip of the plate is divided into two minor areas. The first one consists out of the area of the Minor Northern Flood channel (MNF), the Northern Sand Spit (NSS) and a part of the Main Flood Channel (MFC). The second area consists out of the area of the Minor Southern Flood Channel (MSF), the Southern Sand Spit (SSS), and a part of the Main Ebb Channel (MEC).

For both areas and for each hour of the tidal cycle, figure 154 to 177 display the current pattern computed with the 2D- and the 3D-model. The upper part of each figure displays the current pattern in the selected area computed with the 2D model without any refinement and with a horizontal eddy viscosity of 10 m²/s. The lower part of the figure displays the surface and bottom currents computed with the 3D model without any refinement and with a horizontal eddy viscosity of 10 m²/s and the vertical divided into 10 layers.

9.2.2 Analysis

Figure 154 to 177 display for the whole tidal cycle the current pattern computed with the 2D model (plot above) and the current pattern of surface and bottom currents computed with the 3D model (plot below). A comparison of the different figures leads to the following conclusions.

Comparing the current pattern of the 2D-model with 3D-model, leads to the general conclusion that for most of the hours of the tidal cycle remarkable differences exist in the current direction for both models when the 3D-model computes surface currents with a different direction as the bottom currents. The direction of the vectors as output of the 2D-model at these moments lies in between the direction of the surface and bottom currents.

During the flood and ebb tidal phases (from HW-3h until HW-1h and from HW+2h until HW+5h, figure 158 to 163 and figure 168 to 175) mostly no differences between the velocity and the direction of the currents of the 2D and 3D-model are noticed. The direction of the surface computed by the 3D-model with 10 layers is the same as the direction as the bottom currents. Only at HW+2h (figure 169), HW+3h (figure 171), and HW+4h (figure 173), little differences between the currents computed with both models are noticed in the MEC near the SSS. During this period the 3D-model computes in this area secondary bottom currents directed more northern then the surface currents. When comparing the current pattern of the 2D-model in the MEC with the current of the 3D-model, hardly no differences between the direction of the surface current of the 3D-model and the direction of the vectors computed with the 2D-model is noticed at HW+2h and HW+4h. At HW+3h, vectors with a slightly more northern direction are computed by the 2D-model. The current velocity of the 2D-model is a little bit smaller then the surface velocity computed with the 3D-model.

Higher differences in velocity and directions of the vectors computed with the 2D- and 3D-model are noticed during the slack low and slack high water period. During slack low water (at HW-5h, HW-4h and HW+6h, figures 154, 156 and 176) almost no differences in direction of the current in the MFC is noticed between the current pattern of both the 2D- and 3D-model. The surface currents computed at HW-5h and HW-4h by the 3D-model in the area of the MFC near the downstream end of the NSS are not completely directed parallel to the MFC. The surface current crosses a part of the MFC, while the bottom current flows parallel to the thalweg of the MFC. The current pattern of the 2D-model in this area is directed parallel to the MFC. The 2D-model computes slightly lower velocities in the MFC the 3D-model.

Especially at the ETW the 3D-model computes at HW+6h, HW-5h and HW-4h a bottom current with a direction that differs approximately 90° from the direction of the computed

surface current. The surface currents of the 3D-model at HW+6h are directed almost perpendicular to the NSS, while a bottom current exists parallel to the MNF and the NSS. The current direction of the depth-averaged current of the 2D-model is directed almost parallel to the MEC. The velocity of the 2D-model lies in between the surface and bottom velocity of the 3D-model. The surface current at HW-5h and HW-4h enters the MNF or is likely to spill over the NSS (at the downstream end). The bottom current of the 3D-model is directed more parallel to the MEC. The 2D-model computes a current flowing parallel to the NSS and having a velocity in between the surface and bottom velocity of the 3D-model.

Concerning the current pattern for the area around the SSS (figures 155, 157 and 177), almost no differences between the direction of the vectors computed with both the 2D- and 3D-model are noticed. At HW-5h, the output of the 3D-model shows a large vortex at the surface is appearing around the SSS. Secondary currents directed into a northern direction are computed at the bottom of the MEC (almost perpendicular to the MEC) and in MSF with an almost southern direction (almost perpendicular to the SSS). The surface current in this area is flowing more parallel to the MEC, respectively the MSF. The 2D-model computes also a large vortex around the SSS, with currents flowing parallel to the SSS in the MEC and MSF. The 2D-velocity in the MEC is lower than the 3D-surface velocity, while in the MSF a higher velocity is computed then in 3D.

No differences in velocity or direction are noticed between the current pattern at HW around the NSS computed with the 2D- and the 3D-model (figure 164). In the MEC, contrary, especially in the area near the SSS, the current pattern of the 3D-bottom currents differs almost 45° in direction with the surface currents (figure 165). The surface current flows parallel to the SSS, while the bottom current is crossing the MEC (the direction is almost perpendicular to the SSS). The current pattern computed in this area with the 2D-model has a direction that lies in between the direction of the surface and bottom currents. The velocity of the 2D-model and the velocity of the 3D-surface velocities is almost the same.

At HW+1h (figure 166 and 167), with the ebb phase already present in the Walsoorden area, no differences in direction and velocity are noticed between the current pattern computed with both models at the ETW, MNF and NSS. In the MFC, however, the 3D-model computes secondary bottom currents. While the surface current flows from the MFC over the NSS and enters the MEC almost perpendicular to the thalweg of the MEC, the bottom current is directed a little bit more northern then the thalweg of the MFC. The 2D-model computes for this area a current pattern with a direction almost parallel to the NSS. The velocity of the 2D-model and the surface velocity are almost the same. Concerning the area around the SSS (figure 167), the 3D-model computes especially in the MEC a current pattern with surface currents directed almost to the north bottom currents with a southern direction (perpendicular to the SSS). Consequently, differences in direction of 90°-180° can exist between surface and bottom direction. The 2D-model especially for the area of the MEC with the differences of 180° between surface and bottom direction computes a current pattern with a velocity almost equal to zero and a direction parallel to the MEC. In the MNF and at the SSS, the current patterns of both models are almost not from each other in direction and velocity.

9.3 Comparison with DGPS drifter measurements for variating horizontal eddy viscosity and numbers of vertical layers

9.3.1 General

The following series of figures (figure 178 to 215) displays the comparison of the computed flow pathways and those measured during the field campaign in September/October 2002. Figures 178 to 196 display the influence of changing the horizontal eddy viscosity in the numerical model from 1 m²/s into 10 m²/s. The influence of changing the numbers of layers in the vertical from 5 into 10 is studied in figure 197 to 215.

For the comparison of the flow pathways for both situations of the numerical model with the float tracks measured during the field campaign, the days of the field campaign are selected on which the tidal range almost was the same as the tidal range on June. With this selection method, September 23rd and 24th, October 7th and 8th are selected. Because of the effect of the current at the beginning of the flood phase starting at the tip of the plate and crossing a part of the flood channel before entering it is clearly mentioned on October 4th, the drifter measurements carried out on this day are also selected for the comparison. It should be noticed that for the selected days of the tidal cycle no float tracks were measured during the ebb tidal phase during the period from HW+1h until HW+4h. During the field campaign the drifter measurements were carried out with drifters at 0.8, 2.0 and 5.0 m below the surface. To compare the flow pathways computed with the numerical model and the flow pathways measured during the field campaign the drifters at a depth of 0.8 and 2.0 m below the surface are selected. No distinction is made in the figures between the flow pathways measured at both water depths.

Each figures with the measured and computed flow pathways covers the Walsoorden Sandbar (WSB), the seaward tip of the sandbar (ETW), the Minor Northern and Southern Flood channels (MNF and MSF), the Northern and Southern Sand Spits (NSS and SSS) and the Main Ebb and Flood channels (MEC and MFC). The flow pathways measured during the field campaign are plotted in green, the float tracks computed with the numerical model in red or blue depending on the situation that is plotted on the figure. The contour lines of the bathymetry used in the numerical model are also plotted in the figures together with the labels indicating the depth in meter TAW. The name of the displayed float tracks (as provided in the files from IWA (IWA, 2003), is displayed together with information about the runs of the numerical model in the title of the plot.

9.3.2 Analysis

Before starting with the analysis of the influence of changing the horizontal eddy viscosity and changing the numbers of layers in the numerical model, some general remarks are formulated about the flow pathways computed with the numerical model (figures 178 to figure 215). The flow pathways computed with the numerical model in the MFC follow more or less the gridlines of the numerical model. Especially in the downstream area of the MFC the direction of the computed flow pathways is parallel to the thalweg of the MFC (almost parallel to the gridlines of the model). With the lower water depths from HW-5h until HW-3h, the measured float tracks are directed in a more southern direction. Towards HW, flow pathways are measured with a direction almost parallel to the MFC.

At the ETW the measured float tracks show that the current is divided into a current through the MNF and the MSF (e.g. at HW-5h: figure 178, at HW-4h: figure 180, at HW-2h: figure 186). The flow pathways computed by the numerical model show a current that at the starting points on the ETW follows the measured float tracks. With lower water depths at the WSB, the computed flow pathways flow earlier into the MSF then the measured ones and more float tracks computed by the numerical model are directed into the MSF then measured. Concerning the float tracks with the starting points in the MSF, which are crossing the SSS, with lower water depths at HW-4h and HW-3h (figure 181 and 183), the flow pathways computed by the numerical model are not crossing the SSS, but are directed into the MSF. The fact that at HW-5h the computed flow pathways show already a turning of the current (figure 179) can possibly be explained by a longer appearance of the turning of the tide in the numerical model.

Because of the appearance of the phenomenon that the drifters released during the field campaign around slack low water at the ETW tend to cross a part of the MFC before turning into it, the figures displaying the comparison of the flow pathways measured at October 4th with the computed flow pathways are also given (figure 179, 181, and 184). It can be concluded from these figures that the current crossing the NSS and a part of the MFC is noticed at HW+6h but not anymore at HW-5h. The flow pathways at HW-5h with starting points at the ETW are already flowing into the MNF.

Returning to the influence of changing the horizontal eddy viscosity and the numbers of layers in the numerical model, out of a study of figure 178 to 215 the following general conclusions can be formulated.

At first hardly no effect of changing the horizontal eddy viscosity from 1 into 10 m²/s and changing the numbers of layers from 5 into 10 is noticed on the flow pathways for the period around slack high water (with higher water depths). Nor the length or the direction of the float tracks at HW-2h, HW-1h and HW with starting points in the MNF, the ETW and the MFC is hardly changed by both changes of the numerical model (figure 185 to 191 and figure 204 to 210). Changing the numbers of layers in the vertical from 5 into 10 does also not have any influence on the flow pathways at HW-3h (figure 201 to 203). Only the flow pathways in the MFC computed at HW (figure 188) with a viscosity of 10 m²/s have a length that is longer then those computed with a viscosity of 1 m²/s. These longer float tracks mean a slightly better prediction of the length of the measured float tracks. The flow pathways at the WSB (figure 186) computed with the numerical model with an eddy viscosity of 10 m²/s in the vertical are turning earlier into the MSF then the flow pathways as output of the model with a viscosity of 1m²/s. The same conclusion is found when computing the flow pathways at HW in the MFC and at HW-2h at the WSB with 10 instead of 5 layers in the vertical (figure 205 and 207).

As a second general conclusion, it should be noticed that the difference in velocity and direction resulting out of changing of the numbers of layers in the vertical from 5 into 10 is a very small difference. The influence of changing the horizontal eddy viscosity on the flow pathways starting in the MFC and in the MSF is much higher then the influence of changing the numbers of layers. The highest differences in direction of the float tracks are found

with lower water depths (at HW-5h and HW-4h, figures 187 to 181 and figures 197 to 200) at the ETW.

The influence of the horizontal eddy viscosity on the flow pathways during the period from HW-5h until HW-3h is displayed in figure 178 to 184. The flow pathways in the MFC computed at HW-5h (figure 178) with a viscosity of 10 m²/s tend to follow the gridlines of the numerical model more then the flow pathways out of the computation with a viscosity of 1 m²/s. At HW-3h (figure 182) hardly any difference between the float tracks computed with both models is noticed. The flow pathways starting at the ETW and computed with 10 m²/s at HW-5h and HW-4h (figure 178 and 180) better predict the measured flow pathways then the flow pathways computed with 1 m²/s. The flow pathways starting at HW-4h and HW-3h in the MSF (figure 179 and 181) does not show differences in direction between a computation with 1 and 10 m²/s, but show a lower velocity when computed with 10 m²/s. This means a better simulation of the measured flow pathways at HW-3h and a little bit worse simulation at HW-4h.

Also during the maximum ebb phase (HW+5h, figure 192 and 193) hardly any differences in direction are found when changing the horizontal eddy viscosity from 1 into 10 m²/s. The velocity computed with a viscosity of 10 m²/s at this moment is a little bit higher, resulting into a better prediction of the length of the measured float tracks. At the moment before slack low water with the ebb tidal phase still present (at HW+6h, figure 194 to 196), no differences in direction are noticed at the ETW and the MFC. The direction of the computed float tracks starting at the SSS does not change when changing the horizontal eddy viscosity. The flow pathways starting in the MSF computed with an eddy viscosity of 10 m²/s simulate better the measured float tracks then those computed with 1 m²/s.

The influence of changing the numbers of layers in the vertical for the period from HW-5h until HW-4h and from HW+5h until HW+6h is displayed in figure 197 to 203 and 211 to 215. During the maximum ebb phase (HW+5h, figure 211) and for the moments before slack low water with the ebb tidal phase still present (at HW+6h), changing the numbers of layers does not have any effect on the flow pathways computed in the MFC. As mentioned above, the float tracks in the MSF starting near the SSS and computed with the 10-layer model (figure 211 and 212) are directed slightly more into the MSF. The length of the float tracks is a little bit longer then the length of the flow pathways computed with 5 layers. This makes that the measured flow pathways are a little bit better simulated with 10 layers in the vertical.

With lower water depths at slack low water (HW-5h) and at the beginning of the flood phase (HW-4h), the thinner layers of the numerical model towards the bottom make that the bottom velocity is more precise computed. This also effect the surface velocity and direction and the flow pathways at the ETW and in the MSF. The flow pathways in the MFC (figure 197 and 199) computed at HW-5h and HW-4h with 10 layers in the vertical show a direction and velocity that is not really differing from the flow pathways of the 5-layer model. Concerning the float tracks starting at the ETW, a computation with 10 layers provides a better simulation of the measured flow pathways than a computation with 5 layers. As already mentioned above the numerical model computes at HW-4h flow pathways with starting points in the MSF, but following the MSF instead of crossing the SSS (figure 200).

The float tracks resulting out of a 10-layer computation tend to follow more the thalweg of the MSF then crossing the SSS, resulting into a little bit worse simulation of the measurements.

Changing the numbers of layers from 5 into 10 provides flow pathways corresponding better with the flow pathways measured at October 4th (figure 198 and 200). The division of the current into a current through the MNF and the MSF is better modelled with 10 layers in the vertical. The length of the flow pathways does also correspond better with the length of the measured float tracks.

9.4 Comparison of numerical model results with scale model tests

9.4.1 General

Figure 216 to 227 display for each hour of the tidal cycle a comparison of the instantaneous velocities measured in the scale model and the velocities computed with the numerical model.

Each figure displays the area around the Walsoorden Sand bar (WSB), including the Main Ebb Channel (MEC), the Main Flood Channel (MFC), the Northern and Southern Sand Spits (NSS and SSS) and the Minor Northern and Southern Flood Channels (MNF and MSF). Red vectors display the instantaneous velocity measured in the scale model. This vector field is computed out of the images of the digital cameras. The blue vectors are computed with the numerical model. The numerical model concerns the 3D-model with a horizontal eddy viscosity of 10 m^2/s and the vertical divided into 10 layers. No refinement of the grid is carried out for the numerical model. The vector field displayed in the figures is the output of the numerical model in the upper layer (the surface layer).

As already mentioned in paragraph 2.1.2 the scale model was built in 1990 with the bathymetry of this period. The numerical model, contrary, was run with the bathymetry of 2001. A comparison of both bathymetries in the same paragraph learnt that major differences between both bathymetries were noticed in the MFC and in the MSF. When interpreting the figures these differences in bathymetry should be kept in mind. The contour lines displayed in the background of each figure represent the bathymetry of the numerical model (dd. 2001).

9.4.2 Analysis

Major differences between the current pattern of the numerical model and the current pattern of the scale model are found at the downstream end of the MFC. Due to the erosion of the Schaar van Waarde, the bathymetry of 2001 shows a little sand spit between the Schaar van Waarde and the Schaar van Valkenisse. With lower water depths from HW-5h until HW-3h (figure 216 to 218) the current in the numerical model is flowing from the MEC through the MFC at the northern side of this sand spit into the Schaar van Valkenisse. The current in the scale model flows more parallel to the NSS and then turns into the Schaar van Valkenisse. This phenomenon is less noticed at HW-2h (figure 219) and is not present at HW-1h and HW (figure 220 and 221).

During the entire ebb tidal phase (figure 223 to 227) the current at the downstream end of the MFC in the scale model is directed parallel to the NSS before entering the MEC. The current computed with the numerical model is entering the MEC more perpendicular to the thalweg of it. A possible explanation could be the changed morphology at the upstream end of the MFC. During the last 10 years the upstream end of the WSB is eroded away. It should be noticed here that the same phenomenon is found when comparing the scale model results at HW+4h and HW+5h with the drifter measurements of September 24th and 27th 2002 (figure 117 and 118). The drifters measured during the field campaign flow into a direction more perpendicular to the thalweg of the MEC, while the current in the scale model is directed parallel to the NSS.

During the flood tidal phase (figure 216 to 221), the direction of the vectors measured in the scale model in the MEC is almost the same as the direction computed with the numerical model. With the lower water depths at HW-4h (figure 217) and HW-3h (figure 218), the numerical model computes a little bit lower velocities in the MEC. At these moments also a little difference in direction exists at the ETW and the WSB. Due to the more northern oriented shape of the tip of the WSB in the scale model, the current measured at HW-4h and HW-3h in the scale model is turning earlier into the MSF. Both the velocity of the numerical model and the scale model at the ETW are almost the same.

During the first flood phase (HW-2h and HW-1h), the velocity measured in the MEC in the scale model is almost the same as the velocity computed with the numerical model (figure 219 and 220). The current direction in the scale model at the ETW is also the same as the computed current direction. During this period although higher velocities are measured in the MNF in the scale model. The current in the numerical model is crossing the NSS with a direction more perpendicular to the NSS and with lower velocities then in the scale model

During slack high and low water, the current pattern computed with the numerical model at the ETW and WSB shows directions almost perpendicular to the thalweg of the MEC (figure 221 and 216). The phenomenon of the current at slack low water (HW-5h, figure 216) starting at the ETW and crossing the NSS and a part of the MFC is not noticed in the scale model. The current pattern computed with the numerical model shows a current, which is crossing the MNF and the NSS but is turning almost immediately into the MFC instead of crossing a part of the MFC. Concerning the turning of the current during the slack high water period, the numerical model computes a current at HW+1h (figure 221) is flowing from the MNF over the tip of the WSB and the ETW and is entering the MEC almost perpendicular to the thalweg of it. This was also measured during the field campaign. The only difference between numerical model and scale model at this moment is the numerical model computing a current more perpendicular to the thalweg of the MEC. Due to a larger vortex appearing at HW-5h around the SSS in the numerical model, the numerical model at this location computes lower velocities. Also at HW+1h the scale model provides higher surface velocities above both sand spits (the NSS and SSS). The velocity and direction measured at HW-5h during the scale model tests in the MEC is the same as the velocity and direction computed by the numerical model.

During the scale model tests, an area with almost a velocity almost equal to zero was noticed during the maximum ebb phase (HW+5h and HW+6h) around the tip of the WSB

(figure 226 and 227). This area consisted out of the MSF, MNF and the ETW. The current field as a result of the numerical model, contrary, show significant currents in this area. Consequently the velocity computed by the numerical model in this area is higher then the velocity measured in the scale model.

9.5 Comparison with velocity profiles along transect

9.5.1 General

During the field campaign on June 12th 2002 the vertical velocity profile is measured with ADCP along a transect near Waarde. This velocity profile is compared with the profile computed with the 3D-model with 10 layers in the vertical. Therefore two types of figures are considered. The first type concerns vector plots displaying the measured and computed velocity at 6 different depths below the water level. The second type of plots are contour plots displaying both for the measurements and numerical model computations the current magnitude and direction velocity for the whole transect, as well as the difference between the measured and computed velocity respectively direction.

Before describing into detail both type of figures, the following general remarks should be made about the manipulation of the field data in order to generate these plots.

A first remark concerns the bottom profile measured along the transect during the field campaign and the bottom profile for the same transect in the numerical model. Locating the transect in the grid of the numerical model, let conclude that the transect almost falls together with a gridline in the N-direction of the grid. If the bottom profile of the numerical model between the corresponding starting and ending point of the transect is compared with the profile measured during the field campaign, a shift between both profiles is noticed. The bottom profile of the numerical model does not fall exactly together with the measured profile. To make a comparison possible between the measured and the computed velocity, the bottom profile of the field data is shifted along the transect to provide a better correspondence between both profiles. It should be noticed that this shift of the field data along the transect is different for each hour of the tidal cycle the measurements were carried out.

Secondly it should be noticed that as well as for the field data as for the output of the numerical model, an extrapolation towards the surface and the bottom is carried out. Concerning the velocity and direction computed with the numerical model it should be noticed that both variables are computed for the different layers the model is divided into in the vertical. In order to display the velocity and the direction, both are positioned in the middle of each layer. To have an idea about the value of direction and velocity at the surface and at the bottom, the surface velocity and direction are taken equal to the values in the top layer. The bottom direction is set equal to the direction in the lowest layer, while the velocity is set equal to zero. The same extrapolation is carried out for the field data. The current surface velocity and direction and velocity is set equal to the value measured the closest to the surface. The bottom velocity is set equal to zero, while the current direction is set equal to the lowest measured value.

Before displaying both types of plots as well as the output of the numerical model as the field data are interpolated on a grid. For the first type of plots (the vector plots), the data are interpolated on a rectangular grid with grid cells of 100m along the transect and 1m in the vertical. The second type of plots, the contour plots displaying the current velocity and direction, are the result of an extrapolation on a curvilinear grid. This curvilinear grid is built by the grid cells of the numerical model along the grid line almost falling together with the transect and by the division in layers in the vertical direction. Consequently no extra interpolation is carried out for the numerical model results.

The first type of plot, used for the comparison of the measured and computed velocity profile consists of 6 subplots displaying the current vectors along the transect at 6 different depths (-12mTAW, -8mTAW, -4mTAW, 0m TAW, 2m TAW and 4m TAW). If the water level at the specified moment is lower then the water level indicated in the subplot no vectors are plotted. Therefore the water level computed by the numerical model is also plotted in the title of the plot. It should although be noticed that due to small differences in water level between the numerical model and the field data it is possible that only one type of vectors are plotted (numerical model results or field data). The vectors indicating the current are displayed with reference to the direction of the transect. The real current direction can be found by a superposition of the direction of the transect and the direction indicated by the vectors in the vector plot. Vectors plotted below the transect belong to the flood phase, vectors above the transect belong to the ebb phase. For a better reading of the plots, the flood and ebb direction are also indicated on the plots.

The second type of plots consists out contour plots for the current velocity and direction measured during the field campaign or computed with the numerical model. Each figure contains 6 subplots: the first series of 3 plots are displaying the comparison of the velocity along the transect, the last series of 3 plots are displaying the comparison of the directions. The first plot of the 2 series mentioned above displays the property measured during the field campaign. The second plot contains the value computed with the numerical model and the third plot displays the difference between the numerical model and the field data.

Concerning the current direction in the contour plots it should be noticed that the following convention is used. The positive direction in the figure is measured relative to the normal of the transect pointing in the direction of Hansweert (as displayed in the figure below). This makes that the current during the ebb tidal phase has a direction of almost 360°. It should also be noticed that for the plot with the difference in direction, the absolute value of the difference between numerical model results and field data is plotted.

For both types of plots it should be noticed that the horizontal axis of the plots display the distance along the transect. The origin of this axis is the starting point of the transect near Walsoorden. The point with coördinate 3000 is located in the flood channel near Waarde. Referring to the nomenclature for the different regions around the Walsoorden sandbar (figure 2), the area between coördinate 0 and 1250 lies within the Main Ebb Channel (MEC), the area between 1250 and 1750 will be indicated as the bifurcation area of MEC and MFC. The remaining part of the transect lies within the Main Flood Channel (MFC).

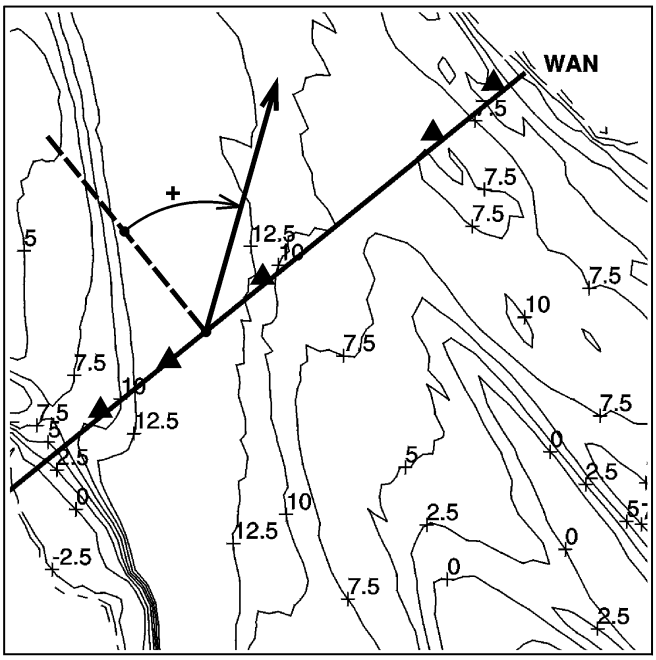

Convention used for defining the directions in the plots

9.5.2 Analysis

Before starting with the analysis of figure 228 to 245 displaying the comparison of the measured and computed velocity profile along the transect, at first some general remarks can be made concerning the current pattern measured during the field campaign.

A first remark concerns the current pattern in the area around the bifurcation point between the MEC and MFC. During the flood phase (HW-5h until HW, figure 228 to 237) and during the first ebb phase (HW+1h, HW+2h and HW+5h, figure 238 to 243), as well as for the surface as for the bottom currents, the current direction is parallel to the NSS. Only during the maximum ebb phase (HW+6h), a surface current exists parallel to the MEC, while a bottom current exists still parallel to NSS. It should be noticed that during these phases the highest velocities of 1-1.5 m/s are measured at the surface of the bifurcation area between MEC and MFC and in the MFC.

A second remark concerns the current pattern along the transect during the slack low and high water period (figures 228-229, 238-239 and 244-245). Due to the turning of the current during these tidal phases, a difference in direction exists between the surface and bottom currents. The field data show that the turning of the current both during slack low water and slack high water appears at first in the MEC near the Schaar van Ossenisse and in the MFC for slack low water. The turning of the current in the MEC appears for both tidal phases first at the bottom and later on at the surface. As also mentioned with the analysis of the scale model tests, at the area of the bifurcation between MEC and MFC the current at HW-5h is directed almost perpendicular to the flood channel.

When for the whole tidal cycle the contour plots with the measured and computed velocity profile along the transect, it is noticed that the contour plots of the velocity computed with

the numerical model show higher velocities towards the bottom then the measured data. A possible explanation for this effect can be found in the extrapolation of the measured and computed velocity towards the bottom. Both for the field data as for the velocity computed with the numerical model, the velocity at the bottom is set manually to zero. Checking the files with the data of the field campaign learns that the lowest measurement is carried out approximately 1 m above the bottom. The middle of the lowest layer in the numerical model contrary is located maximum 0.20m above the bottom (the middle of a layer with thickness of 2% of the total water depth above the bottom = maximum water level of 5 m + bottom depth of 15 m in the ebb channel). Due to the interpolation of the field data and the data of the numerical model on the curvilinear grid, manually setting the velocity at the bottom to zero can result into lower velocities towards the bottom for the contour plots of the field data.

Especially during the ebb and the flood phase (from HW-3h until HW-1h and HW+2h, figures 231-235 and 240-241), out of the comparison of the vector plots and the contour plots displaying the directional profile of the measured and computed currents follows that the direction of surface and bottom currents are well predicted by the numerical model. For these tidal phases, a difference in direction between the numerical model and the field data lower then 22.5° is noticed. Only at HW+2h the numerical model computes a surface current directed more perpendicular to the MEC (figure 241). The field data for this moment show a surface currrent parallel to the MFC.

The surface current computed with the numerical model at HW+5h and HW+6h (figure 242 to 245) in the MEC is directed more into the Schaar van Ossenisse, while the measured surface current more likely to follow the MEC. The field data at HW (figure 236-237) show that in the MEC near the Schaar van Ossenisse, the turning of the current is already present. This is not the case for the numerical model, resulting into differences in direction of 90° in the MEC.

The velocity profile computed with the numerical model for these tidal phases is almost of the same shape as the measured velocity profile. Besides the above-mentioned effect of the numerical model providing higher velocities towards the bottom, probably due to the interpolation on the curvilinear grid, the difference between the velocity computed with the numerical model and the field data is mostly not higher then 0.1 m/s. At HW-2h and HW-1h (figure 233 and 235) 0.2 m/s lower surface velocities are computed with the numerical model near the land boundaries of the numerical model in the MEC and the MFC. At HW+5h and HW+6h (figure 243 and 245) the numerical model computes also 0.2-0.5m/s lower surface velocities and 0.2 m/s lower surface velocities at HW in the MEC and MFC (figure 237) .

Concerning the turning of the current at slack low and slack high water, the following conclusions follow out of the comparison of the vector and contour plots for HW+1h and HW-5h (figures 228-229 and 238-238).

The turning of the current at HW-5h (figures 228 and 229) computed by the numerical model appears first in the MEC near the Schaar van Ossenisse and in the MFC. This was also noticed in the contour plot of the field data. The turning of the current in the MEC

during the field campaign at first measured at the bottom of the MEC is not noticed in the results of the numerical model, which makes that differences in direction of 180° exist at the bottom of the MEC. This is probably the result of the moment of slack low water of the numerical model and the field data not falling exactly together. The surface current computed around this moment with the numerical model in the area of the bifurcation point between MEC and MFC is directed almost perpendicular to the flood channel, while the bottom current is still flowing into the ebb direction almost parallel to the NSS. This was also noticed in the field data. At the surface of the MFC and in the area near the bifurcation between MFC and MEC, the numerical model computes +/- 0.2 m/s lower velocities, while 0.2 m/s higher velocities are computed at the bottom of the MEC.

At HW+1h (figures 238 and 239) the numerical model computes in the area of the MEC where the Schaar van Ossenisse enters the MEC a surface current directed parallel with the MEC and a bottom current directed into the Schaar van Ossenisse. This was also noticed during the field campaign. In the middle of the MEC, the surface and bottom current computed by the numerical model are directed almost parallel to the MEC, while the field data indicated an already turning bottom current. Also for the area of the bifurcation between MEC and MFC, the numerical model computes a bottom current flowing parallel to the NSS into the upstream direction, contrary to the field data showing an already turning current for this area. The surface current is as well as for the field data as for the numerical model flowing parallel to the MEC. The numerical model provides a 0.1 m/s lower surface velocity in the MFC then the field data. During slack high water, up to 0.25 m/s lower surface velocities are computed in the MEC where the Schaar van Ossenisse enters the MEC and up to 0.2 m/s higher surface and bottom velocities in the area of the bifurcation point between MEC and MFC.

Remarkable is the situation computed with the numerical model in the MFC (figure 239). The surface current is directed into the ebb direction almost parallel to the MFC. The bottom current, contrary, seems to cross the flood channel with an ebb direction. This is not present in the field data and provides a difference in direction of 135-180° in this area. Checking this phenomenon in the output of the numerical model, it is found that during the turning of the tide the numerical model computes vortices in the surface and bottom layer with an opposite direction.

9.6 Comparison of salinity with field data

9.6.1 General

During the field campaign of June 12th 2002, the salinity was measured at 5 points lying on the transect near Waarde. For each hour of the tidal cycle, figures 246 to 269 compare the salinity computed with the numerical model with the salinity measured in 4 of these 5 points (i.e. points WC1N, WC2N, WC3N and WC4N).

Each figure with the comparison of the measured and computed salinity in one of these locations displays the measured salinity (green line) together with the salinity computed with the 3D model with 5 layers in the vertical (blue line) and the 3D-model with 10 layers in the vertical (red line). Concerning the salinity computed with the numerical model the following

remarks should be made. The numerical model concerns the 3D-model without any grid refinement and with a horizontal eddy viscosity of 10 m²/s. The salinity for each layer is displayed at the middle of this layer. The value of the salinity at the surface and at the bottom of the vertical profile is then determined using a constant extrapolation (the value is set equal to the salinity computed in respectively the highest and lowest layer). The salinity concentrations measured during the field campaign, contrary, are measured close enough to the surface and to the bottom. Therefore, the field data are displayed in the figures without performing any extrapolation.

As already mentioned in the previous paragraph, the bottom profile measured during the field campaign is shifted towards the bottom profile of the numerical model along the transect. For displaying the figures with the comparison of field data and numerical model results, no extra shift of the bottom profile of the numerical model or field data is carried out, in order to let coincide the measured and computed bottom profile. On the other hand, both the bottom level measured during the field campaign and the bottom level of the numerical model is displayed in each figure. Because of a possible difference between the water level measured during the field campaign and the water level computed with numerical model, both water levels are also displayed in each figure.

Referring to the nomenclature for the different regions around the Walsoorden sandbar (figure 2), location WC1N and WC2N will be referred to as the Main Ebb Channel (MEC), locations WC3N and WC4N as the Main Flood Channel (MFC).

9.6.2 Analysis

Before starting with the analysis of the comparison of the measured and computed salinity profiles, a short description of the appearance of the salinity profile in MEC and MFC is given.

Out of the field data follows that for the area around the Walsoorden sandbar, a salinity concentration between 12.5 and 22.5 ppt is measured. Especially during the flood phase for most of the locations a constant profile in depth is measured. At HW-5h (figures 246 and 247) a constant salinity of 16 ppt is measured in the MEC and a value of 15 in the MFC. During the flood phase, these constant values increase from 16 ppt at HW-4h in the MEC and MFC, to 18 ppt at HW –3h, 20 ppt at HW-2h and 21-22 ppt at HW-1h (figures 248 to 255). It should be noticed that for the MEC, 1-2 ppt lower values are measured then in the MFC and in the MEC. Only in the MEC near the Schaar van Ossenisse (location WC1N) and in the MFC (at location WC4n), the salinity slightly diminishes towards the surface at HW-2h and HW-1h (a difference of +/- 0.5 ppt exists between the bottom and the surface).

During slack low and slack high water, the salinity measured at the bottom is higher then at the surface. Due to the fresh water flow from upstream to downstream and the salinity intrusion by the flood at HW+6h and HW-5h a salinity concentration of 12.5 ppt is measured at the surface of the MEC (figures 246 and 268). The concentration at the bottom of the MEC is 16-17 ppt at this moment. Lower differences of 1.5 ppt between surface and bottom salinity concentrations are measured at HW+6h in the MEC (location WC2N, figure 268) and in the MFC (figure 269). This lower difference between surface and bottom salin-

ity concentration is also mentioned during the slack high water period. At HW and HW+1h (figures 256 to 259) at the surface a 0.5-1.0 ppt lower concentration is measured then at the bottom. At these moments a salinity between 18 ppt (in the MFC) and 21 ppt (in the MEC) is measured at the different locations.

At HW+2h the salinity concentration at the surface of the MEC is +/- 2.5 ppt lower then at the bottom. With lower water depths later on during the first ebb phase (HW+3h and HW+4h), this difference in salinity between the surface and the bottom of the MEC (location WC1N, figures 262 and 264) diminishes, resulting in a constant profile in depth of 13 ppt at HW+4h. Contrary for location WC2N in the MEC the rather low difference of 1.0 ppt between surface and bottom at HW+2h (figure 260) increases towards HW+3h and HW+4h (figure 262 and 264), resulting into a almost linear profile in depth at HW+4h. At this moment of the tidal cycle a difference between the salinity at the surface and at the bottom of 2.5 ppt is noticed. In the MFC channel, except for the area with lower water depths near the banks of the river (location WC4N, figure 263), the difference in salinity between surface and bottom is lower (+/- 1.0 ppt) and also resulting into a constant profile in depth at the end of the maximum ebb phase (HW+4h, figure 265).

Comparing the measured salinity with the field data provides the general conclusion that salinity computed by the numerical model during the flood phase is lower then the field data, while during the ebb tidal phase higher salinity concentrations are computed. This effect of the numerical model providing lower concentrations during the ebb phase and higher during the flood phase makes that for the maximum flood period (HW-2h and HW-1h, figures 252 to 255) a rather good correspondence exists between the computed and measured salinity profiles.

Comparing the salinity profile measured during slack low and slack high water with the computed profiles let conclude that the moment of slack low and slack high water of the numerical model is not appearing at exactly the same moment as with the field data. In the MEC and the MFC at HW+6h (figures 268-269) the salinity profile computed by the numerical model is constant in depth. The field data at this moment show already a 1-2.5 ppt lower surface salinity. Consequently at HW-5h (figure 246-247) the numerical model computes salinity profiles with a 1.0 ppt lower salinity at the surface then at the bottom corresponding to field measurements which are already constant in depth. The salinity profile computed by the numerical model for location WC2N in the middle of the MEC at HW-5h (figure 246) shows the same shape as the measured profile. The change between the lower surface values and the higher bottom concentrations appears at almost the same depth. The difference of 1.0 ppt between surface and bottom salinity is lower then the difference notice in the field data (2.5 ppt.). The salinity computed by the numerical model at HW+5h and HW+6h is, except for location WC2N at HW-5h, 2-2.5 ppt higher then the measured salinity (figures 266 to 269).

Concerning the slack high water period, the numerical model computes at HW constant salinity profiles in the MEC and MFC (figures 256-257), while the field data show already 0.5-1.0 ppt lower surface concentrations, because of the turning of the current. The shape of the computed salinity profile at HW+1h (figures 258-259) corresponds better with the shape of the measured profile. The difference in salinity between top and bottom of 0.5-1.0

ppt is a little bit higher then the difference measured during the field campaign. The computed salinity at HW and HW+1h is, except for the MEC near the Schaar van Ossenisse (location WC1N, figure 256 and 258) at HW, for all locations in MEC and MFC 1.0-2.0 ppt higher than the measured salinity concentrations at the same moments.

The moment of slack low water in the 3D-computation not appearing at the same moment as in nature makes that at HW-4h the salinity profile in the MEC (figure 248) computed with the numerical model shows 1-2ppt higher salinity concentrations at the bottom then at the surface. The influence of the turning of the current with lower concentrations at the surface due to the fresh water flow during ebb tide is still present. At the bottom of the MEC and in the MFC, already a salinity profile constant in depth is computed. At HW-4h and HW-3h (figures 248 to 251), the numerical model provides for the MEC, ETW and MFC salinity profiles which are constant in depth and which differ only 0.5-1.0 ppt from the field data.

Later on, at HW-2h and HW-1h, the difference between the measured and computed constant salinity profiles increases in the MEC towards 1.0 ppt (figures 252 and 254). The numerical model provides for this location lower concentrations then the field data. In the MFC and at the ETW, the underestimation of the field data by 1.0 ppt at HW-2h (figure 253) diminishes towards HW-1h (figure 255) resulting into a rather good prediction of the field data by the numerical model.

It should be mentioned at this point that during the period from HW-2h until HW for all locations a rather high difference exist between the bottom level of the numerical model and the bottom level that was measured during the field campaign. The differences in bottom level can reach 3 -4 meter.

During the ebb tidal phase at HW+2h and HW+3h the numerical model computes in the MEC (figures 260 and 262) a salinity profile with at the surface 0.5-1.0 ppt lower salinity concentrations then at the bottom. The computed salinity profile in the MFC at HW+2h and HW+3h (figures 261 and 263) and in the MEC and MFC at HW+4h and HW+5h (figures 264 to 267) is constant in depth. During the field campaign, due to the fresh water flow from upstream to downstream, especially in the MEC (location WC2N from HW+2h until HW+4h) and in the flood channel (location WC3N at HW+2h) a salinity profile with a surface salinity being 1.0-2.0 ppt lower than the bottom salinity is measured. Generally, the 3D-numerical model provides an overestimation of the measured salinity with 2 –2.5 ppt.

Changing the numbers of layers for the 3D-model from 5 into 10 does not significantly change much the computed salinity profile. The 10-layer model mostly provides a more fluently curved salinity profile. During the period from HW+1h until HW+6h, it can be stated that the 10-layer model provides slightly higher salinity concentrations then the 5-layer model, while in general for the flood phases (HW-5h until HW) slightly lower concentrations are computed with 10 layers in the vertical.

9.7 Comparison of velocity profiles with field data measured on 03/06/03

9.7.1 General

During the field campaign of June 3rd 2003 the velocity profile at location Kaloo, Scaldis and Veremans was measured each 10 minutes with ADCP and each 30 minutes with the AZTM. In order to compare the computed velocity profile with the measured profile, for each location and for each hour of the tidal cycle 2 measurements are selected.

All figures (figure 270 to 300) display for each hour of the tidal cycle and for each location the measured and computed velocity and direction. The current velocity (unit: m/s) is displayed on the bottom X-axis, the direction (units: ° with reference to the geographical North) is displayed on the top X-axis. On the Y-axis of the plot, the depth in meter TAW can be read. As well as for the field data as for the output of the numerical model, the current velocity is displayed as a full line, the direction as a dotted line. The field data, both for current and direction are plotted in green. To have and idea about the influence of the numbers of layers in the vertical used in the 3D-model, both the current direction and velocity are computed with the 3D-model with 5 layers in the vertical (plotted in blue) and with the 3D-model with 10 layers in the vertical (plotted in red).

As already mentioned with the analysis of the velocity profile along the transect near Waarde, a possible shift can exist between the bottom profile measured during the field campaign and the bottom profile of the transect defined in the numerical model. Because not that much information is available on this shift, for displaying the figures with the comparison of the velocity profile, no extra manipulations of field data or results of the numerical model are carried out to let coincide the measured and computed bottom. To have an idea about the difference between the measured and computed bottom level, both bottom levels are displayed in each figure (by a black line). Because of a possible difference between the measured and computed water level, a black line in each figure indicates the water level of the numerical model and the water level of the field data.

Concerning the velocity and direction computed with the numerical model, the output of each layer of the numerical model is represented at the middle of the layer. To have an idea about the current velocity and direction at the surface and at the bottom, an extrapolation towards surface and bottom is carried out. The current velocity at the bottom is set equal to 0 m/s and the surface velocity is set equal to the velocity in the upper layer. The current direction at the bottom and at the surface is respectively set equal to the current direction computed in the lowest and the highest layer.

The same extrapolation is carried out for the field measurements. The surface velocity and direction is set equal to the velocity and direction of the highest point that is measured during the field campaign. The value of bottom velocity is set equal to 0 m/s and the bottom direction equal to the lowest point that is measured. It should be noticed here that this extrapolation method could provide problems with the interpretation of the figures, especially when the velocity is measured in a few points because of the low water depth (e.g. location Scaldis for the period around slack low water).

Because of the absence of an ADCP-device on the Veremans during the field campaign, it should be noticed that for location Veremans the velocity computed with the numerical model is compared with the AZTM-measurements, instead of a comparison with the ADCP-measurements as for location Kaloo and Scaldis. To have and indication of the difference between the current velocity and direction measured with the ADCP and the AZTM, for each moment a measurement was carried out, the mean current velocity and the mean current direction is computed. For location Kaloo and Scaldis, these velocities and directions are displayed in the figures below. Out of these figures follows that in general the velocity and direction measured with the ADCP and the AZTM are almost the same.

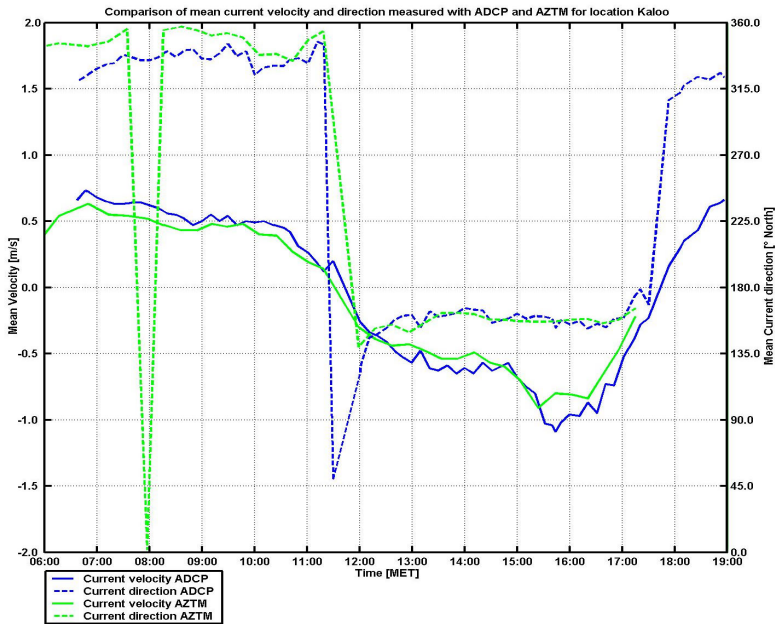

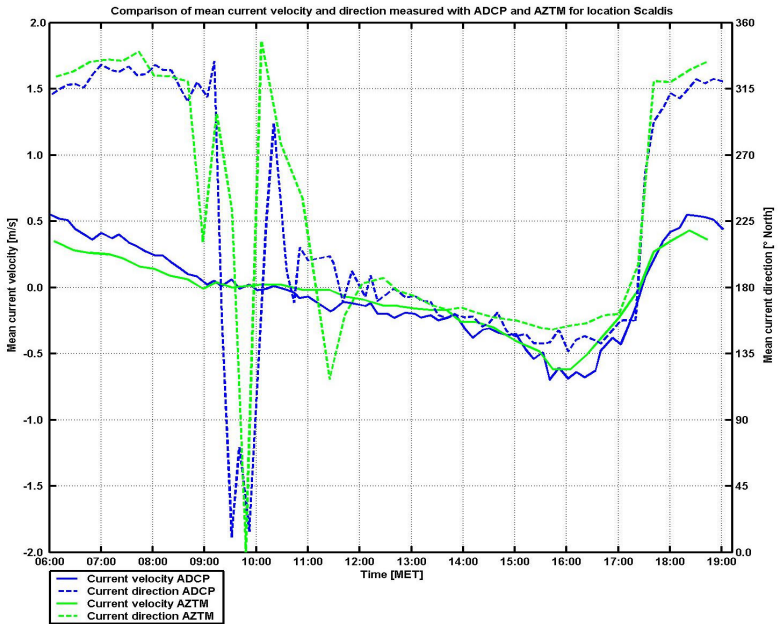

9.7.2 Analysis

At first some general remarks are formulated on the velocity profile that is measured during the field campaign at locations Kaloo, Veremans and Scaldis.

A first remark concerns the current direction for location Kaloo (the bifurcation area between MEC and MFC) during the period from HW+4h until HW+6h. At HW+4h (figure 294) a surface current is measured almost parallel to the NSS. The bottom current at this moment is directed parallel to the MEC. This situation changes at HW+5h and HW+6h (figures 297 and 299) into a surface current parallel to the MEC and a bottom current parallel to the NSS. Together with this changing current direction, also the current velocity changes. At HW+4h the measured bottom velocity (parallel to the MEC) is higher then the surface velocity. After the changing of the directions, the surface velocity at HW+6h becomes higher then the bottom velocity (due to the lower velocities on the tip of the plate) resulting into a sort of step profile for the measured velocity.

The phenomenon of the drifters crossing a part of the flood channel before turning into it, noticed the first hour after slack low water during the drifter measurements at October 4th 2002) is also found when studying the velocity profile measured at location Kaloo and Veremans (figures 270 and 271). The direction of the surface current changes from direction 25° North (parallel to MEC) over 60°-70° degrees to 90° North (almost perpendicular to MFC). From HW-4h until HW-1h (figures 273 to 283) current directions between 135 and 180° North (parallel to the MFC) are measured. It should be mentioned that from the ADCP/AZTM-measurements follows that this phenomenon is only present at the surface. The current direction at the bottom turns much earlier to the direction 180°, which makes that the current at the bottom is flowing almost parallel to the MFC.

During the slack low water period (at HW+6h and HW-5h, figures 270, 271 and 298) high differences appear between the surface and bottom directions for locations Kaloo and Veremans. Because of the influence of the salinity the turning of the current at slack low and high water appears first for currents near the bottom and then for currents in the surface layers. Differences of 45-90° can exist between the direction of the surface and bottom currents during this period. During the slack high water period (at HW and HW+1h, figures 285-286 and 288-289), the difference in direction between surface and bottom currents is lower. The profile of the current direction is almost constant in depth.

Concerning the current pattern at HW+1h, out of the ADCP-measurements for locations Kaloo and Veremans (figures 288-289) follows that the current flowing from the MFC, through the MNF enters the MEC almost perpendicular to the thalweg of the MEC (current direction between 270° and 315° North). During the ebb tidal phase (from HW+2h until HW+6h, figure 291 to figure 300) the current for both locations is almost parallel to the MEC.

During the period from HW-4h until HW-1h (figures 274 to 284) an almost logarithmic velocity profile is measured at locations Kaloo and Veremans. In the MNF (location Scaldis) the velocity profile varies from a constant profile at HW-4h and HW-3h (figures 275 and 278) into a logarithmic profile during the period with higher water depths from HW-2h until HW+2h (figures 281, 284, 287, 290 and 293). A velocity profile with low surface velocities

and higher bottom velocities is measured at HW-5h for locations Kaloo and Veremans (figures 270 and 271). The reason is the t he turning of the current at slack low and slack high water appearing first at the bottom. A last remark concerns the directions measured at location Scaldis during the slack low water period (HW-5h and HW+6h , figures 270 and 300). During this period directions are measured which differ much from top to bottom. With lower water depths in the MNF an area exists with a velocity almost equal to zero. .

The analysis of figures 270 to 300 the current pattern measured with ADCP/AZTM at locations Kaloo, Veremans and Scaldis will be divided into at first a analysis of the measured and computed current directions and secondly the analysis of the measured and computed velocity profile.

Out of the comparison of measured and computed directions for the 3 locations follows the conclusion that in general the directions are well predicted by the numerical model for the flood phase. During this tidal phase the constant directional profile measured at HW-4h until HW-1h on locations Kaloo and Veremans (figures 273-274, 276-277, 279-280, and 282-283) and on location Scaldis at HW-3h until HW-1h (figures 278, 281 and 284) is also computed with the numerical model. The difference between the computed and measured directions is less then 10°.

Due to the low water depths in the MNF (location Scaldis) during the period from HW+4h until HW+6h (figures 296, 298 and 300) and from HW-5h until HW-4h (figures 272 and 275), the current profile is measured in only a few points on the vertical (2-4 points). The directions measured during the field campaign at HW+4h and HW+5h (figures 296 and 298) show high differences between the direction of the surface and bottom currents in the MNF. The numerical model computes also directional profiles consisting out of different directions for surface and bottom currents, but these differences are less significant. Therefore differences in direction of 90°-135° between measurements and numerical model results can exist. It should be noticed here that the extrapolation of the measured directions in combination with the few points measured on the vertical could lead to a wrong interpretation of the figures.

As mentioned above at HW+6h and HW-5h differences up to 90° between surface and bottom directions are measured during the field campaign for locations Kaloo and Veremans. The directional profile at HW-5h (figures 270 and 271) for these locations computed with the numerical model falls together with the measured profile. Out of a comparison of the directional profile at HW-4h (figures 273 and 274) with the measured profile follows that the turning of the tide at slack low water takes longer in the numerical model then was measured during the field campaign. The directional profile during the field measurements becomes sooner a constant profile in depth. The same effect is noticed during slack high water (HW+1h, figures 288-289). The numerical model computes velocity profiles with a surface direction that differs up to 45° with the bottom direction. This difference is significantly higher than then the difference between the measured surface and bottom direction.

The comparison of the measured and computed velocity leads to the following conclusions. As a general conclusion follows that for most of the hours of the tidal cycle the numerical model computes a logarithmic velocity profile. Due to the logarithmic representa-

tion for solving the turbulence equations of the k-ε-model in the numerical model mostly a logarithmic profile will be found. Only during the slack low water period (HW+6h and HW-5h), the first ebb phase (HW-4h), the slack high water period (HW+1h only for location Kaloo) a different velocity profile is computed.

Consequently, for all moments a logarithmic velocity profile is measured during the field campaign the numerical model provides a velocity profile with the same shape as the measured profile. This is noticed for location Kaloo and Veremans from HW-3h until HW-1h (figures 276-277, 279-280 and 282-283) and for location Scaldis from HW-2h until HW+2h (figures 281, 284, 287, 290 and 293). The following 2 paragraphs give a brief overview of the analysis of these figures. It should be noticed that due to the logarithmic shape of the measured and computed velocity profile the differences between the computed and measured velocities and the measured velocities itself indicated in the analysis below appear at the surface.

The numerical model underestimates the measured velocity (0.5-0.75 m/s) with 0.1-0.2 m/s at HW-4h for location Kaloo (figure 273) and 0.125-0.25m/s at HW-4h and HW-3h for location Veremans (figures 274 and 277). This underestimation during the first flood phase changes into a rather good prediction of the field data during the flood phase (at HW-3h for location Kaloo and HW-3h and HW-2h for location Veremans, figures 276, 277 and 280). Finally an overestimation of the measured velocity (0.75-0.85m/s) with 0.125-0.25 m/s is computed at HW-2h and HW-1h for location Kaloo (figure 279 and 282) and at HW-1h for location Veremans (figure 283). During the ebb tidal phase (HW+2h and HW+4h) the numerical model underestimates the field data measured at location Veremans (0.5 m/s at HW+2h and 0.75 m/s at HW+4h) with 0.1-0.15m/s at the surface (figures 292 and 295).

For location Scaldis, almost no difference between measured and computed velocity is noticed at HW-4h (figure 275). This good correspondence between measured and computed velocity changes into a 0.05-0.1 m/s higher velocity computed by the numerical model at HW-2h (figure 281) and 0.125 m/s higher velocities then measured (0.75 m/s) computed at HW-1h (figure 284). During the slack high water period an overestimation of the measured velocity (0.125-0.375 m/s) by the numerical model of 0.2-0.25 m/s is noticed at HW (figure 287) and an underestimation of the field data (0.375 – 0.5 m/s) of 0.2-0.25 m/s at HW+1h (figure 290). During the first ebb phase (at HW+2h, figure 293) these underestimation of the measured velocity (0.5 – 0.625 m/s) by the numerical model decreases to 0.1-0.125m/s.

As above-mentioned the current for location Kaloo at HW-4h (figure 273-274) is directed almost perpendicular to the MFC. During this period as well as for location Kaloo as for location Veremans the surface velocity is lower then the bottom velocity. The numerical model with approximately 0.1-0.2 m/s underestimates the measured surface velocity of 0.5-0.75 m/s.

Higher differences between the computed and measured velocity profile can exist when the numerical model computes a velocity profile with a logarithmic shape and a profile with an other shape is measured during the field data. For these moments it is more difficult to conclude something about the difference between the numerical model and the field data.

The almost constant velocity profile measured at location Scaldis at HW-4h and HW-3h (figures 275 and 278) and the logarithmic profile computed by the numerical model makes that the numerical model overestimates the surface velocity of 0.3 m/s with 0.05 m/s and underestimates the bottom velocity with 0.05-0.1 m/s. For location Veremans, rather high bottom velocities of 0.5m/s are measured at the beginning of the slack high water period (HW, figure 286). The surface velocity at this moment is +/- 0.15 m/s lower than the bottom velocity. The numerical model computes a logarithmic shape of the velocity profile. Consequently rather high differences of 0.25 m/s exist between the measured surface velocities (0.25 m/s) and the velocity in the upper layer of the numerical model.

During the period from HW+4h until HW+6 differences in measured and computed velocity profile are noticed for location Kaloo, due to the above-mentioned effect that together with the current direction from a bottom current parallel to the MEC and a surface current parallel to the NSS at HW+4h, changing into a bottom current parallel to the NSS and a surface current parallel to the MEC at HW+5h and HW+6h, a changing surface and bottom velocity exists.. At HW+4h (figure 294) the measured velocity profile shows higher velocities at the bottom then at the surface. The numerical model although computes a logarithmic profile, resulting in a rather good modelled bottom velocity and an overestimation of the surface velocity with 0.1-0.15 m/s. At HW+5h (figure 297) the situation changes into a sort of step profile with higher surface velocities and lower bottom velocities. This makes that also for this period the bottom velocity is rather good modelled but that the computed surface velocity lies 0.1-0.15m/s lower than the measured velocity.

Other differences between measured and computed velocity profile are found during the slack low and high water period. At the end of the ebb tidal period (at HW+6h), the velocity profile for location Kaloo (figure 299) as output of the numerical model shows an almost constant velocity in the bottom layers and constant higher surface velocities (as was already mentioned above). The numerical model computes +/- 0.15 m/s higher velocities then the field data (of 0.10-0.25 m/s at the bottom and 0.25-0.35m/s at the bottom). At HW-5h the almost logarithmic shape of the velocity profile computed with the numerical model for the locations Kaloo, and Veremans corresponds relatively good with the shape measured during the field campaign (figures 270-271). The computed and measured velocity profiles almost fall together. Because the turning of the current is appearing faster in nature then in the numerical model, the numerical model computes at HW-4h (figure 273-274) surface currents, which differ 45° from the bottom currents. Consequently also 0.25 m/s lower surface velocities are measured.

Towards slack high water (HW) the velocity profile measured at location Kaloo (figure 285) shows almost constant lower values at the bottom and constant higher values at the surface. Due to the fact that the moment slack high water on June 3rd 2003 does not entirely correspond with the moment of slack low water in the numerical model, this jump in the velocity profile is noticed at moments later on in the velocity profiles computed with the numerical model (figure 288).

Because of the low water depths in the MNF at HW+6h and HW-5h, for location Scaldis only one or two measuring points over the vertical are present, which makes it difficult to compare the shape of the measured and computed velocity profile. Although it can be

stated that the numerical model computes 0.1-0.15 m/s higher velocities for this location (figures 272 and 300). With relation to the measurements this is almost the double of the field data.

Changing the numbers of layers in the 3D-model from 5 into 10, results especially for the velocity profile measured at the 3 locations during the slack low water period into a better prediction of the shape of the velocity profile. A computation with 10 layers in the vertical provides during this period a more fluently curved velocity profile. During the whole tidal cycle the velocity profile computed with the 10-layer model shows velocities in the bottom layer which are better modelled then with 5 layers.

9.8 Influence of grid refinement in M- and N-direction

9.8.1 General

To study the influence of grid refinement, the area around the plate of Walsoorden is refined 3 times in both the M- and N-direction. Due to the increase of the number of grid cells and the smaller timestep needed for the computation, the computational time will increase a lot. Therefore, the technique of domain decomposition is used. sing this technique, the original grid is divided into 3 subgrids (indicated in figure 301): a first grid from the downstream boundary until Ossenisse called subdomain 1, a second grid from Ossenisse until Zandvliet and Berendrecht called subdomain 2 and the last grid from Zandvliet and Berendrecht until the downstream boundary of the original grid. After the definition of the grids only subdomain 2 containing the area around the plate of Walsoorden, is refined 3 times in M- and N-direction. The resulting grid size in M- and N-direction is visualised in figure 302.

As a first indication of the effect of grid refinement on the current velocity and direction and water level, a 2D run with the refined grid is carried out. Due to the higher resolution of refined grid, it was needed to decrease the horizontal eddy viscosity to 1 m²/s and the horizontal eddy diffusivity to 5 m²/s. In order to fulfil the Courant-criterium it was needed to lower the time step of 0.250 minutes into 0.10 minutes or 6 seconds.

To study the influence of grid refinement, the output of the run with the refined grid is compared with the output of a 2D-computation without refinement with a horizontal eddy viscosity of 1m²/s and a time step of 0.250 minutes (figure 303 to 315). For this comparison the area around the tip of the plate of Walsoorden is divided into 2 minor areas. The first one consists out of the area of the Minor Northern Flood channel (MNF), the Northern Sand Spit (NSS) and a part of the Main Flood Channel (MFC). The second one consists out of the area of the Minor Southern Flood Channel (MSF), the Southern Sand Spit (SSS), and a part of the Main Ebb Channel (MEC).

For each area and for each hour of the tidal cycle a figure comparing the current velocity or water level computed with the numerical model without any refinement with the model with grid refinement in M- and N-direction. The plot above in each figure displays a contour plot of the velocity or the water level computed with the numerical model without refinement, the lower plot displays the contour plot for the output of the numerical model with the grid refined in both the M- and N-direction.

9.8.2 Analysis

Figure 303 to 315 compare for the area around the NSS and SSS the current velocity computed with the numerical model without refinement with the velocity computed with the model refined into both the M- and N-direction. Out of these figures follows the general conclusion that due to the grid refinement locally small differences in velocity exist between the original model and the refined model.

Comparing the velocity computed at HW-4h (figure 303) with the original and the refined model makes clear that the NSS, which is falling dry at this moment , is better represented when using the refined grid instead of the grid without refinement. Also a part of the WSB that falls dry at this moment is better modelled. Comparing the velocity computed with the original and the refined model learns that in the MFC, for the area where the MNF enters into the MFC, 0.1 m/s higher velocities are computed when using the refined grid. Remarkable is the little increase of the velocity in the thalweg of the MEC (figure 304) at the same moment.

During the maximum flood period (at HW-1h), the refined model computes a slightly higher velocity of 0.1m/s in the MNF and at the tip of the WSB (figure 305). Due to the better representation of the bathymetry, the area of the WSB that falls dry at this moment is better modelled when using the refined grid. Concerning the area around the SSS (figure 306), approximately 0.1-0.15 m/s higher velocities are measured above the SSS, especially for the area where the SSS reaches the WSB. The area in the MEC with velocities between 1.35 m/s and 1.50 m/s extends further into the downstream direction whit the usage of the refined grid.

Refining the grid 3 times in both the M- and N-direction provides at HW+3h slightly lower velocities in the area of the MEC near the boundary of the SSS and the MEC (figure 308). The area with velocities higher then 1.2 m/s extends further downstream when using the grid without any refinement. The appearance of lower velocities computed with the refined grid is also found in the area of the MFC near the NSS (figure 307). In the middle of the MFC 0.1 m/s lower velocities are computed with grid refinement.

During the slack low water period (at HW+6h), the grid refinement in both directions makes that up to 0.1 m/s lower velocities are computed in the MEC (figure 310), slightly higher velocities in the area where the flow through the MSF passes the SSS before entering the MEC. For the area around the NSS (figure 309), the major consequence of grid refinement is that the area of the NSS falling dry at slack low water is better represented. Not that many differences in velocity are noticed between the plot with the output of the refined and the output of the mode, which was not refined.

Concerning the influence of grid refinement on the water level, figure 311 to 315 show differences of a few centimetres between the water level computed with the refined grid and the water level computed with the original grid. During the ebb tidal period, up to 4 cm lower water levels are computed with the refined grid at HW+3h (figure 312 and 313) around the tip of the WSB. Where a water level of 2.96 m was computed around the tip of the WSB with the original grid, a water level of 2.92 m is computed with the refined grid. The area in the MEC where a water level of 3.0 m. is computed with the original grid does

not extend that much into the downstream direction, when the water level is computed with the refined grid. During the first flood period (at HW-4h, figure 311) a higher difference in water level between the output of the refined and the original grid is computed for the area around the NSS. Figure 314 and 315 show that also during the slack low water period up to 2 cm lower water levels are computed around the Walsoorden sandbar with grid refinement.

9.9 Conclusions

The flow patterns around the sand bar of Walsoorden are highly complex because of the secondary currents around the bifurcation of the main ebb and flood channel and because of the saline intrusion in the Scheldt. For this reason a 3D hydrodynamical model is necessary to analyse the flow fields in the research area.

With the constant eddy viscosity concept for exchange of horizontal turbulence, no distinction can be made between the effects of a low or a high value (within realistic margins of 1 to 10 m^2/s) for the eddy viscosity on the flow patterns around the research area. Especially during the periods with lower water depths (the period around slack low water and the first flood phase) small changes in the flow pattern can be noticed just on the tip of the Walsoorden sand bar. These changes however do not diminish significantly the differences between the flow pathways found in nature and modelled.

Changing the numbers of layers in the vertical of the 3D-model does not significantly change the length or direction of the flow pathways, but influences the vertical velocity and salinity profiles. Increasing the numbers of layers better predicts the velocity profile near the bottom.

The comparison of vertical velocity and salinity profiles shows that the numerical model results predict well the field data during the period from maximum flood to high water. During the other phases of the tide important deviations occur with overestimations or underestimation of the velocity magnitude with a factor of even 2. However these deviations are not straightforward in one same direction, which makes it difficult to define a cause for these deviations.

Increasing the resolution of the numerical grid shows non neglectable changes in the flow pattern on certain locations of the research area, especially near the sand spits and the minor flood channels. These changes are on both velocity magnitude and flow direction. Unfortunately there are not enough measurements available to decide if the higher resolution produces better results.

10 APPENDIX C

10.1 Use of artificial sediments in the physical model

To study the behaviour of the sediments that occur in the area of the sand bar of Walsoorden, the main characteristics of these sediments have to be scaled in a such a way that the sediment dynamics in the scale model is similar to the sediment dynamics in reality (or prototype)

The main characteristics of non-cohesive sediments like sand are represented by their grain size distribution (average grain size diameter d_{50} and other grain size diameters like d_{90}), the absolute density of the sediments ρ_s and the porosity percentage p of the air volume in the sediment .

In Rijkswaterstaat-DZL 2002 it can be found that in the vicinity of the sandbar of Walsoorden d_{50} has an average value of 134 µm but with a standard deviation of 40 µm. This means that d_{50} varies approximately between 95 µm and 170 µm. During the field campaign of June 3th 2003 (PAET, 2003c) the sediment samples taken in the three locations shown in figure 47 all had more or less a d_{50} of 190 µm. It is chosen to restrain the value measured during this last field campaign to characterise the sediment.

The absolute density ρ_s of sand is assumed to be always 2650 kg/m³.

The sediment dynamics of the prototype material has to be simulated by the following available artificial sediments at Flanders Hydraulics Research:

Artificial sediment	**ρ_s (kg/dm³)**	**d_{50} mm**	**P %**
Bakelite big	1.35	0.85	46
Bakelite fine	1.35	0.36	42
Fine sand	2.65	0.10	42
Nacre	1.22	0.42	36
Polystyrene big	1.05	2.45	41
Polystyrene fine	1.06	0.45	42

Characteristics available artificial sediments at Flanders Hydraulics Research

To simulate the sediment dynamics of the prototype with this artificial material in the scale model, an approach is followed as explained below.

10.2 Physical model laws

10.2.1 Scaling laws for water motion

In the scale tidal model of the Scheldt in use at Flanders Hydraulics Research, the water movement is scaled according to the *roughness condition* and within the assumption that *Froude similarity* exists.

If the scale of a physical quantity X in a scale model is defined as:

$$\boxed{N_X = \frac{I_p}{I_m}}$$

with I_p value of quantity X in prototype

I_X value of quantity X in scale model

we get the next scaling laws for the water motion (fully developed turbulent flow):

Froude condition $$N_U = N_v^{1/2} \quad (1)$$

Roughness condition $$N_C = \frac{N_h^{1/2}}{N_v^{1/2}} \quad (2)$$

In which represent : U: velocity magnitude

v: vertical dimension

h: horizontal dimension

C: roughness according to the Chezy formula

During the construction of the tidal scale model in 1991 it was chosen to take the next scaling values for the vertical and horizontal dimensions, in order to meet the requirements of the available pump capacity, space facility in Flanders Hydraulics Research and accuracy for measuring water levels and flow velocities in the scale model itself:

$$N_v = 100$$

$$N_h = 400$$

This leads to the next scale values:

$$N_U = 10$$

$$N_C = 2$$

In order to reproduce the flow velocities in a scale model according to the Froude similarity, it is not always necessary tot fulfill the roughness condition. This condition is needed when a large part of the prototype is scaled for which the differences in water level at the same moment from one side of the prototype to the other side are significant,. For the tidal

model of the Scheldt the roughness condition has been fulfilled because 120 km of the river has been modelled. However, if we just look at the location of Walsoorden at one specific moment of the tide, the roughness condition does not necessarily have to be fulfilled because the water level differences over just the Walsoorden area at one moment are very small and the flow pattern at that moment is not influenced significantly by the roughness of that area, but primarely by the geometry of channels and flats in the scale model.

10.2.2 Scaling laws for sediment motion

The motion of sediments in a river bed depends entirely on the mechanical character of the flow which generates it. On the other hand, motion of sediments is accompanied by features of its own (such as diffusion of particles in liquid fluid, sand waves, etc.) that affect the motion of fluid to a considerable extent. This means that transport of sediment and the transporting fluid are interdependent.

In this context there is no reason to assume that scale values for the grain size of the sediment will yield the same values for the scale laws for sediment transport as for the scale laws for sand wave length, sand wave height etc.

Therefore, when dealing with motion of sediment, the safest approach for modelling with artificial sediments is to use in the scale model granular material that is geometrically similar to that of the prototype. Most commonly, the quantity d_{50} is used to describe the geometry of the sediments. Furthermore, the motion of sediments is also determined by the specific weight ρ_s of the material in relation to the specific weight of the fluid ρ and by the fall velocity w.

As a result we can define the scale values for the sediment characteristics as follows:

$$\boxed{N_d = \frac{d_{50,p}}{d_{50,m}}}$$

$$\boxed{N_{\Delta\rho} = N_{\rho_s - \rho} = \frac{\rho_{s,p} - \rho_p}{\rho_{s,m} - \rho_m}}$$

$$\boxed{N_w = \frac{w_p}{w_m}}$$

With the values for the characteristics of the available artificial sediments, we can transform the table above into a table with scale values that are applicable for the scale model. For the prototype values a d_{50} of 170 µm has been chosen.

Artificial sediment	$\mathbf{N_d}$(d_{50} = 190 µm)	$\mathbf{N_{\Delta\rho}}$
Bakelite big	0.223	4.714
Bakelite fine	0.528	4.714
Fine sand	1.900	1.000
Nacre	0.452	7.500
Polystyrene big	0.078	33.000
Polystyrene fine	0.422	27.500

Scaling values of the characteristic sediment parameters for the available artificial sediments

To conclude: in a scale model in which sediment transport and fluid motion are modelled at the same time, for a given set of scales for the horizontal and vertical dimensions five other scales have to be applied, being N_U, N_C, N_d, N_w and $N_{\Delta\rho}$.

As mentioned before motion of fluid can be scaled if the Froude and Roughness condition are respected. If this is the case N_U and N_C can be written as a function of N_v and N_h only.

To reproduce sediment transport similarity in the scale model correctly, other conditions will have to be respected in order to find N_d, N_W and $N_{\Delta\rho}$ as a function of N_v and N_h only. In literature several methods can be found that define these conditions.

<u>Remark</u>: In the paragraphs below the conditions to fulfill for sediment transport similarity are focused on bedload transport only. This means that the fall velocity of the sediment doesn't need to be scaled correctly as it has no influence on the amount of sediment transport. The search for conditions that can define N_w as a function of N_v and N_h only, is therefore not treated anymore below.

SEDIMENT TRANSPORT MODELLING ACCORDING TO THE SHIELDS DIAGRAM

In order to reproduce sediment bedload transport similarity it is only needed to have similarity in the parameters that influence the incipient motion of sediment particles. According to the well-known Shields diagram, these parameters are defined as the grain size Reynolds number $R_*$and the densimetric Froude F_* number as seen in the figure below.

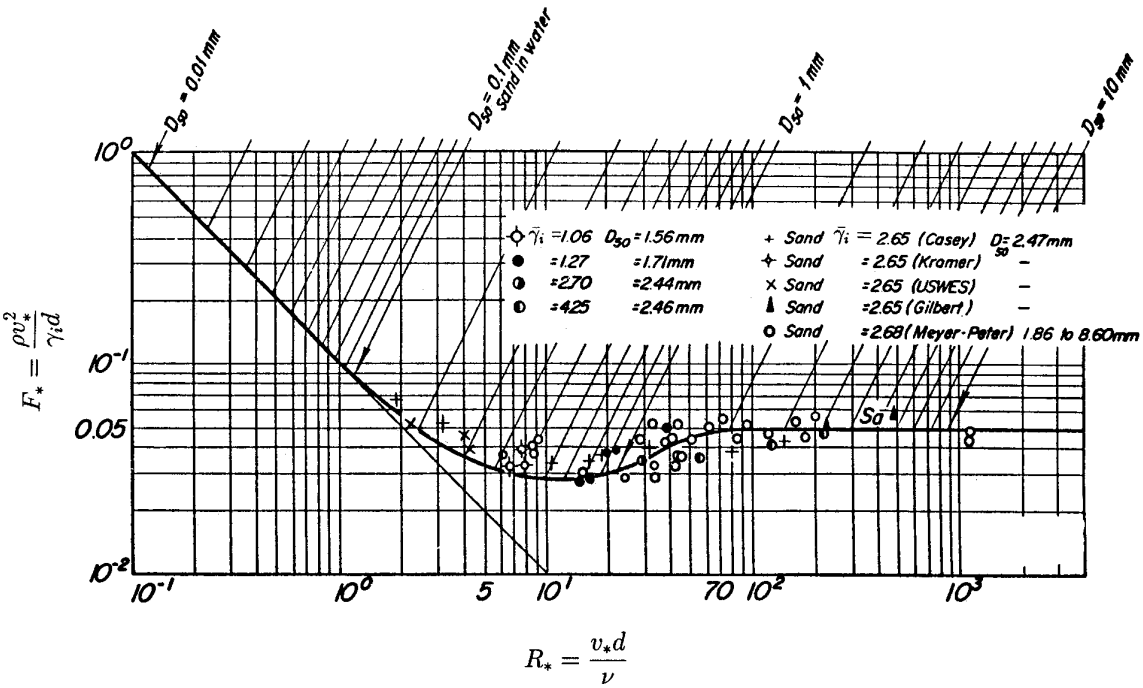

Shields diagram for incipiënt motion of sediments in uniform flow

In the Shields diagram each axis represents a dimensionless number in which the used physical quantities have the following meaning:

$v_* = \sqrt{\frac{\tau_b}{\rho}}$ is the shear velocity

τ_b is the shear stress on the bottom of the river- or seabed

$\gamma_i = (\rho_s - \rho)g$ is the submerged sediment specific weight

The Shields-diagram has to be interpreted in such a way that if the acting value for the shear stress leads to combinations for R_* and F_* which are lying above the critical combinations as shown in the diagram, than sediment transport will occur.

Similarity of incipient motion means that these dimensionless numbers have the same values both in prototype as in the scale model which leads to the following conditions for the sediment transport scale values:

Grain size Reynolds condition: $N_v N_d N_h^{-1/2} = 1$ (3)

Densimetric Froude condition: $N_v^2 N_h^{-1} N_{\Delta\rho}^{-1} N_d^{-1} = 1$ (4)

For the design of a scale model in which fluid motion and bedload transport are modelled at the same time, the equations (1) to (4) have to be used to make a practical choice for the scale values of the five scale quantities. This means that in theory any scale value is possible.

However during the design of the tidal scale model in1991, only the motion of free surface water flow was taken into account. The whole electro-mechanical steering of the scale

model is therefore exclusively based on the Froude condition. This results in scale values that cannot be changed for the following scale quantities:

Scale value for vertical dimension: $N_v = 100$

Scale value for horizontal dimension: $N_h = 400$

Scale value for flow velocity magnitude: $N_U = 10$

Scale value for the time of hydraulic processes: $N_t = 40$

With the scale values above the equations (1) and (2) are fulfilled. But this is not the case for the equations (3) and (4). These equations result in the following scale values for the characteristics for the artificial sediment:

$$N_d = 0.2$$

$$N_{\Delta\rho} = 125$$

When we compare this with the values in the table above, then it is clear that none of the available artificial sediments would be capable of reproducing complete sediment transport similarity. Polystyrene is the material that would come the closest to the desired scaling law values.

SEDIMENT TRANSPORT MODELLING ACCORDING TO THE IDEAL VELOCITY SCALE

Instead of looking directly at the Shields-diagram to derive scaling laws for sediment transport, it is also possible to look at formulae in which the sediment transport rate as function of certain parameters is described. This leads to a scaling law for the flow velocity that does not necessarily generate the same scale values for the flow velocity when following Froude's law. This also effects the hydraulic time scale values. If the velocity scale value has the same value as when using Froude's law, it is said that the 'ideal velocity' scale is reached. If this is the case, then this approach is identical to the first approach.

Normally the physical model is capable in using other velocity scale values to reproduce the tides and the flow in the scale model. However the calibration of the tides and flows in the scale model has never been carried out for such scale values and also the electromechanical steering of the physical model has not been designed for it. It is therefore wise to look for artificial material that allows to reach the 'ideal velocity' scale.

According to the way the roughness of the riverbed is related to a characteristic diameter of the sediment, many variations exist in scale law conditions that follow the transport formulae approach. The simplest of them is the following:

$$N_U = N_C \sqrt{N_{\Delta\rho} N_d} \qquad (5)$$

In this formulae N_C represents the total resistance coëfficiënt according to the Chezy formulation. As the average Chezy coëfficiënt for the Walsoorden area is considered to have a value of 90, then in combination with the experimental values found for this coëfficiënt the scale values for the Chezy coëfficiënt for each of the available artificial sediments can be found.

As the polystyrene fine material was especially bought for this research, no experimental values of the characteristic Chezy coëfficiënt of this material were known. For this new experiments in a special flume should have been carried out, but unfortunately the available flume at Flanders Hydraulics Research was occupied during the whole research period. However from detailed analysing the behaviour of the fine polystyrene in the physical model it could be seen that this new material creates dunes with a large wave length and a higher height from crest to through than compared with the big polystyrene or the big bakelite. Therefore a Chezy value of 30 seems to be a realistic value

Artificial sediment	**Chezy value ($m^{1/2}/s$)**	**N_C**	**N_U** (d_{50} = 190 µm)
Bakelite big	27	3.333	3.421
Bakelite fine	29	3.103	4.894
Fine sand	35	2.571	3.544
Nacre	28	3.214	5.920
Polystyrene big	31	2.903	4.644
Polystyrene fine	30	3.000	10.222

Chezy coëfficiënt for the artificial sediments for Froude numbers of 0.15 à 0.25

From the table above it can be seen that the velocity scale value N_U deviates from the value that would result out of Froude's law (equation (1)). According to Froude's law N_U should have a value of 10 when N_V is 100. If polystyrene fine with a d_{50} of 450 µm would be used, then N_U would result in a value of approximately 10, meaning that the 'ideal velocity scale' in that particular case is reached.

10.2.3 Relaxation of the scaling law conditions

From the paragraph above it can be concluded that out of six available artificial sediments only polystyrene comes the closest to the desired scaling law values for the purpose of simulating the sediment transport processes for bedload.

As polystyrene is a very lightweight material which could give difficulties for practical use, it is worthwhile to look if the other artificial sediments could be used if some of the scaling law conditions are relaxated. This means that these conditions do not need to be fulfilled if the aspects for which they should be applied can be more or less neglected in the whole of the sediment transport processes in prototype. Froude's law will always be applied otherwise the hydraulic steering of the physical model should be modified.

<u>Relaxation of the roughness condition</u>

When we look at the area of interest, then as mentioned before, it is clear that during a short time interval of the tide, the water level changes are very small compared to the water depths in the area. This means that the roughness of the river bed has no significant

influence on these water levels for which in return it is not needed to fulfill the roughness equation expressed trough equation (2). Relaxation of the roughness condition brings however no solution. The five scale values are now combined by only three equations and as two of the scale values are prescribed, the equations (3) and (4).will still have one unique solution for the scale values N_d and $N_{\Delta\rho}$, and these values are the ones mentioned above.

Relaxation of the grain size Reynolds condition and the roughness condition

To get more flexibility in choosing the scale values, it is also possible to relaxate the grain size Reynolds condition R_*. In the Shields-diagram it is seen that, for values of R_* bigger than 70 to 100, the densimetric Froude number F_* becomes independent of the grain size Reynolds number R_*. This means that if the scale values for F_* and R_* are still in that region of the Shields-diagram, then the Grain size Reynolds condition has not to be taken into account.

When both roughness condition and grain size Reynolds condition are relaxated, then only equation (1) and (4) have to be applied. Equation (4) can be rewritten as follows:

$$N_{\Delta\rho}N_d = N_v^2 N_h^{-1} = 25$$

Calculating $N_{\Delta\rho}N_d$ for the remaining five artificial sediments results in the following table.

Artificial sediment	$\mathbf{N_{\Delta\rho}N_d}$($d_{50}$ = 190 µm)
Bakelite big	1.053
Bakelite fine	2.488
Fine sand	1.900
Nacre	3.392
Polystyrene big	2.559
Polystyrene fine	11.611

Transformed scaling values when relaxating roughness condition and Grain size Reynolds condition

From the table above it can be seen that for none of the available artificial sediments the applicable scale values allow to meet the densimetric Froude condition. Furthermore it is also clear that the sediment transport processes both in prototype and definitely in the physical model are not lying in the appropriate zone of the Shields diagram.

CONCLUSION

Designing the tidal Western Scheldt scalemodel into a physical model in which hydraulic processes and sediment bedload transport processes are modelled according to respectively Froude's law, the roughness condition and the Shields diagram could be best carried out with the use of **fine polystyrene**.

Only then the ideal velocity scale is reached which allows to keep the hydraulic steering of the physical model which is designed according to Froude's Law during the experiments with artificial sediment.

In principal experiments should be carried out to define more precisely the Chezy coëfficiënt of the artificial sediments. As already mentioned this was not possible during this research because of the unavailability of experimental flumes. However, the tests carried out in the physical model with polystyrene suggest that the big polystyrene grains have a too high level of incipient motion when using a velocity scale of 10, while the fine polystyrene grains seem to have a too low level of incipient motion when using a velocity scale of 10.

For this reason it is better to use the fine polystyrene as a material that can give qualitative insight in the sediment dynamics around the sand bar of Walsoorden. Due to the apparently too low level of inicpiënt motion, the experiments will lead to a conservative approach of the dumping strategy because the amounts of sediment settling and remaining on the tip of the sandbar will be underestimated.

Remark:

The use of fine polystyrene during the experiments has shown a certain scale effect caused by the hydrofobic behaviour of the polystyrene. During each tidal cycle in the physical model an amount of polystyrene is thrown on the intertidal area. The material in these area's always became a little dry which led to the fact that during the next tidal cycle when this material became wet again, flocs of the artificial sediment started to float. This means that each tidal cycle a small amount of material was lost and was always driven upstream in the physical model. The more tidal cycles were run in the physical model, the bigger the scale effect because the resulting amount of lost floating material became higher and higher.

10.3 Additional scaling laws

The scale law for sediment transport rate (m³/s) is expressed as follows:

$$N_{Q_s} = N_d^{3/2} N_{\Delta\rho}^{1/2} N_h$$

This formula results in the following scale value for the sediment transport rate when using fine polystyrene:

$$N_{Q_s} = N_d^{3/2} N_{\Delta\rho}^{1/2} N_h = 576$$

The time scale for sediment transport processes is not the same as for hydraulic processes as can be seen in the formula below:

$$N_{t,mor} = \frac{N_h^{3/2}}{N_d}$$

This results in scale value of

$$N_{t,mor} = \frac{N_h^{3/2}}{N_d} = 18947$$

This means that sediment transport processes in the physical model happen almost 475 times faster than the hydraulic processes. Or expressed otherwise: the effect of one tidal cycle in the physical model generates transport processes on the artificial sediment with which corresponds the morphological effect in reality of 475 tides .

11 LITERATURE

[1]. FLANDERS HYDRAULICS RESEARCH (FHR), 1994. “Model 500.2-Overzichtsmodel Westerchelde-Bouw en ijking van het model”, December 1994.

[2]. FHR, 1990. “Vergelijkende studie beweegbare materialen”, February 1990

[3]. FHR, 2002a. “Onderzoeksplan Model 678 – LTV Schelde estuarium – Alternatieve stortstrategie voor de platen van Walsoorden – eerste stand van zaken”; May 2002.

[4]. FHR, 2002b. “Onderzoeksplan Model 678 – LTV Schelde estuarium – Alternatieve stortstrategie voor de platen van Walsoorden – definitieve versie voor Pro-Ses”; August 2002.

[5]. FHR, 2003. “ALTERNATIVE DUMPING STRATEGY WALSOORDEN: Physical and numerical modelling of tidal currents around the Plate of Walsoorden – Draft Report to PROSES”; June 2003.

[6]. GERMAN ASSOCIATION FOR WATER RESOURCES AND LAND IMPROVEMENT, 1980. “Hydraulic Modelling”, September 1980.

[7]. MM, 2002a. Minutes of the meeting of July 4th 2002.

[8]. MM, 2002b. Minutes of the meeting of December 13th 2002.

[9]. MM, 2003a. Minutes of the meeting with MID Zeeland of January 16th 2003.

[10]. MM, 2003b. Minutes of the meeting with environmental organisations of January 17th 2003.

[11]. MM, 2003c. Minutes of the meeting with the dredging companies of March 11th 2003.

[12]. MM, 2003d. Minutes of the meeting with Dr. P. Meire of March 11th 2003.

[13]. INSTITUT FÜR WASSERBAU – BREMEN (IWA), 2003. “Current measurements in the Westerschelde – September and October 2002”, January 2003.

[14]. PAET, 2001a. “Improving navigation conditions in the Westerschelde and managing its estuarine environment – How to harmonise accessibility, safetyness and naturalness?”; January 2001.

[15]. PAET, 2001b. “Management strategy for the Westerschelde and for its estuarine environment – An addendum to the Final Report with a proposal for an alternative dredging strategy”; May 2001.

[16]. PAET, 2002a. “Proposal for experiments on the Westerschelde scale model”; July 2002.

[17]. PAET, 2002b. “Note on field experiments and modelling to assess alternative strategies for the disposal of dredging materials in the Westerschelde”; September 2002.

[18]. PAET, 2003a. “Field surveys for morphological studies in Walsoorden – Short note on sediment measurements”; January 2003.

[19]. PAET, 2003b. “Note on numerical simulation problems: mathematics, numerics, Delft3D software, Walsoorden application”; June 2003.

[20]. PAET, 2003c. “Observations of Sediment Transport on the Plaat van Walsoorden”; in Preparation.

[21]. PAET, 2003d. “The Feasibility of Morphological Dredging as a Tool for Managing the Westerschelde”; September 2003.

[22]. Rijkswaterstaat-RIKZ, 2001. “Morfologische ontwikkeling Westerschelde 1931 – 2000”, November 2001.

[23]. Rijkswaterstaat-DZL, 2002. “MOVE - De toestand van de bodem van de Westerschelde aan het begin van de verruiming 48’/43’ – Herziene T0 voor de bodem van de Westerschelde”, June 2002.

[24]. Rijkswaterstaat-RIKZ, 2002. “Verbeteren SCALWEST model. Bouw SCALWEST2000 model – Eindrapport deel I en II”, September 2002.

[25]. Rijkswaterstaat-RIKZ, 2001. “Operationalisering RANNDELTA III model – Bouw en afregeling”, October 2001.

[26]. IMDC, 2002. “Studie densiteitsstromingen in het kader van LTV – Stroom- en saliniteitsmeting te Waarde uitgevoerd op 12/06/2002”, December 2002.

FIGURES

Figure 001 Overview of the Westerschelde

Figure 002 Nomenclatura for the different regions in the research area.

Figure 003 Overview of the construction of the physical model.

Figure 004 Comparison bathymetry of physical model (1989-1990) with bathymetry as measured in 2000-2001

Figure 005 Isovel lines for velocity measured in the scale model at HW-5h and HW-4h

Figure 006 Isovel lines for velocity measured in the scale model at HW-3h and HW-2h

Figure 007 Isovel lines for velocity measured in the scale model at HW-1h and HW

Figure 008 Isovel lines for velocity measured in the scale model at HW+1h and HW+2h

Figure 009 Isovel lines for velocity measured in the scale model at HW+3h and HW+4h

Figure 010 Isovel lines for velocity measured in the scale model at HW+5h and HW+6h

Figure 011 Numerical model train used by Rijkswaterstaat to simulate tidal propagation from the North Sea into the inland estuaries, rivers and waterways

Figure 012 Numerical grid of the Rijkswaterstaat SCALWEST 2000 model

Figure 013 Modified SCALWEST numerical grid

Figure 014 Validation results of the modified SCALWEST model (June 1st – June 13th 2002 boundary conditions) Locations Vlissingen and Walsoorden

Figure 015 Validation results of the modified SCALWEST model (June 1st – June 13th 2002 boundary conditions) Locations Antwerpen and Hemiksem

Figure 016 Validation results of the modified SCALWEST model (June 1st – June 13th 2002 boundary conditions) Locations Walem and Melle

Figure 017 Validation results of the modified SCALWEST model. Calculated depth averaged salinity compared with measured point salinity (15 % – 25 % below the water surface)

Figure 018 Nesting of the detailed Walsoorden numerical grid into the modified numerical grid of the SCALWEST model (for 2D and 3D modelling)

Figure 019 Bathymetry of the SCALWEST model and basic 3D model (based on surveys of 2000-2001).

Figure 020 Isovel lines for surface and bottom velocity at HW-5h. Numerical model: 3D model, no refinement, 10 layers

Figure 021 Current pattern computed with the numerical model at HW-5h. Numerical model: 3D model, no refinement, 10 layers, horizontal eddy viscosity 10m²/s

Figure 022 Isovel lines for surface and bottom velocity at HW-4h. Numerical model: 3D model, no refinement, 10 layers

Figure 023 Current pattern computed with the numerical model at HW-4h. Numerical model: 3D model, no refinement, 10 layers, horizontal eddy viscosity 10m²/s

Figure 024 Isovel lines for surface and bottom velocity for HW-3h. Numerical model: 3D model, no refinement, 10 layers

Figure 025 Current pattern computed with the numerical model at HW-3h. Numerical model: 3D model, no refinement, 10 layers, horizontal eddy viscosity 10m²/s

Figure 026 Isovel lines for surface and bottom velocity for HW-2h. Numerical model: 3D model, no refinement, 10 layers

Figure 027 Current pattern computed with the numerical model at HW-2h. Numerical model: 3D model, no refinement, 10 layers, horizontal eddy viscosity 10m²/s

Figure 028 Isovel lines for surface and bottom velocity for HW-1h. Numerical model: 3D model, no refinement, 10 layers

Figure 029 Current pattern computed with the numerical model at HW-1h. Numerical model: 3D model, no refinement, 10 layers, horizontal eddy viscosity 10m²/s

Figure 030 Isovel lines for surface and bottom velocity for HW. Numerical model: 3D model, no refinement, 10 layers

Figure 031 Current pattern computed with the numerical model at HW. Numerical model: 3D model, no refinement, 10 layers, horizontal eddy viscosity 10m²/s

Figure 032 Isovel lines for surface and bottom velocity for HW+1h. Numerical model: 3D model no refinement, 10 layers

Figure 033 Current pattern computed with the numerical model at HW+1h. Numerical model: 3D model, no refinement, 10 layers, horizontal eddy viscosity 10m²/s

Figure 034 Isovel lines for surface and bottom velocity for HW+2h. Numerical model: 3D model, no refinement, 10 layers

Figure 036 Isovel lines for surface and bottom velocity for HW+3h. Numerical model: 3D model, no refinement, 10 layers

Figure 037 Current pattern computed with the numerical model at HW+3h. Numerical model: 3D model, no refinement, 10 layers, horizontal eddy viscosity 10m²/s

Figure 038 Isovel lines for surface and bottom velocity at HW+4h. Numerical model: 3D model, no refinement, 10 layers

Figure 039 Current pattern computed with the numerical model at HW+4h. Numerical model: 3D model, no refinement, 10 layers, horizontal eddy viscosity 10m²/s

Figure 040 Isovel lines for surface and bottom velocity at HW+5h. Numerical model: 3D model, no refinement, 10 layers

Figure 041 Current pattern computed with the numerical model at HW+5h. Numerical model: 3D model, no refinement, 10 layers, horizontal eddy viscosity 10m²/s

Figure 042 Isovel lines for surface and bottom velocity at HW+6h. Numerical model: 3D model, no refinement, 10 layers

Figure 043 Current pattern computed with the numerical model at HW+6h. Numerical model: 3D model, no refinement, 10 layers, horizontal eddy viscosity 10m²/s

Figure 044 Image of the GPS drifters used during the field campaign from 23th September to 10th October 2002.

Figure 045 General overview of the measurements with GPS drifters carried out from 23th September to 10th October 2002. Above: flood; Below: ebb

Figure 046 Overview of transect and CTD-measuring points during the field campaign of 12/06/2002.

Figure 047 Overview of measuring points during the field campaign of 03/06/2003

Figure 048 Dumping location P1 (experiment 301). Tides 4 and 7

Figure 049 Dumping location P1 (experiment 301). Tides 10 and 13.

Figure 050 Dumping location P1 (experiment 301). Tide 16

Figure 051 Dumping location M2 (experiment 302). Tides 4 and 7

Figure 052 Dumping location M2 (experiment 302). Tides 10 and 13

Figure 053 Dumping location M2 (experiment 302). Tides 16 and 23

Figure 054 Dumping location M3 (experiment 303). Tides 4 and 7

Figure 055 Dumping location M3 (experiment 303). Tides 10 and 13

Figure 056 Dumping location M4 (experiment 304). Tides 4 and 7

Figure 057 Dumping location M4 (experiment 304). Tides 10 and 13

Figure 058 Dumping location M4 (experiment 304). Tide 16

Figure 059 Dumping location L2 (experiment 305). Tides 4 and 7

Figure 060 Dumping location L2 (experiment 305). Tides 10 and 13

Figure 061 Dumping location L2 (experiment 305). Tide 16

Figure 062 Dumping Location R2-R3 (experiment 307). Tides 4 and 7

Figure 063 Dumping location R2-R3 (experiment 307). Tides 10 and 13

Figure 064 Dumping location R2-R3 (experiment 307). Tides 16 and 73

Figure 065 Dumping location as used near the ‘Schaar van Waarde’ before 1995. Tides 4 and 7

Figure 066 Dumping location as used near the ‘Schaar van Waarde’ before 1995. Tides 10 and 13

Figure 067 Dumping location as used near the ‘Schaar van Waarde’ before 1995. Tides 16 and 73

Figure 068 Effect of alternative dumping strategy. Proposal for the shape of the plate of Walsoorden

Figure 069 Effect of alternative dumping strategy. Difference between expected and present bathymetry

Figure 070 Effect of alternative dumping strategy. Overview of transects and points used for the comparison.

Figure 071 Effects of alternative dumping strategy. Discharge through transect Schaar van Waarde (above). Difference in discharge between expected and present situation (below).

Figure 072 Effect of alternative dumping strategy. Discharge through transect Schaar van Waarde 2 (above). Difference in discharge between expected and present situation (below).

Figure 073 Effect of alternative dumping strategy. Discharge through transect Zuidergat (above). Difference in discharge between expected and present situation (below).

Figure 074 Effect of alternative dumping strategy. Discharge through transect Zuidergat 2 (above). Difference in discharge between expected and present situation (below).

Figure 075 Effect of alternative dumping strategy. Velocity at location Baalhoek (above). Difference in velocity between expected and present situation (below).

Figure 076 Effect of alternative dumping strategy. Velocity at location Valkenisse (above). Difference in velocity between expected and present situation (below).

Figure 077 Effect of alternative dumping strategy. Velocity at location Waarde (above). Difference in velocity between expected and present situation (below).

Figure 078 Effect of alternative dumping strategy. Velocity at location Walsoorden (above). Difference in velocity between expected and present situation (below).

Figure 079 Licensed dumping zone near the flood channel of Waarde, suited for in situ test of 500000 m³ sand.

Figure 080 Preferable location for dumping 500000m³ sand during the in-situ test and expected transport direction of the sediments.

Figure 081 Desired development of the Sandbar of Walsoorden

Figure 082 Tidal curves used in the physical model. Water levels at the downstream boundary. Blue (reality); Red (model)

Figure 083 Tidal curves used in the physical model. Water levels measured around the research area. Blue(reality); Red (model)

Figure 084 Effect of removing the roughness elements in the scale model. Water level measured at Hansweert and Waarde.

Figure 085 Effect of removing the roughness elements in the scale model. Water level measured at Schaar van de Noord and Bath.

Figure 086 Zones in the physical model in which instantaneous velocity vectors could be measured with the aid of the digital cameras.

Figure 087 Vectors computed out of the pictures with the digital cameras

Figure 088 Zones in the physical model in which flow pathways could be measured with the aid of the Hasselblad cameras

Figure 089 Image taken with Hasselblad camera.

Figure 090 Selected tidal curves for comparison of scale model tests with field data.

Figure 091 Comparison of instantaneous velocities at HW-5h. Scale model - Field data 24/09/02.

Figure 092 Comparison of instantaneous velocities at HW-5h. Scale model - Field data 04/10/02.

Figure 093 Comparison of instantaneous velocities at HW-5h. Scale model - Field data 07/10/02

Figure 094 Comparison of instantaneous velocities at HW-5h. Scale model - Field data 08/10/02

Figure 095 Comparison of instantaneous velocities at HW-4h. Scale model - Field data 24/09/02

Figure 096 Comparison of instantaneous velocities at HW-4h. Scale model - Field data 04/10/02

Figure 097 Comparison of instantaneous velocities at HW-4h. Scale model - Field data 07/10/02

Figure 098 Comparison of instantaneous velocities at HW-4h. Scale model - Field data 08/10/02

Figure 099 Comparison of instantaneous velocities at HW-3h. Scale model - Field data 24/09/02

Figure 100 Comparison of instantaneous velocities at HW-3h. Scale model - Field data 04/10/02

Figure 101 Comparison of instantaneous velocities at HW-3h. Scale model - Field data 07/10/02

Figure 102 Comparison of instantaneous velocities at HW-3h. Scale model - Field data 08/10/02

Figure 103 Comparison of instantaneous velocities at HW-2h. Scale model - Field data 24/09/02

Figure 104 Comparison of instantaneous velocities at HW-2h. Scale model - Field data 04/10/02

Figure 105 Comparison of instantaneous velocities at HW-2h. Scale model - Field data 07/10/02

Figure 106 Comparison of instantaneous velocities at HW-2h. Scale model - Field data 08/10/02

Figure 107 Comparison of instantaneous velocities at HW-1h. Scale model - Field data 24/09/02

Figure 108 Comparison of instantaneous velocities at HW-1h. Scale model - Field data 04/10/02

Figure 109 Comparison of instantaneous velocities at HW-1h. Scale model - Field data 07/10/02

Figure 110 Comparison of instantaneous velocities HW-1h. Scale model - Field data 08/10/02

Figure 111 Comparison of instantaneous velocities for HW. Scale model - Field data 24/09/02

Figure 112 Comparison of instantaneous velocities for HW. Scale model - Field data 04/10/02

Figure 113 Comparison of instantaneous velocities for HW+1h. Scale model - Field data 04/10/02

Figure 114 Comparison of instantaneous velocities at HW+2h. Scale model - Field data 27/09/02

Figure 115 Comparison of instantaneous velocities at HW+3h. Scale model - Field data 26/09/02

Figure 116 Comparison of instantaneous velocities at HW+3h. Scale model - Field data 27/09/02

Figure 117 Comparison of instantaneous velocities for HW+4h. Scale model - Field data 27/09/02

Figure 118 Comparison of instantaneous velocities at HW+5h. Scale model - Field data 24/09/02

Figure 119 Comparison of instantaneous velocities at HW+5h. Scale model - Field data 07/10/02

Figure 120 Comparison of instantaneous velocities at HW+6h. Scale model - Field data 04/10/02

Figure 121 Comparison of instantaneous velocities at HW+6h. Scale model - Field data 07/10/02

Figure 122 Comparison of instantaneous velocities at HW+6h. Scale model - Field data 08/10/02

Figure 123 Comparison of flow pathways at HW-5h. Scale model - method 2 - Field data 07/10/02

Figure 124 Comparison of flow pathways at HW-4h. Scale model - method 1 - Field data: 07/10/02, 08/10/02

Figure 125 Comparison of flow pathways at HW-4h. Scale model - method 1 - Field data: 04/10/02

Figure 126 Comparison of flow pathways at HW-4h. Scale model - method 2 - Field data: 04/10/02, 07/10/02

Figure 127 Comparison of flow pathways at HW-3h. Scale model - method 1 - Field data: 07/10/02, 08/10/02

Figure 128 Comparison of flow pathways at HW-3h. Scale model - method 1 - Field data: 24/09/02, 04/10/02

Figure 129 Comparison of flow pathways at HW-3h. Scale model - method 2 - Field data: 04/10/02, 07/10/02

Figure 130 Comparison of flow pathways at HW-2h. Scale model - method 1 - Field data: 07/10/02, 08/10/02

Figure 131 Comparison of flow pathways at HW-2h. Scale model - method 1 - Field data: 24/09/02, 04/10/02

Figure 132 Comparison of flow pathways at HW-2h. Scale model - method 2 - Field data: 04/10/02, 07/10/02

Figure 133 Comparison of flow pathways at HW-1h. Scale model - method 1 - Field data: 07/10/02, 08/10/02

Figure 134 Comparison of flow pathways at HW-1h. Scale model - method 1 - Field data: 04/10/02

Figure 135 Comparison of flow pathways at HW-1h. Scale model - method 2 - Field data: 04/10/02, 07/10/02

Figure 136 Comparison of flow pathways at HW. Scale model - method 1 (above) - method 2 (below) - Field data 04/10/02

Figure 137 Comparison of flow pathways at HW-4h and HW-3h. Scale model - Field data: overview

Figure 138 Comparison of flow pathways at HW-2h and HW-1h. Scale model - Field data: overview

Figure 139 Comparison of flow pathways at HW. Scale model - Field data: overview

Figure 140 Comparison of the numerical grid of the original SCALWEST model (black) with the modified SCALWEST model (red) upstream of Prosperpolder.

Figure 141 Detailed views of the Rijkswaterstaat SCALWEST 2000 numerical grid.

Figure 142 Details of the modified SCALWEST numerical grid.

Figure 143 Validation results of the original Scalwest model upstream of the Dutch-Belgian border.

Figure 144 Validation results of the modified Scalwest model after improving grid schematisation of the Belgian part of the Scheldt.

Figure 145 Details of the numerical grid of the SCALWEST model which is also the same grid for the basic 3D grid around the Walsoorden area.

Figure 146 Grid Size in M-direction of the SCALWEST model or basic 3D model

Figure 147 Grid Size in N-direction of the SCALWEST model or basic 3D model

Figure 148 Coëfficiënt of orthogonality of the curvilinear numerical grid of the SCALWEST model or basic 3D model

Figure 149 Smoothness in M-direction of the curvilinear numerical grid of the SCALWEST model or basic 3D model

Figure 150 Smoothness in N-direction of the curvilinear numerical grid of the SCALWEST model or basic 3D model.

Figure 151 Bottom Roughness coëfficiënt (according to Manning) of the SCALWEST model or basic 3D model

Figure 152 Courant number of the SCALWEST model and basic 3D model for a numerical time step of 0.25 minutes.

Figure 153 Courant number of the SCALWEST model and basic 3D model for a numerical time step of 0.125 minutes.

Figure 154 Current pattern at HW-5h for the area around NSS. 2D-model (above)-3D-model (below): no refinement, horizontal eddy viscosity 10 m²/s; 3D-model: 10 layers.

Figure 155 Current pattern at HW-5h for the area around SSS 2D-model (above)-3D-model (below): no refinement, horizontal eddy viscosity 10 m²/s; 3D-model: 10 layers

Figure 156 Current pattern at HW-4h for the area around NSS 2D-model (above)-3D-model (below): no refinement, horizontal eddy viscosity 10 m²/s; 3D-model: 10 layers

Figure 157 Current pattern at HW-4h for the area around SSS 2D-model (above)-3D-model (below): no refinement, horizontal eddy viscosity 10 m²/s; 3D-model: 10 layers

Figure 158 Current pattern at HW-3h for the area around NSS 2D-model (above)-3D-model (below): no refinement, horizontal eddy viscosity 10 m²/s; 3D-model: 10 layers

Figure 159 Current pattern at HW-3h for the area around SSS 2D-model (above)-3D-model (below): no refinement, horizontal eddy viscosity 10 m²/s; 3D-model: 10 layers

Figure 160 Current pattern at HW-2h for area around NSS 2D-model (above)-3D-model (below): no refinement, horizontal eddy viscosity 10 m²/s; 3D-model: 10 layers

Figure 161 Current pattern at HW-2h for the area around SSS 2D-model (above)-3D-model (below): no refinement, horizontal eddy viscosity 10 m²/s; 3D-model: 10 layers

Figure 162 Current pattern at HW-1h for the area around NSS 2D-model (above)-3D-model (below): no refinement, horizontal eddy viscosity 10 m²/s; 3D-model: 10 layers

Figure 163 Current pattern at HW-1h for the area around SSS 2D-model (above)-3D-model (below): no refinement, horizontal eddy viscosity 10 m²/s; 3D-model: 10 layers

Figure 164 Current pattern at HW for the area around NSS 2D-model (above)-3D-model (below): no refinement, horizontal eddy viscosity 10 m²/s; 3D-model: 10 layers

Figure 165 Current pattern at HW for the area around SSS 2D-model (above)-3D-model (below): no refinement, horizontal eddy viscosity 10 m²/s; 3D-model: 10 layers

Figure 166 Current pattern at HW+1h for the area around NSS 2D-model (above)-3D-model (below): no refinement, horizontal eddy viscosity 10 m²/s; 3D-model: 10 layers

Figure 167 Current pattern at HW+1h for the area around SSS 2D-model (above)-3D-model (below): no refinement, horizontal eddy viscosity 10 m²/s; 3D-model: 10 layers

Figure 168 Current pattern at HW+2h for the area around NSS 2D-model (above)-3D-model (below): no refinement, horizontal eddy viscosity 10 m²/s; 3D-model: 10 layers

Figure 169 Current pattern at HW+2h for the area around SSS 2D-model (above)-3D-model (below): no refinement, horizontal eddy viscosity 10 m²/s; 3D-model: 10 layers

Figure 170 Current pattern at HW+3h for the area around NSS 2D-model (above)-3D-model (below): no refinement, horizontal eddy viscosity 10 m²/s; 3D-model: 10 layers

Figure 171 Current pattern at HW+3h for the area around SSS 2D-model (above)-3D-model (below): no refinement, horizontal eddy viscosity 10 m²/s; 3D-model: 10 layers

Figure 172 Current pattern at HW+4h for the area around NSS 2D-model (above)-3D-model (below): no refinement, horizontal eddy viscosity 10 m²/s; 3D-model: 10 layers

Figure 173 Current pattern at HW+4h for the area around SSS 2D-model (above)-3D-model (below): no refinement, horizontal eddy viscosity 10 m²/s; 3D-model: 10 layers

Figure 174 Current pattern at HW+5h for the area around NSS 2D-model (above)-3D-model (below): no refinement, horizontal eddy viscosity 10 m²/s; 3D-model: 10 layers

Figure 175 Current pattern at HW+5h for the area around SSS 2D-model (above)-3D-model (below): no refinement, horizontal eddy viscosity 10 m²/s; 3D-model: 10 layers

Figure 176 Current pattern at HW+6h for the area around NSS 2D-model (above)-3D-model (below): no refinement, horizontal eddy viscosity 10 m²/s; 3D-model: 10 layers

Figure 177 Current pattern at HW+6h for the area around SSS 2D-model (above)-3D-model (below): no refinement, horizontal eddy viscosity 10 m²/s; 3D-model: 10 layers

Figure 178 Comparison of flow pathways at HW-5h. Influence of horizontal eddy viscosity (1 m²/s – 10 m²/s). Numerical model: 3D model, no refinement, 5 layers

Figure 179 Comparison of flow pathways at HW-5h. Influence of horizontal eddy viscosity (1 m²/s – 10 m²/s) Numerical model: 3D model, no refinement, 5 layers

Figure 180 Comparison of flow pathways at HW-4 h. Influence of horizontal eddy viscosity (1 m²/s – 10 m²/s) Numerical model: 3D model, no refinement, 5 layers

Figure 181 Comparison of flow pathways at HW-4 h. Influence of horizontal eddy viscosity (1 m²/s – 10 m²/s) Numerical model: 3D model, no refinement, 5 layers

Figure 182 Comparison of flow pathways at HW-3h. Influence of horizontal eddy viscosity (1 m²/s – 10 m²/s). Numerical model: 3D model, no refinement, 5 layers

Figure 183 Comparison of flow pathways at HW-3 h. Influence of horizontal eddy viscosity (1 m²/s – 10 m²/s) Numerical model: 3D model, no refinement, 5 layers

Figure 184 Comparison of flow pathways at HW-3 h. Influence of horizontal eddy viscosity (1 m²/s – 10 m²/s) Numerical model: 3D model, no refinement, 5 layers

Figure 185 Comparison of flow pathways at HW-2h. Influence of horizontal eddy viscosity (1 m²/s – 10 m²/s) Numerical model: 3D model, no refinement, 5 layers

Figure 186 Comparison of flow pathways at HW-2h. Influence of horizontal eddy viscosity (1 m²/s – 10 m²/s) Numerical model: 3D model, no refinement, 5 layers

Figure 187 Comparison of flow pathways at HW-1h. Influence of horizontal eddy viscosity (1 m²/s – 10 m²/s) Numerical model: 3D model, no refinement, 5 layers

Figure 188 Comparison of flow pathways at HW. Influence of horizontal eddy viscosity (1 m²/s – 10 m²/s) Numerical model: 3D model, no refinement, 5 layers

Figure 189 Comparison of flow pathways at HW. Influence of horizontal eddy viscosity (1 m²/s – 10 m²/s) Numerical model: 3D model, no refinement, 5 layers

Figure 190 Comparison of flow pathways at HW. Influence of horizontal eddy viscosity (1 m²/s – 10 m²/s) Numerical model: 3D model, no refinement, 5 layers

Figure 191 Comparison of flow pathways at HW. Influence of horizontal eddy viscosity (1 m²/s – 10 m²/s) Numerical model: 3D model, no refinement, 5 layers

Figure 192 Comparison of flow pathways at HW+5h. Influence of horizontal eddy viscosity (1 m²/s – 10 m²/s) Numerical model: 3D model, no refinement, 5 layers

Figure 193 Comparison of flow pathways at HW+5h. Influence of horizontal eddy viscosity (1 m²/s – 10 m²/s) Numerical model: 3D model, no refinement, 5 layers

Figure 194 Comparison of flow pathways at HW+6h. Influence of horizontal eddy viscosity (1 m²/s – 10 m²/s) Numerical model: 3D model, no refinement, 5 layers

Figure 195 Comparison of flow pathways at HW+6h. Influence of horizontal eddy viscosity (1 m²/s – 10 m²/s) Numerical model: 3D model, no refinement, 5 layers

Figure 196 Comparison of flow pathways at HW+6h. Influence of horizontal eddy viscosity (1 m²/s – 10 m²/s) Numerical model: 3D model, no refinement, 5 layers

Figure 197 Comparison of flow pathways at HW-5h. Numerical model: 3D model, no refinement, horizontal eddy viscosity 10 m²/s, 5 layers - 10 layers

Figure 198 Comparison of flow pathways at HW-5h. Numerical model: 3D model, no refinement, horizontal eddy viscosity 10 m³/s, 5 layers - 10 layers

Figure 199 Comparison of flow pathways at HW-4h. Numerical model: 3D model, no refinement, horizontal eddy viscosity 10 m³/s, 5 layers - 10 layers

Figure 200 Comparison of flow pathways at HW-4h. Numerical model: 3D model, no refinement, horizontal eddy viscosity 10 m³/s, 5 layers - 10 layers

Figure 201 Comparison of flow pathways at HW-3h. Numerical model: 3D model, no refinement, horizontal eddy viscosity 10 m³/s, 5 layers - 10 layers

Figure 202 Comparison of flow pathways at HW-3h. Numerical model: 3D model, no refinement, horizontal eddy viscosity 10 m³/s, 5 layers - 10 layers

Figure 203 Comparison of flow pathways at HW-3h. Numerical model: 3D model, no refinement, horizontal eddy viscosity 10 m³/s, 5 layers - 10 layers

Figure 204 Comparison of flow pathways at HW-2h. Numerical model: 3D model, no refinement, horizontal eddy viscosity 10 m³/s, 5 layers - 10 layers

Figure 205 Comparison of flow pathways at HW-2h. Numerical model: 3D model, no refinement, horizontal eddy viscosity 10 m³/s, 5 layers - 10 layers

Figure 206 Comparison of flow pathways at HW-1h. Numerical model: 3D model, no refinement, horizontal eddy viscosity 10 m³/s, 5 layers - 10 layers

Figure 207 Comparison of flow pathways at HW. Numerical model: 3D model, no refinement, horizontal eddy viscosity 10 m³/s, 5 layers 10 layers

Figure 208 Comparison of flow pathways at HW. Numerical model: 3D model, no refinement, horizontal eddy viscosity 10 m³/s, 5 layers - 10 layers

Figure 209 Comparison of flow pathways at HW. Numerical model: 3D model, no refinement, horizontal eddy viscosity 10 m³/s, 5 layers - 10 layers

Figure 210 Comparison of flow pathways at HW.Numerical model: 3D model, no refinement, horizontal eddy viscosity 10 m³/s, 5 layers - 10 layers

Figure 211 Comparison of flow pathways at HW+5h. Numerical model: 3D model, no refinement, horizontal eddy viscosity 10 m³/s, 5 layers - 10 layers

Figure 212 Comparison of flow pathways at HW+5h. Numerical model: 3D model, no refinement, horizontal eddy viscosity 10 m³/s, 5 layers - 10 layers

Figure 213 Comparison of flow pathways at HW+6h. Numerical model: 3D model, no refinement, horizontal eddy viscosity 10 m³/s, 5 layers - 10 layers

Figure 214 Comparison of flow pathways at HW+6h. Numerical model: 3D model, no refinement, horizontal eddy viscosity 10 m³/s, 5 layers - 10 layers

Figure 215 Comparison of flow pathways at HW+6h. Numerical model: 3D model, no refinement, horizontal eddy viscosity 10 m³/s, 5 layers - 10 layers

Figure 216 Comparison of surface velocity at HW-5h. Scale model-Numerical model: 3D model, no refinement, 10 layers, horizontal eddy viscosity 10 m²/s

Figure 217 Comparison of surface velocity at HW-4h.Scale model-Numerical model: 3D model, no refinement, 10 layers, horizontal eddy viscosity 10 m²/s

Figure 218 Comparison of surface velocity at HW-3h.Scale model-Numerical model: 3D model, no refinement, 10 layers, horizontal eddy viscosity 10 m²/s

Figure 219 Comparison of surface velocity at HW-2h. Scale model-Numerical model: 3D model, no refinement, 10 layers, horizontal eddy viscosity 10 m²/s

Figure 220 Comparison of surface velocity at HW-1h. Scale model-Numerical model: 3D model, no refinement, 10 layers, horizontal eddy viscosity 10 m²/s

Figure 221 Comparison of surface velocity at HW. Scale model-Numerical model: 3D model, no refinement, 10 layers, horizontal eddy viscosity 10 m²/s

Figure 222 Comparison of surface velocity at HW+1h. Scale model-Numerical model: 3D model, no refinement, 10 layers, horizontal eddy viscosity 10 m²/s

Figure 223 Comparison of surface velocity at HW+2h. Scale model-Numerical model: 3D model, no refinement, 10 layers, horizontal eddy viscosity 10 m²/s

Figure 224 Comparison of surface velocity at HW+3h. Scale model-Numerical model: 3D model, no refinement, 10 layers, horizontal eddy viscosity 10 m²/s

Figure 225 Comparison of surface velocity at HW+4h. Scale model-Numerical model: 3D model, no refinement, 10 layers, horizontal eddy viscosity 10 m²/s

Figure 226 Comparison of surface velocity at HW+5h. Scale model-Numerical model: 3D model, no refinement, 10 layers, horizontal eddy viscosity 10 m²/s

Figure 227 Comparison of surface velocity at HW+6h. Scale model-Numerical model: 3D model, no refinement, 10 layers, horizontal eddy viscosity 10 m²/s

Figure 228 Comparison of velocity profile along transect at HW-5h (vectorplot). Numerical model: 3D model, no refinement, 10 layers, horizontal eddy viscosity 10 m²/s

Figure 229 Comparison of velocity profile along transect at HW-5h contourplot). Numerical model: 3D model, no refinement, 10 layers, horizontal eddy viscosity 10 m²/s

Figure 230 Comparison of velocity profile along transect at HW-3h (vectorplot). Numerical model: 3D model, no refinement, 10 layers, horizontal eddy viscosity 10 m²/s

Figure 231 Comparison of velocity profile along transect at HW-3h contourplot). Numerical model: 3D model, no refinement, 10 layers, horizontal eddy viscosity 10 m²/s

Figure 232 Comparison of velocity profile along transect at HW-2h (vectorplot). Numerical model: 3D model, no refinement, 10 layers, horizontal eddy viscosity 10 m²/s

Figure 233 Comparison of velocity profile along transect at HW-2h contourplot). Numerical model: 3D model, no refinement, 10 layers, horizontal eddy viscosity 10 m²/s

Figure 234 Comparison of velocity profile along transect at HW-1h (vectorplot). Numerical model: 3D model, no refinement, 10 layers, horizontal eddy viscosity 10 m²/s

Figure 235 Comparison of velocity profile along transect at HW-1h contourplot). Numerical model: 3D model, no refinement, 10 layers, horizontal eddy viscosity 10 m²/s

Figure 236 Comparison of velocity profile along transect at HW (vectorplot). Numerical model: 3D model, no refinement, 10 layers, horizontal eddy viscosity 10 m²/s

Figure 237 Comparison of velocity profile along transect at HW contourplot). Numerical model: 3D model, no refinement, 10 layers, horizontal eddy viscosity 10 m²/s

Figure 238 Comparison of velocity profile along transect at HW+1h (vectorplot). Numerical model: 3D model, no refinement, 10 layers, horizontal eddy viscosity 10 m²/s

Figure 239 Comparison of velocity profile along transect at HW+1h (contourplot). Numerical model: 3D model, no refinement, 10 layers, horizontal eddy viscosity 10 m²/s

Figure 240 Comparison of velocity profile along transect at HW+2h (vectorplot). Numerical model: 3D model, no refinement, 10 layers, horizontal eddy viscosity 10 m²/s

Figure 241 Comparison of velocity profile along transect at HW+2h (contourplot). Numerical model: 3D model, no refinement, 10 layers, horizontal eddy viscosity 10 m²/s

Figure 242 Comparison of velocity profile along transect at HW+5h (vectorplot). Numerical model: 3D model, no refinement, 10 layers, horizontal eddy viscosity 10 m²/s

Figure 243 Comparison of velocity profile along transect at HW+5h (contourplot). Numerical model: 3D model, no refinement, 10 layers, horizontal eddy viscosity 10 m²/s

Figure 244 Comparison of velocity profile along transect at HW+6h (vectorplot). Numerical model: 3D model, no refinement, 10 layers, horizontal eddy viscosity 10 m²/s

Figure 245 Comparison of velocity profile along transect at HW+6h (contourplot). Numerical model: 3D model, no refinement, 10 layers, horizontal eddy viscosity 10 m²/s

Figure 246 Comparison of salinity profile at HW-5h. Field data: point WC1N, WC2N. Numerical model: 3D model, no refinement, 10 layers, horizontal eddy viscosity 10 m²/s

Figure 247 Comparison of salinity profile at HW-5h. Field data: point WC3N, WC4N. Numerical model: 3D model, no refinement, 10 layers, horizontal eddy viscosity 10 m²/s

Figure 248 Comparison of salinity profile at HW-4h. Field data: point WC1N, WC2N. Numerical model: 3D model, no refinement, 10 layers, horizontal eddy viscosity 10 m²/s

Figure 249 Comparison of salinity profile at HW-4h. Field data: point WC3N, WC4N. Numerical model: 3D model, no refinement, 10 layers, horizontal eddy viscosity 10 m²/s

Figure 250 Comparison of salinity profile at HW-3h. Field data: point WC1N, WC2N. Numerical model: 3D model, no refinement, 10 layers, horizontal eddy viscosity 10 m²/s

Figure 251 Comparison of salinity profile at HW-3h. Field data: point WC3N, WC4N. Numerical model: 3D model, no refinement, 10 layers, horizontal eddy viscosity 10 m²/s

Figure 252 Comparison of salinity profile at HW-2h. Field data: point WC1N, WC2N. Numerical model: 3D model, no refinement, 10 layers, horizontal eddy viscosity 10 m²/s

Figure 253 Comparison of salinity profile at HW-2h. Field data: point WC3N, WC4N. Numerical model: 3D model, no refinement, 10 layers, horizontal eddy viscosity 10 m²/s.

Figure 254 Comparison of salinity profile at HW-1h. Field data: point WC1N, WC2N. Numerical model: 3D model, no refinement, 10 layers, horizontal eddy viscosity 10 m²/s

Figure 255 Comparison of salinity profile at HW-1h. Field data: point WC3N, WC4N. Numerical model: 3D model, no refinement, 10 layers, horizontal eddy viscosity 10 m²/s

Figure 256 Comparison of salinity profile at HW. Field data: point WC1N, WC2N. Numerical model: 3D model, no refinement, 10 layers, horizontal eddy viscosity 10 m²/s

Figure 257 Comparison of salinity profile at HW. Field data: point WC3N, WC4N. Numerical model: 3D model, no refinement, 10 layers, horizontal eddy viscosity 10 m²/s

Figure 258 Comparison of salinity profile at HW+1h. Field data: point WC1N, WC2N. Numerical model: 3D model, no refinement, 10 layers, horizontal eddy viscosity 10 m²/s

Figure 259 Comparison of salinity profile at HW+1h. Field data: point WC3N, WC4N. Numerical model: 3D model, no refinement, 10 layers, horizontal eddy viscosity 10 m²/s

Figure 260 Comparison of salinity profile at HW+2h. Field data: point WC1N, WC2N. Numerical model: 3D model, no refinement, 10 layers, horizontal eddy viscosity 10 m²/s

Figure 261 Comparison of salinity profile at HW+2h. Field data: point WC3N, WC4N. Numerical model: 3D model, no refinement, 10 layers, horizontal eddy viscosity 10 m²/s

Figure 262 Comparison of salinity profile at HW+3h. Field data: point WC1N, WC2N. Numerical model: 3D model, no refinement, 10 layers, horizontal eddy viscosity 10 m²/s

Figure 263 Comparison of salinity profile at HW+3h. Field data: point WC3N, WC4N. Numerical model: 3D model, no refinement, 10 layers, horizontal eddy viscosity 10 m²/s

Figure 264 Comparison of salinity profile at HW+4h. Field data: point WC1N, WC2N. Numerical model: 3D model, no refinement, 10 layers, horizontal eddy viscosity 10 m²/s

Figure 265 Comparison of salinity profile at HW+4h. Field data: point WC3N, WC4N. Numerical model: 3D model, no refinement, 10 layers, horizontal eddy viscosity 10 m²/s

Figure 266 Comparison of salinity profile at HW+5h. Field data: point WC1N, WC2N. Numerical model: 3D model, no refinement, 10 layers, horizontal eddy viscosity 10 m²/s

Figure 267 Comparison of salinity profile at HW+5h. Field data: point WC3N, WC4N. Numerical model: 3D model, no refinement, 10 layers, horizontal eddy viscosity 10 m²/s

Figure 268 Comparison of salinity profile at HW+6h. Field data: point WC1N, WC2N. Numerical model: 3D model, no refinement, 10 layers, horizontal eddy viscosity 10 m²/s

Figure 269 Comparison of salinity profile at HW+6h. Field data: point WC3N, WC4N. Numerical model: 3D model, no refinement, 10 layers, horizontal eddy viscosity 10 m²/s

Figure 270 Comparison of velocity profile at HW-5h. Field data: 03/06/03;Location Kaloo. Numerical model: 3D model, no refinement, 5-10 layers, horizontal eddy viscosity 10 m²/s

Figure 271 Comparison of velocity profile at HW-5h. Field data: 03/06/03;Location Veremans. Numerical model: 3D model, no refinement, 5-10 layers, horizontal eddy viscosity 10 m²/s

Figure 272 Comparison of velocity profile at HW-5h. Field data: 03/06/03;Location Scaldis. Numerical model: 3D model, no refinement, 5-10 layers, horizontal eddy viscosity 10 m²/s

Figure 273 Comparison of velocity profile at HW-4h. Field data: 03/06/03;Location Kaloo. Numerical model: 3D model, no refinement, 5-10 layers, horizontal eddy viscosity 10 m²/s

Figure 274 Comparison of velocity profile at HW-4h. Field data: 03/06/03;Location Veremans. Numerical model: 3D model, no refinement, 5-10 layers, horizontal eddy viscosity 10 m²/s

Figure 275 Comparison of velocity profile at HW-4h. Field data: 03/06/03;Location Scaldis. Numerical model: 3D model, no refinement, 5-10 layers, horizontal eddy viscosity 10 m²/s

Figure 276 Comparison of velocity profile at HW-3h. Field data: 03/06/03;Location Kaloo. Numerical model: 3D model, no refinement, 5-10 layers, horizontal eddy viscosity 10 m²/s

Figure 277 Comparison of velocity profile at HW-3h. Field data: 03/06/03;Location Veremans. Numerical model: 3D model, no refinement, 5-10 layers, horizontal eddy viscosity 10 m²/s

Figure 278 Comparison of velocity profile at HW-3h. Field data: 03/06/03;Location Scaldis. Numerical model: 3D model, no refinement, 5-10 layers, horizontal eddy viscosity 10 m²/s

Figure 279 Comparison of velocity profile at HW-2h. Field data: 03/06/03;Location Kaloo. Numerical model: 3D model, no refinement, 5-10 layers, horizontal eddy viscosity 10 m²/s

Figure 280 Comparison of velocity profile at HW-2h. Field data: 03/06/03;Location Veremans. Numerical model: 3D model, no refinement, 5-10 layers, horizontal eddy viscosity 10 m²/s

Figure 281 Comparison of velocity profile at HW-2h. Field data: 03/06/03;Location Scaldis. Numerical model: 3D model, no refinement, 5-10 layers, horizontal eddy viscosity 10 m²/s

Figure 282 Comparison of velocity profile at HW-1h. Field data: 03/06/03;Location Kaloo. Numerical model: 3D model, no refinement, 5-10 layers, horizontal eddy viscosity 10 m²/s

Figure 283 Comparison of velocity profile at HW-1h. Field data: 03/06/03;Location Veremans. Numerical model: 3D model, no refinement, 5-10 layers, horizontal eddy viscosity 10 m²/s

Figure 284 Comparison of velocity profile at HW-1h. Field data: 03/06/03;Location Scaldis. Numerical model: 3D model, no refinement, 5-10 layers, horizontal eddy viscosity 10 m²/s

Figure 285 Comparison of velocity profile at HW. Field data: 03/06/03; Location Kaloo. Numerical model: 3D model, no refinement, 5-10 layers, horizontal eddy viscosity 10 m²/s

Figure 286 Comparison of velocity profile at HW. Field data: 03/06/03;Location Veremans. Numerical model: 3D model, no refinement, 5-10 layers, horizontal eddy viscosity 10 m²/s

Figure 287 Comparison of velocity profile at HW. Field data: 03/06/03 Location Scaldis. Numerical model: 3D model, no refinement, 5-10 layers, horizontal eddy viscosity 10 m²/s

Figure 288 Comparison of velocity profile at HW+1h. Field data: 03/06/03;Location Kaloo. Numerical model: 3D model, no refinement, 5-10 layers, horizontal eddy viscosity 10 m²/s

Figure 289 Comparison of velocity profile at HW+1h. Field data: 03/06/03;Location Veremans. Numerical model: 3D model, no refinement, 5-10 layers, horizontal eddy viscosity 10 m²/s

Figure 290 Comparison of velocity profile at HW+1h. Field data: 03/06/03;Location Scaldis. Numerical model: 3D model, no refinement, 5-10 layers, horizontal eddy viscosity 10 m²/s

Figure 291 Comparison of velocity profile at HW+2h. Field data: 03/06/03;Location Kaloo. Numerical model: 3D model, no refinement, 5-10 layers, horizontal eddy viscosity 10 m²/s

Figure 292 Comparison of velocity profile at HW+2h. Field data: 03/06/03;Location Veremans. Numerical model: 3D model, no refinement, 5-10 layers, horizontal eddy viscosity 10 m²/s

Figure 293 Comparison of velocity profile at HW+2h. Field data: 03/06/03;Location Scaldis. Numerical model: 3D model, no refinement, 5-10 layers, horizontal eddy viscosity 10 m²/s

Figure 294 Comparison of velocity profile at HW+4h. Field data: 03/06/03;Location Kaloo. Numerical model: 3D model, no refinement, 5-10 layers, horizontal eddy viscosity 10 m²/s

Figure 295 Comparison of velocity profile at HW+4h. Field data: 03/06/03;Location Veremans. Numerical model: 3D model, no refinement, 5-10 layers, horizontal eddy viscosity 10 m²/s

Figure 296 Comparison of velocity profile at HW+4h. Field data: 03/06/03;Location Scaldis. Numerical model: 3D model, no refinement, 5-10 layers, horizontal eddy viscosity 10 m²/s

Figure 297 Comparison of velocity profile at HW+5h. Field data: 03/06/03;Location Kaloo. Numerical model: 3D model, no refinement, 5-10 layers, horizontal eddy viscosity 10 m²/s

Figure 298 Comparison of velocity profile at HW+5h. Field data: 03/06/03;Location Scaldis. Numerical model: 3D model, no refinement, 5-10 layers, horizontal eddy viscosity 10 m²/s

Figure 299 Comparison of velocity profile at HW+6h. Field data: 03/06/03;Location Kaloo. Numerical model: 3D model, no refinement, 5-10 layers, horizontal eddy viscosity 10 m²/s

Figure 300 Comparison of velocity profile at HW+6h. Field data: 03/06/03;Location Scaldis. Numerical model: 3D model, no refinement, 5-10 layers, horizontal eddy viscosity 10 m²/s

Figure 301 Grids for domain decomposition. Subdomain 1 (black), Subdomain 2 (Red), Subdomain 3 (Green)

Figure 302 Gridsize for subdomain 2 after refinement in M-and N-direction.

Figure 303 Influence of grid refinement in M- and N-direction on velocity at HW-4h (area around NSS) Numerical model: 2D-model, horizontal eddy viscosity 1 m²/s

Figure 304 Influence of grid refinement in M- and N-direction on velocity at HW-4h (area around SSS) Numerical model: 2D-model, horizontal eddy viscosity 1 m²/s

Figure 305 Influence of grid refinement in M- and N-direction on velocity at HW-1h (area around NSS) Numerical model: 2D-model, horizontal eddy viscosity 1 m²/s

Figure 306 Influence of grid refinement in M- and N-direction on velocity at HW-1h (area around SSS) Numerical model: 2D-model, horizontal eddy viscosity 1 m²/s

Figure 307 Influence of grid refinement in M- and N-direction on velocity at HW+3h (area around NSS) Numerical model: 2D-model, horizontal eddy viscosity 1 m²/s

Figure 308 Influence of grid refinement in M- and N-direction on velocity at HW+3h (area around SSS) Numerical model: 2D-model, horizontal eddy viscosity 1 m²/s

Figure 309 Influence of grid refinement in M- and N-direction on velocity at HW+6h (area around NSS) Numerical model: 2D-model, horizontal eddy viscosity 1 m²/s

Figure 310 Influence of grid refinement in M- and N-direction on velocity at HW+6h (area around SSS) Numerical model: 2D-model, horizontal eddy viscosity 1 m²/s

Figure 311 Influence of grid refinement in M- and N-direction on waterlevel at HW-4h (area around NSS). Numerical model: 2D-model, horizontal eddy viscosity 1 m²/s

Figure 312 Influence of grid refinement in M- and N-direction on waterlevel at HW+3h (area around NSS). Numerical model: 2D-model, horizontal eddy viscosity 1 m²/s

Figure 313 Influence of grid refinement in M- and N-direction on waterlevel at HW+3h (area around SSS). Numerical model: 2D-model, horizontal eddy viscosity 1 m²/s

Figure 314 Influence of grid refinement in M- and N-direction on waterlevel at HW+6h (area around NSS). Numerical model: 2D-model, horizontal eddy viscosity 1 m²/s

Figure 315 Influence of grid refinement in M- and N-direction on waterlevel at HW+6h (area around SSS). Numerical model: 2D-model, horizontal eddy viscosity 1 m²/s.

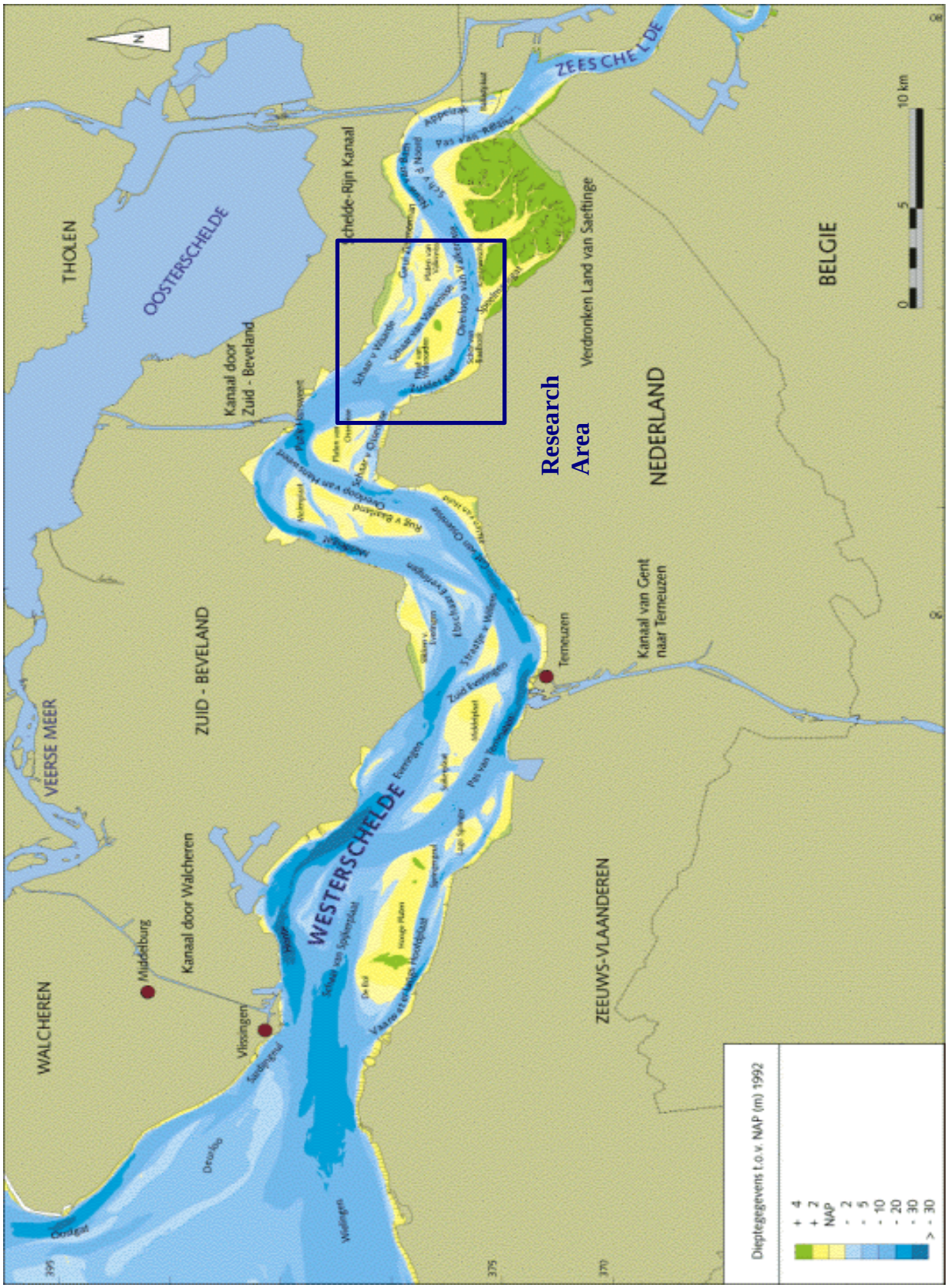

Alternative dumping strategy **Results of physical and numerical modelling**	Overview of the Westerschelde

MINISTERIE VAN DE VLAAMSE GEMEENSCHAP **AFDELING WATERBOUWKUNDIG LABORATORIUM EN HYDROLOGISCH ONDERZOEK**	Figure 001	**MODEL 678/1**

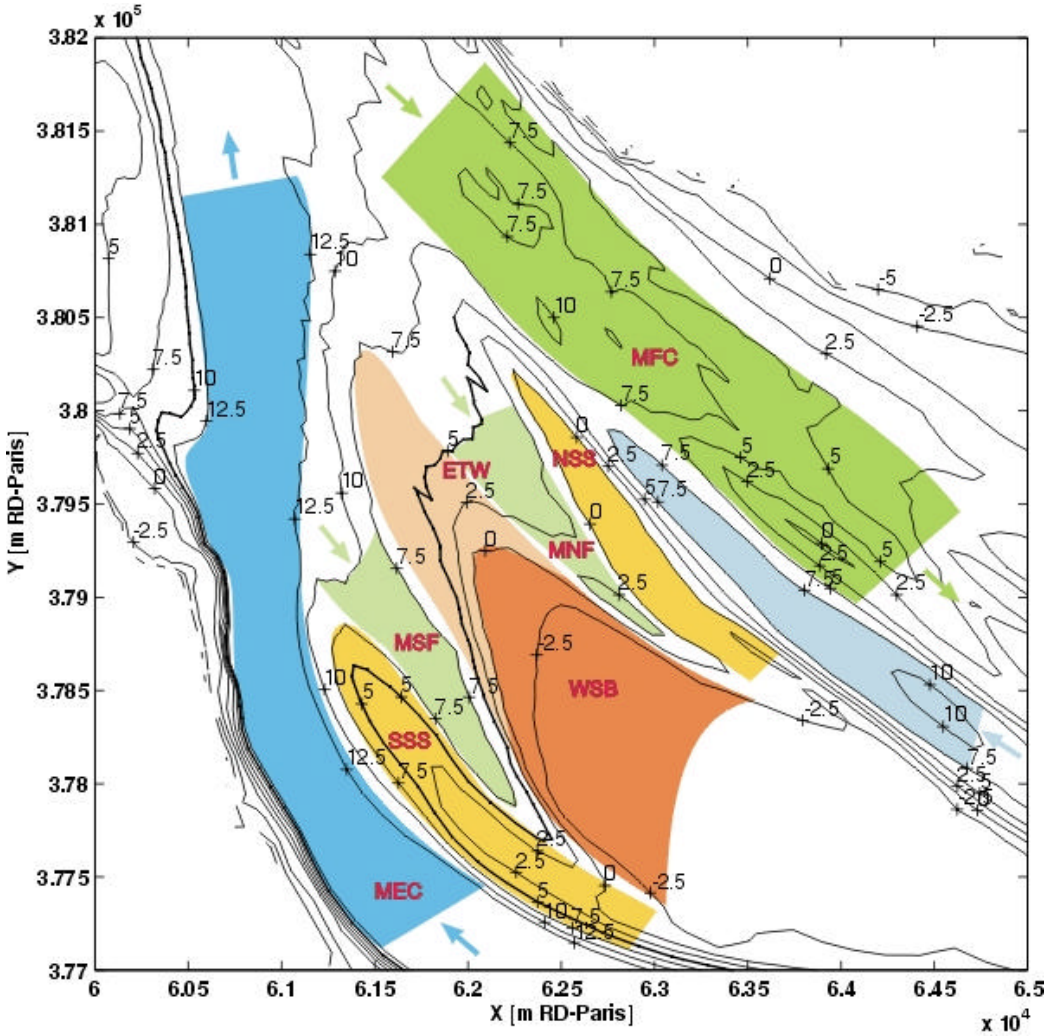

Sandbar under flood flow attack (WSB)
Main ebb channel (MEC)
Main flood channel (MFC)
Strong ebb flow in flood channel
Minor flood channel (MNF & MSF)
Sand spit (NSS & SSS)
+ Depth contours in meters TAW

Alternative dumping strategy **Results of physical and numerical modelling**	Nomenclatura for the different regions in the research area.

MINISTERIE VAN DE VLAAMSE GEMEENSCHAP **AFDELING WATERBOUWKUNDIG LABORATORIUM EN HYDROLOGISCH ONDERZOEK**	Figure 002	**MODEL 678/1**

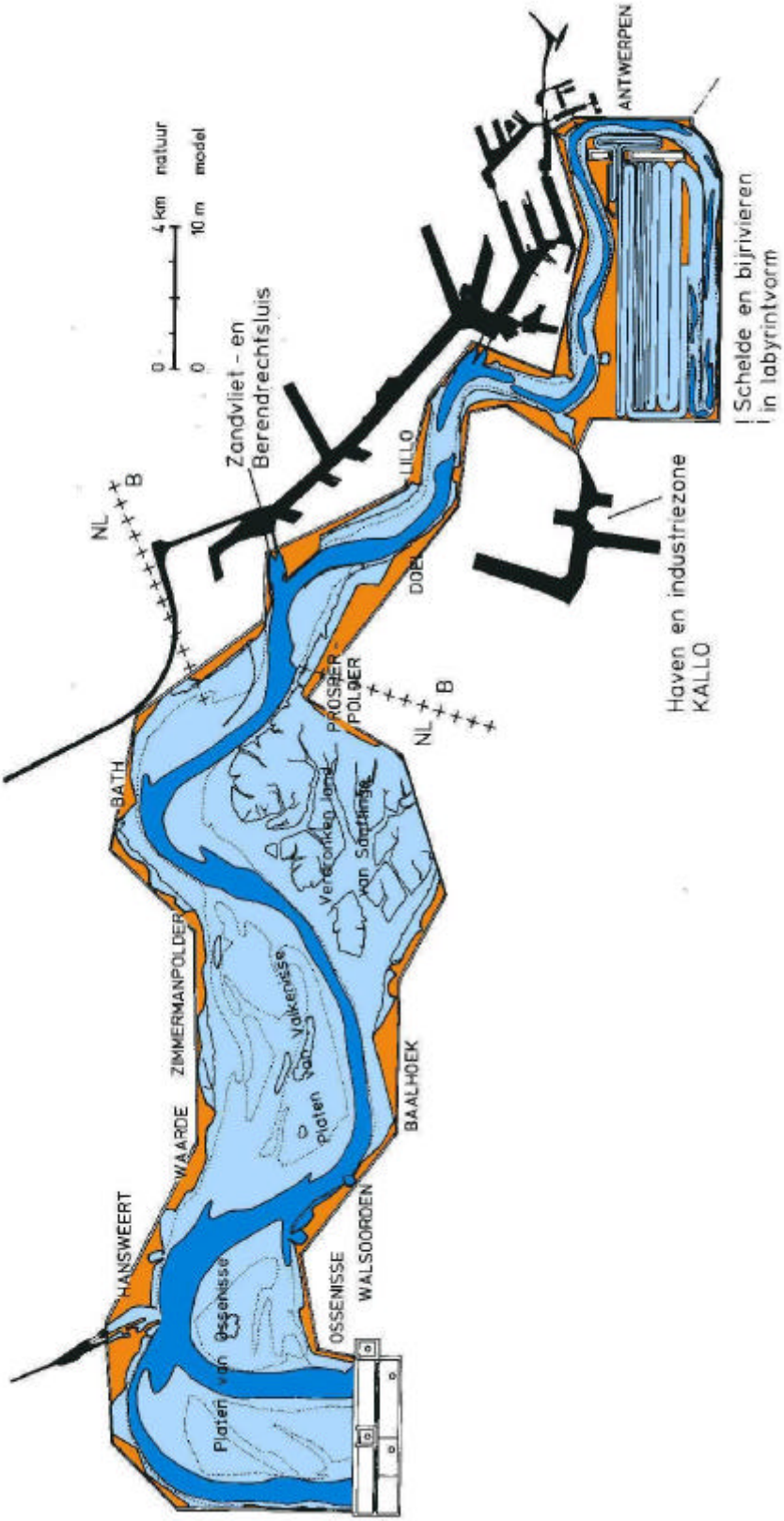

Alternative dumping strategy **Results of physical and numerical modelling**	Overview of the construction of the physical model.

MINISTERIE VAN DE VLAAMSE GEMEENSCHAP **AFDELING WATERBOUWKUNDIG LABORATORIUM EN HYDROLOGISCH ONDERZOEK**	Figure 003	**MODEL 678/1**

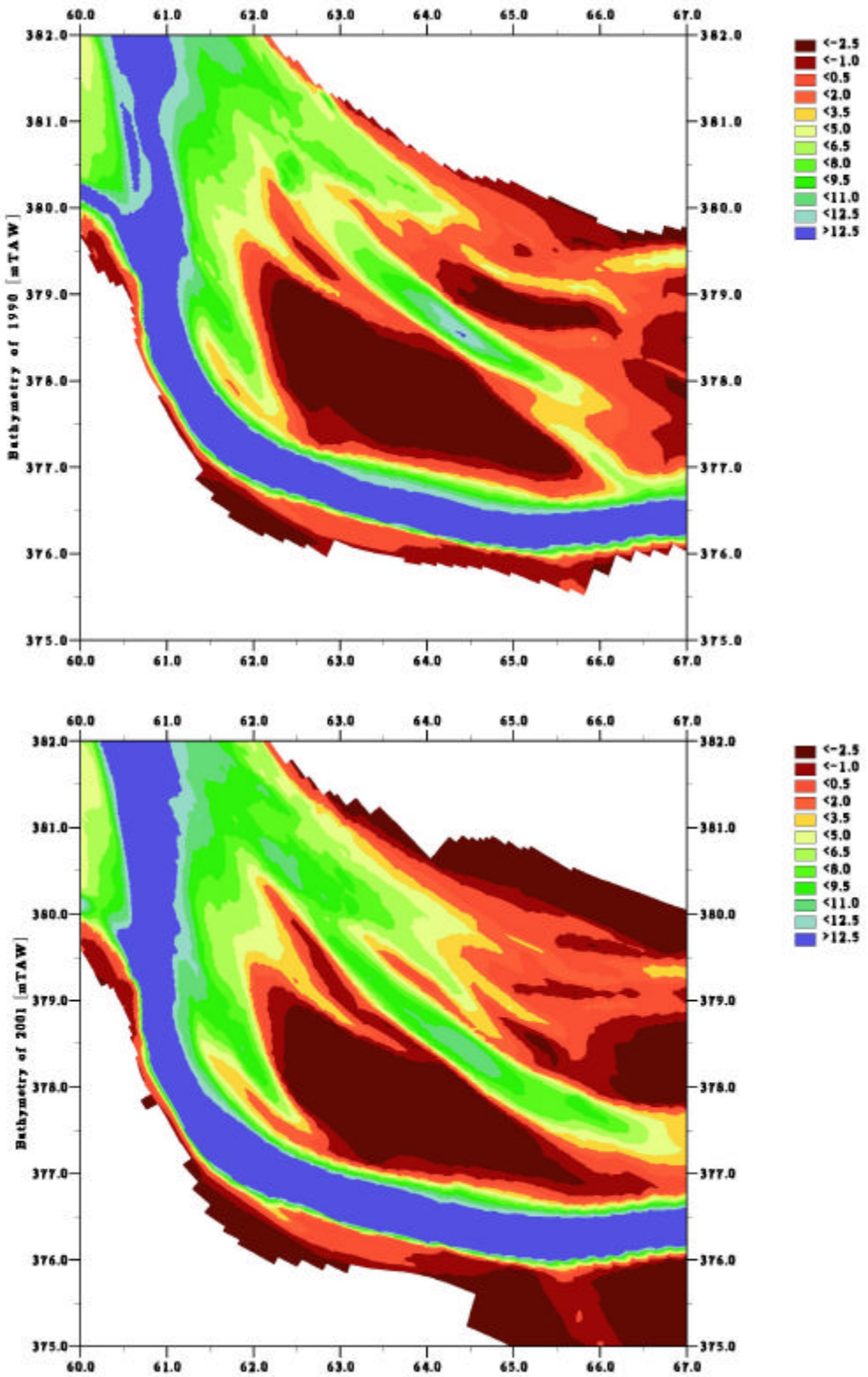

Alternative dumping strategy
Results of physical and numerical modelling

Comparison bathymetry of physical model (1989-1990) with bathymetry as measured in 2000-2001

MINISTERIE VAN DE VLAAMSE GEMEENSCHAP

AFDELING WATERBOUWKUNDIG LABORATORIUM EN HYDROLOGISCH ONDERZOEK

Figure 004

MODEL 678/1

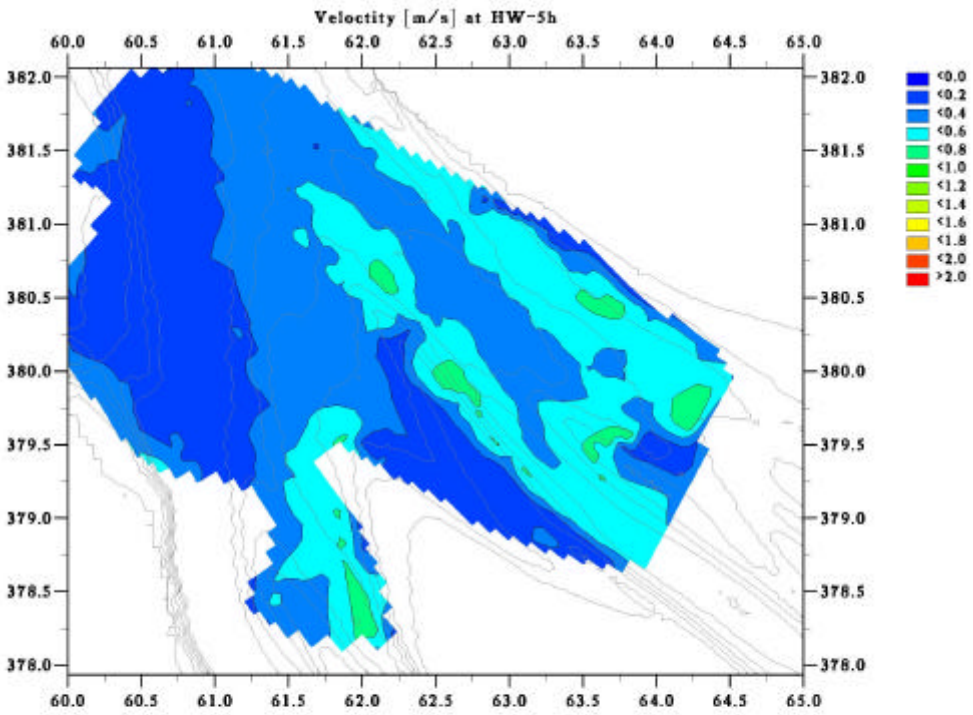

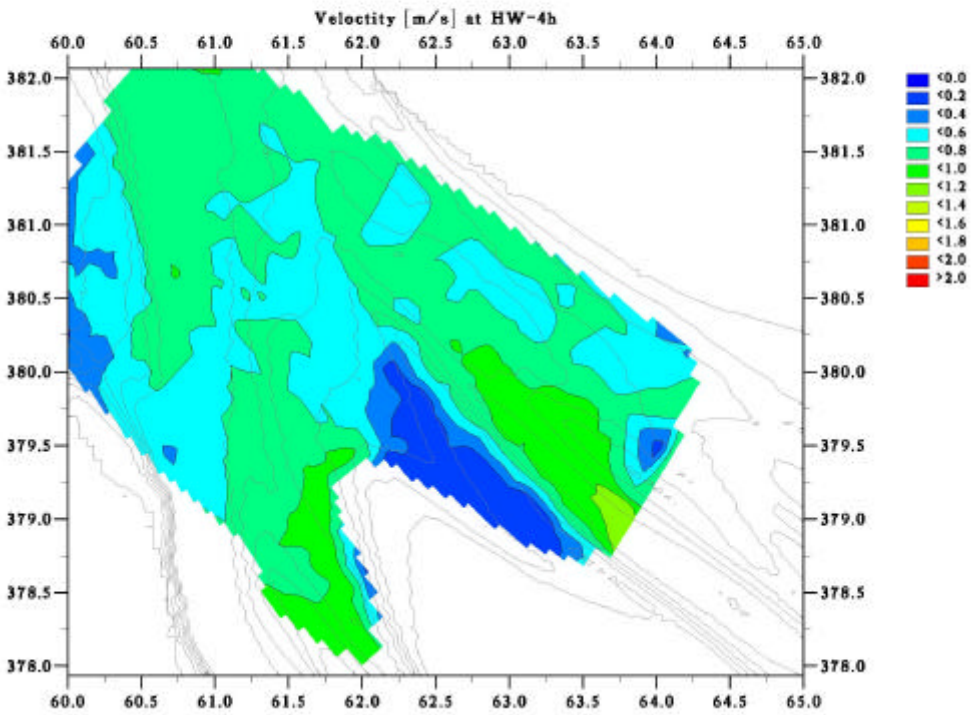

Alternative dumping strategy **Results of physical and numerical modelling**	Isovel lines for velocity measured in the scale model at HW-5h and HW-4h

MINISTERIE VAN DE VLAAMSE GEMEENSCHAP **AFDELING WATERBOUWKUNDIG LABORATORIUM EN HYDROLOGISCH ONDERZOEK**	Figure 005	**MODEL 678/1**

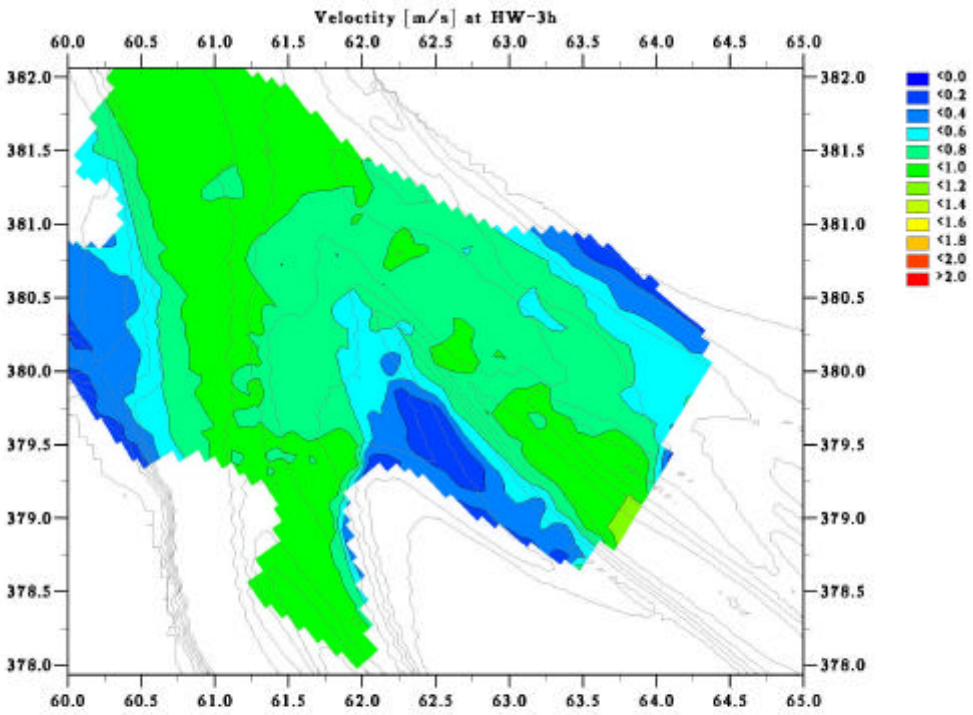

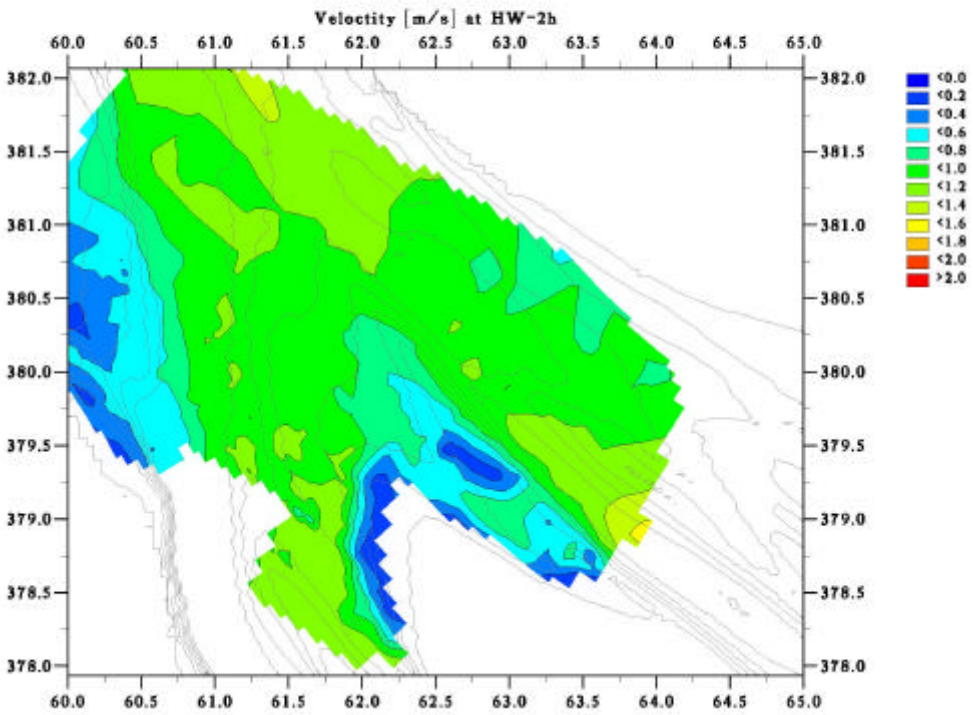

Alternative dumping strategy **Results of physical and numerical modelling**	Isovel lines for velocity measured in the scale model at HW-3h and HW-2h

MINISTERIE VAN DE VLAAMSE GEMEENSCHAP **AFDELING WATERBOUWKUNDIG LABORATORIUM EN HYDROLOGISCH ONDERZOEK**	Figure 006	**MODEL 678/1**

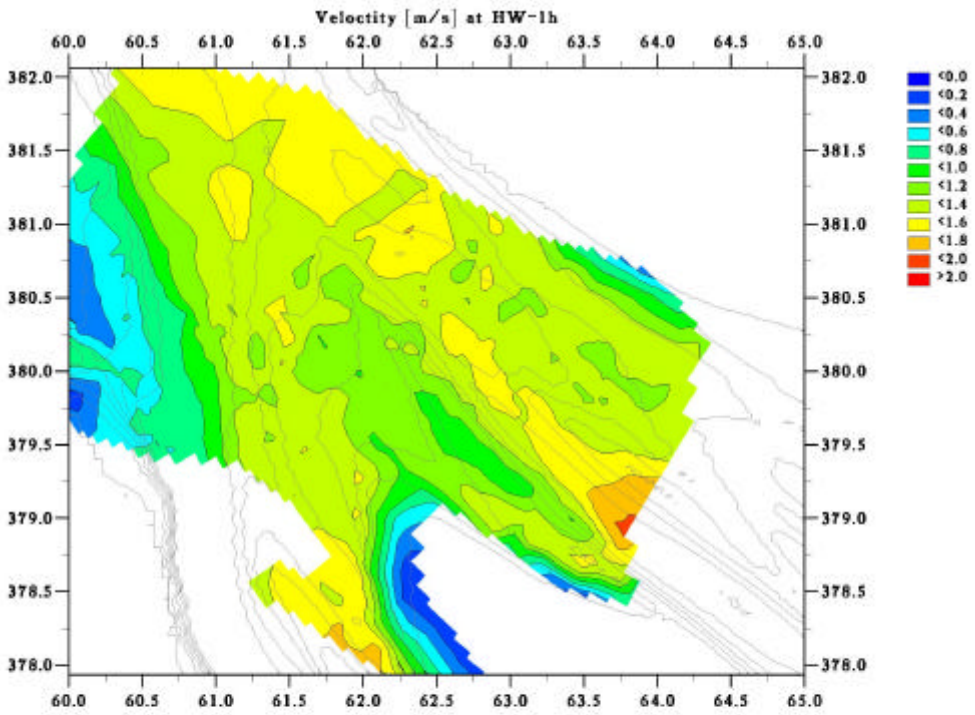

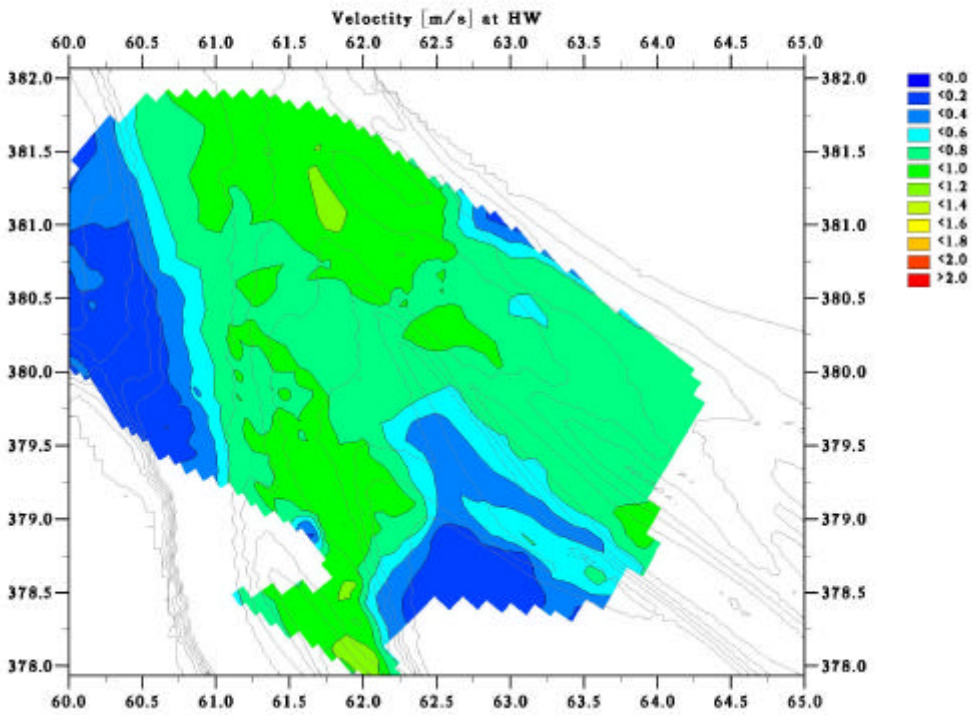

Alternative dumping strategy **Results of physical and numerical modelling**	Isovel lines for velocity measured in the scale model at HW-1h and HW

MINISTERIE VAN DE VLAAMSE GEMEENSCHAP **AFDELING WATERBOUWKUNDIG LABORATORIUM EN HYDROLOGISCH ONDERZOEK**	Figure 007	**MODEL 678/1**

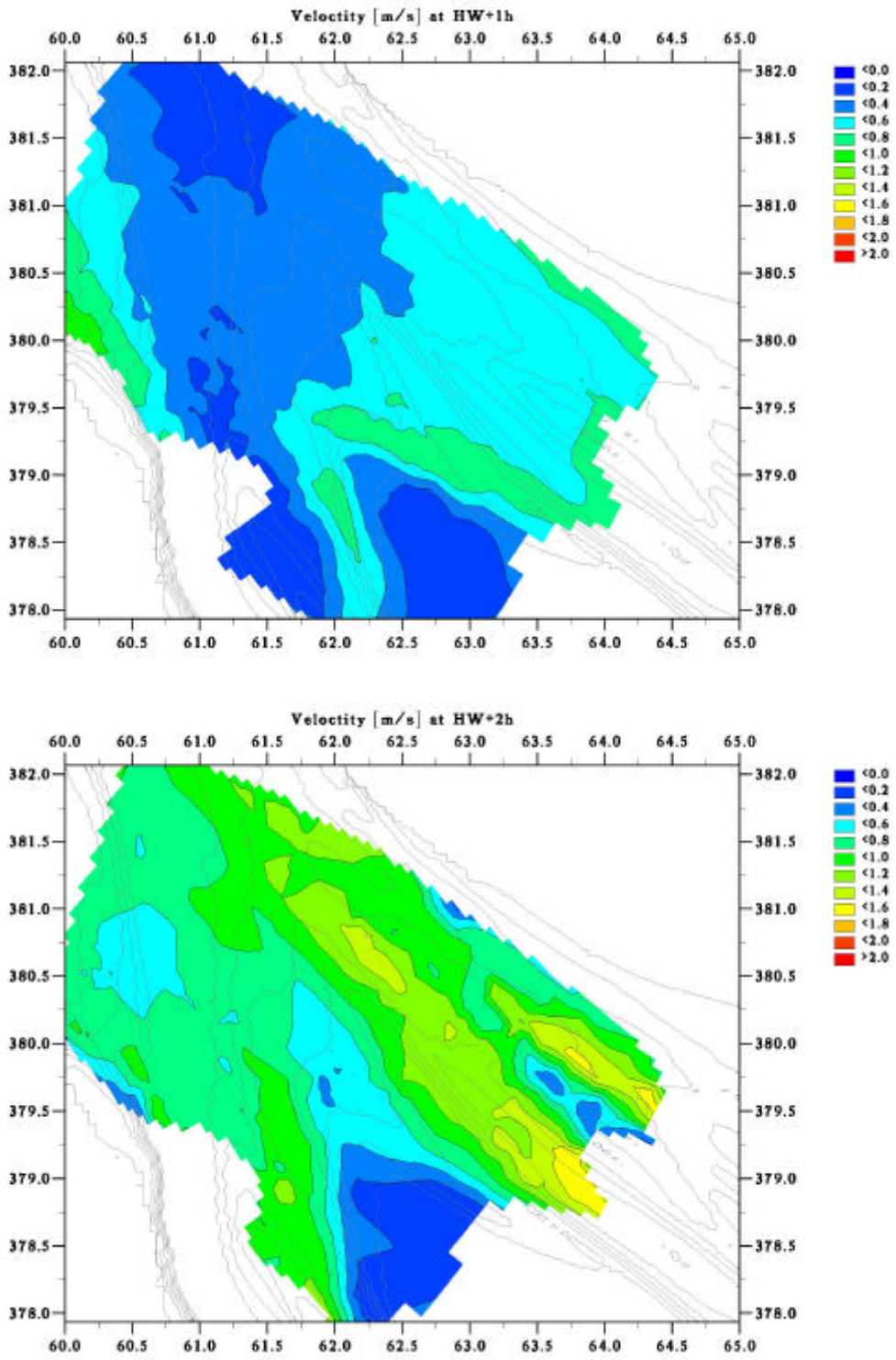

Alternative dumping strategy **Results of physical and numerical modelling**	Isovel lines for velocity measured in the scale model at HW+1h and HW+2h

MINISTERIE VAN DE VLAAMSE GEMEENSCHAP **AFDELING WATERBOUWKUNDIG LABORATORIUM EN HYDROLOGISCH ONDERZOEK**	Figure 008	**MODEL 678/1**

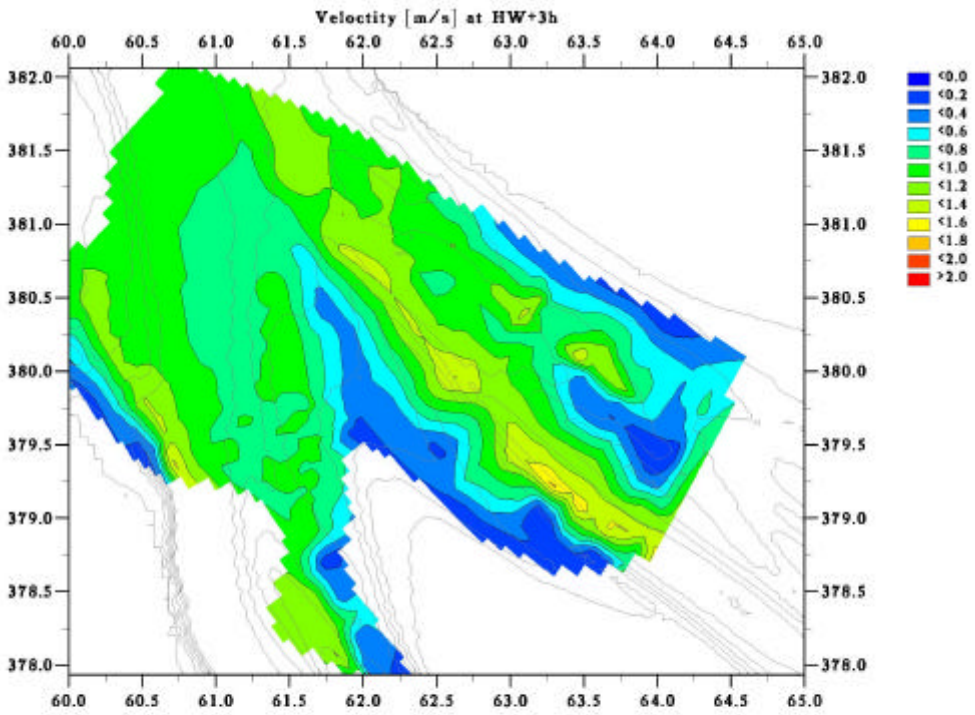

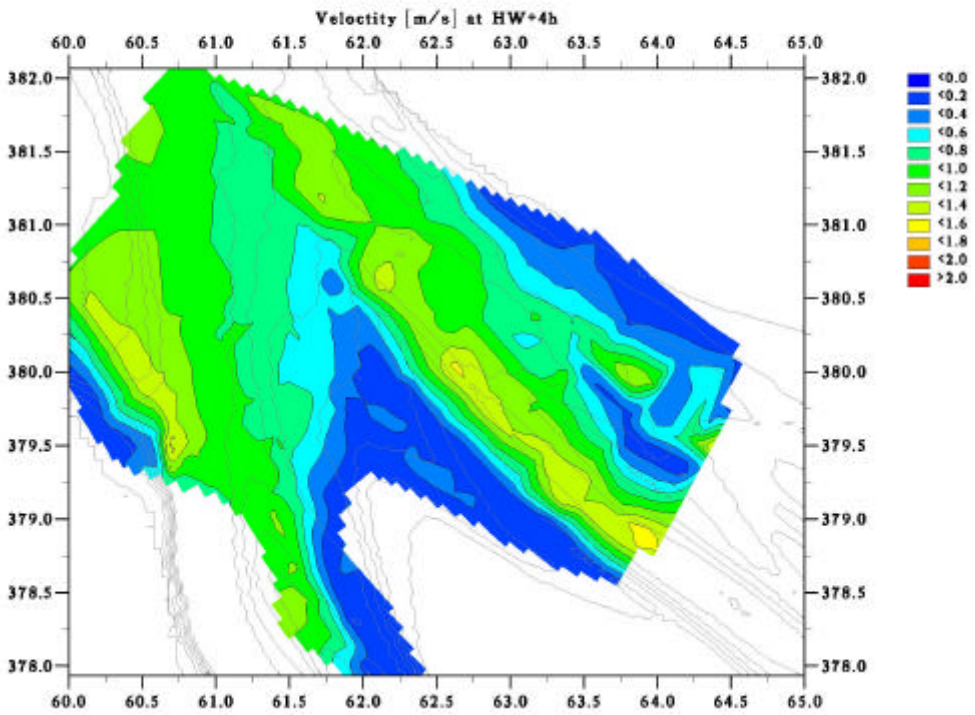

Alternative dumping strategy **Results of physical and numerical modelling**	Isovel lines for velocity measured in the scale model at HW+3h and HW+4h

MINISTERIE VAN DE VLAAMSE GEMEENSCHAP **AFDELING WATERBOUWKUNDIG LABORATORIUM EN HYDROLOGISCH ONDERZOEK**	Figure 009	**MODEL 678/1**

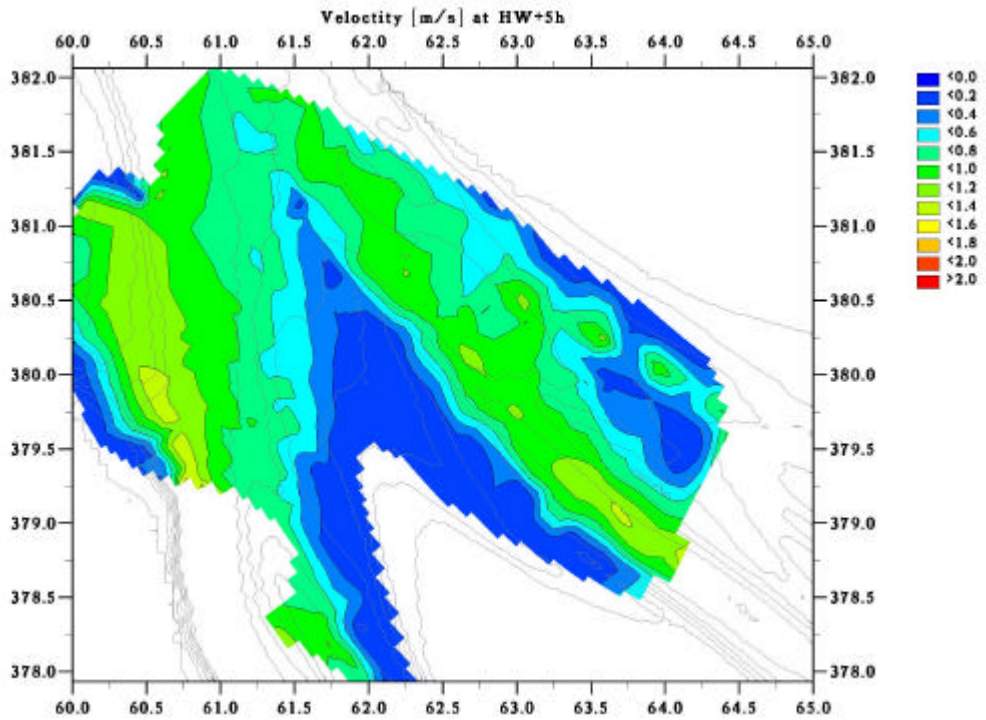

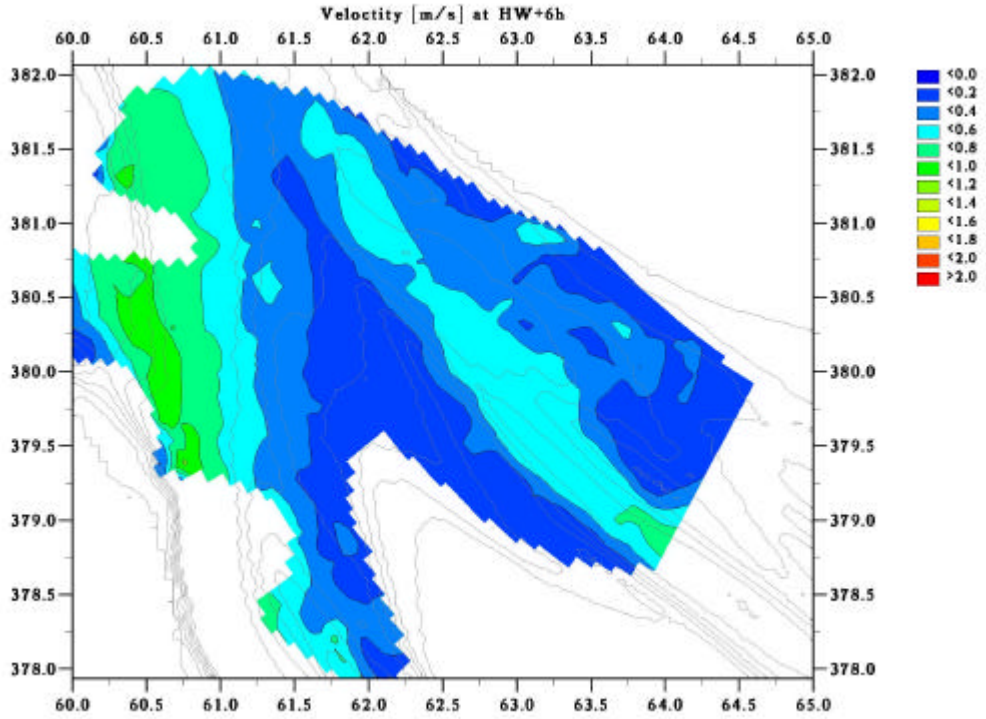

Alternative dumping strategy **Results of physical and numerical modelling**	Isovel lines for velocity measured in the scale model at HW+5h and HW+6h

MINISTERIE VAN DE VLAAMSE GEMEENSCHAP **AFDELING WATERBOUWKUNDIG LABORATORIUM EN HYDROLOGISCH ONDERZOEK**	Figure 010	**MODEL 678/1**

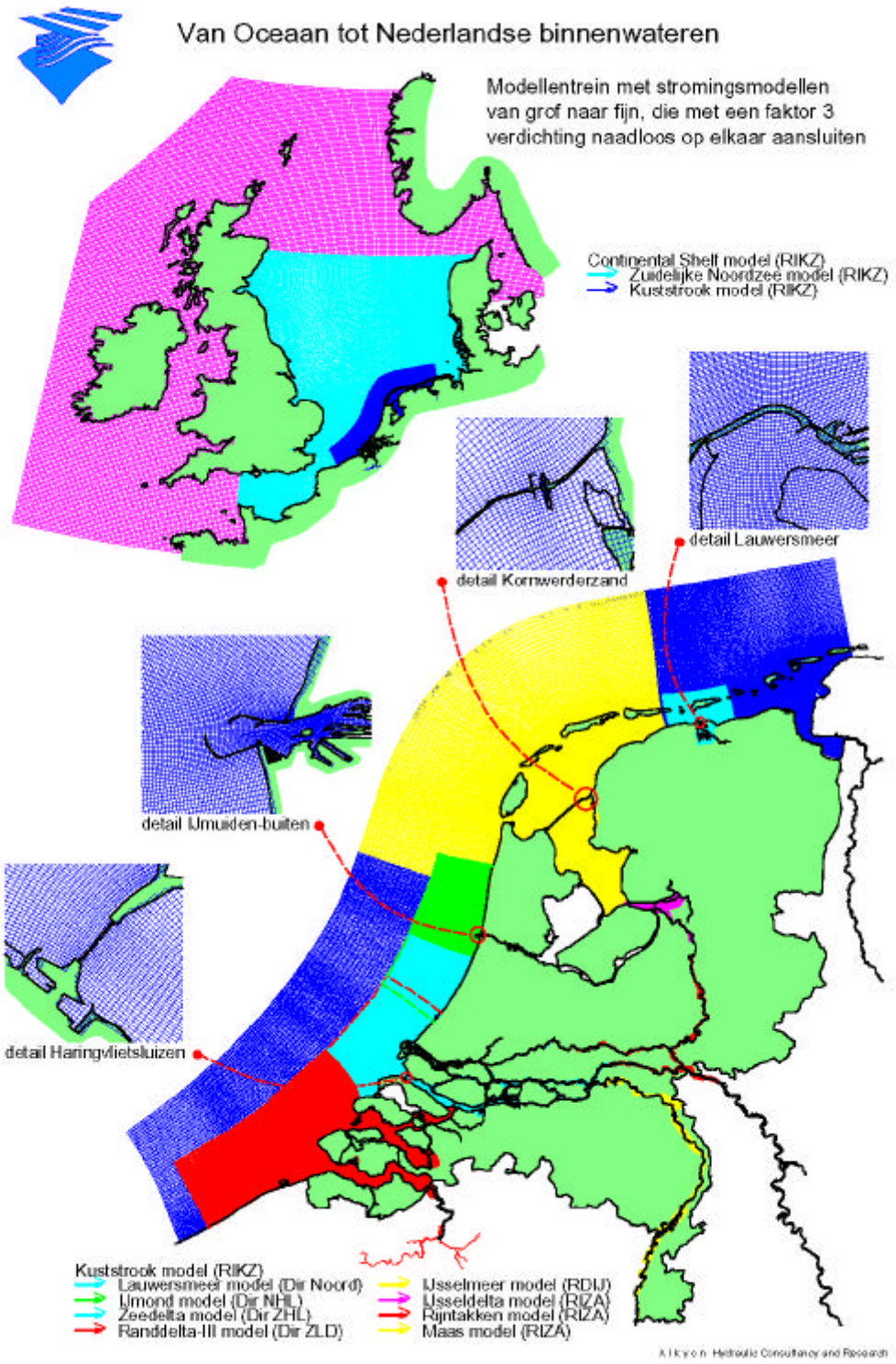

Alternative dumping strategy **Results of physical and numerical modelling**	Numerical model train used by Rijkswaterstaat to simulate tidal propagation from the North Sea into the inland estuaries, rivers and waterways.

MINISTERIE VAN DE VLAAMSE GEMEENSCHAP **AFDELING WATERBOUWKUNDIG LABORATORIUM EN HYDROLOGISCH ONDERZOEK**	Figure 011	**MODEL 678/1**

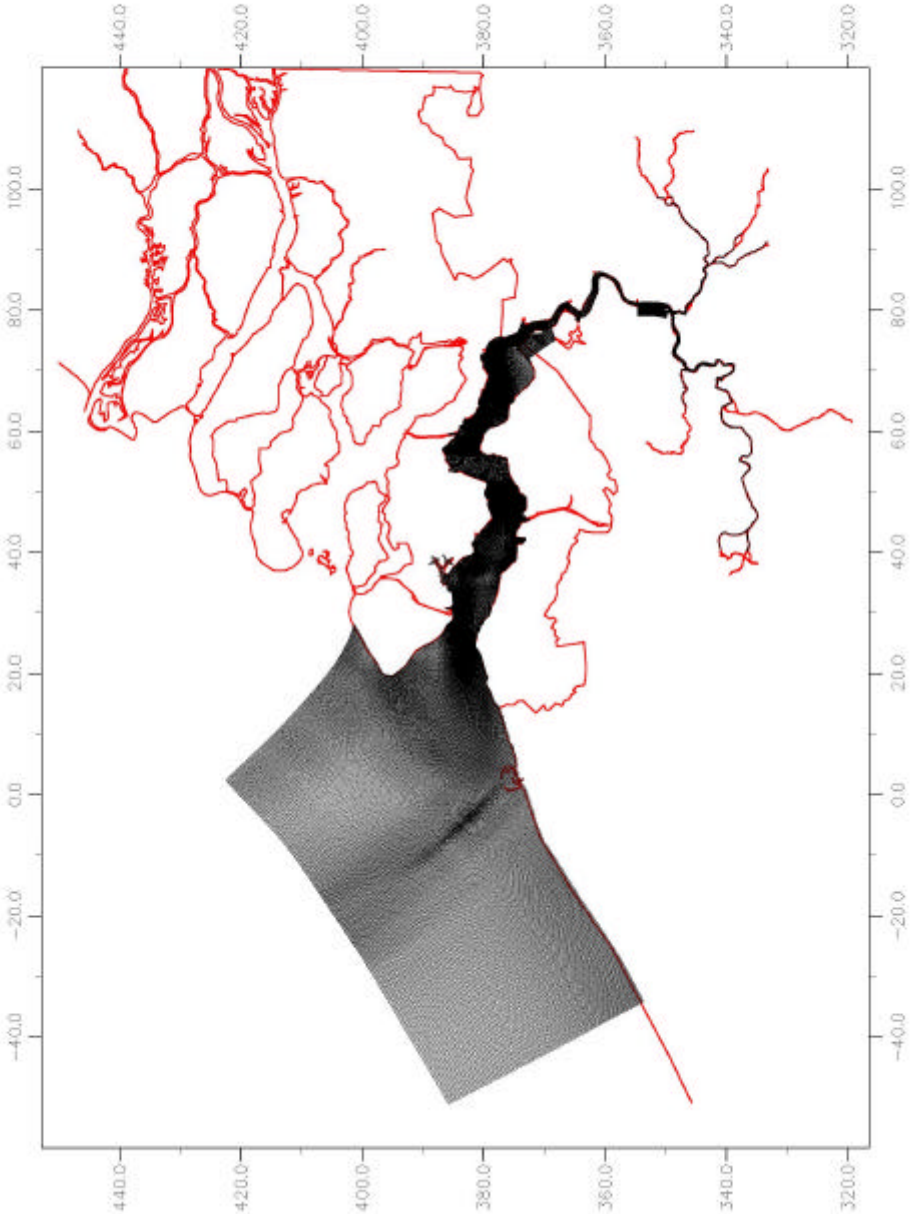

Alternative dumping strategy **Results of physical and numerical modelling**	Numerical grid of the Rijkswaterstaat SCALWEST 2000 model.

MINISTERIE VAN DE VLAAMSE GEMEENSCHAP **AFDELING WATERBOUWKUNDIG LABORATORIUM EN HYDROLOGISCH ONDERZOEK**	Figure 012	**MODEL 678/1**

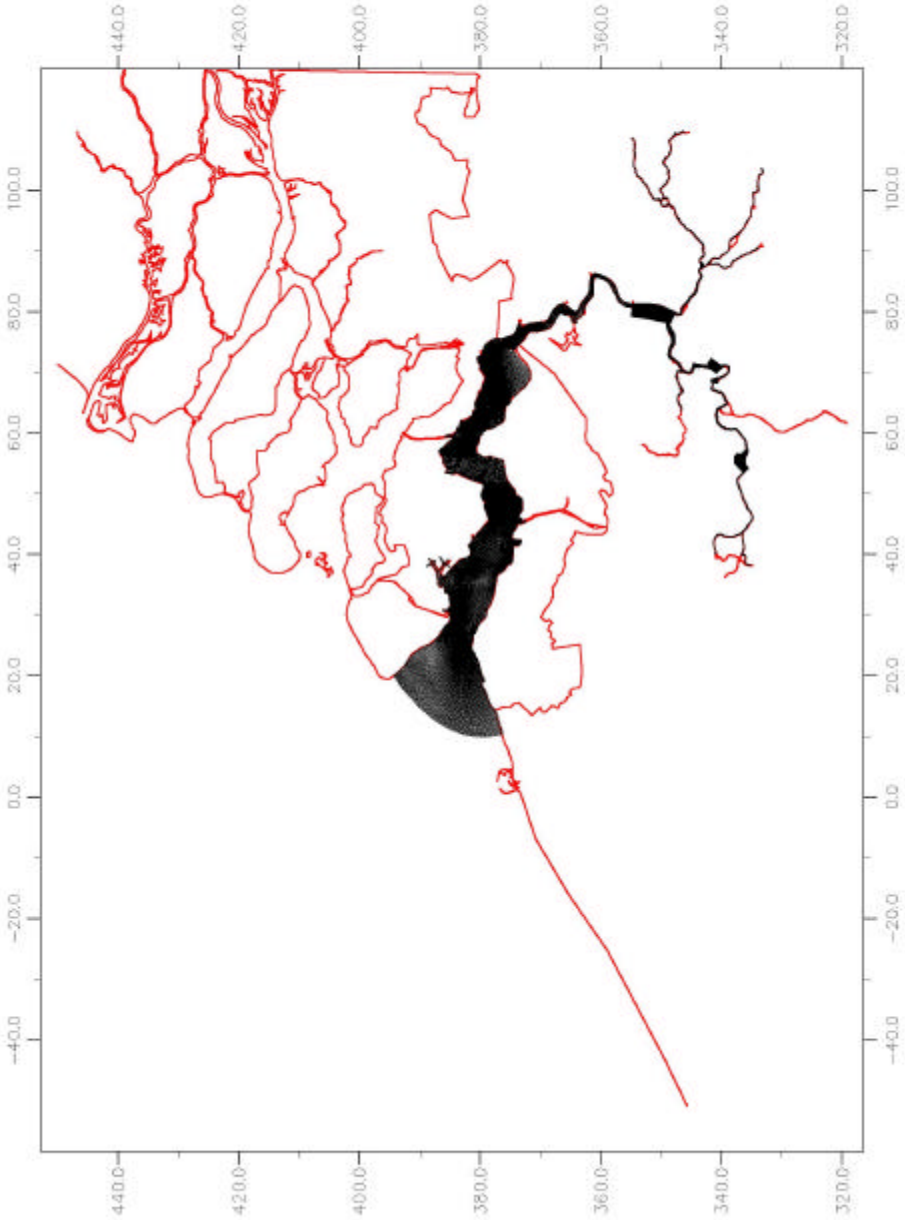

Alternative dumping strategy **Results of physical and numerical modelling**	Modified SCALWEST numerical grid	
MINISTERIE VAN DE VLAAMSE GEMEENSCHAP **AFDELING WATERBOUWKUNDIG LABORATORIUM EN HYDROLOGISCH ONDERZOEK**	Figure 013	**MODEL 678/1**

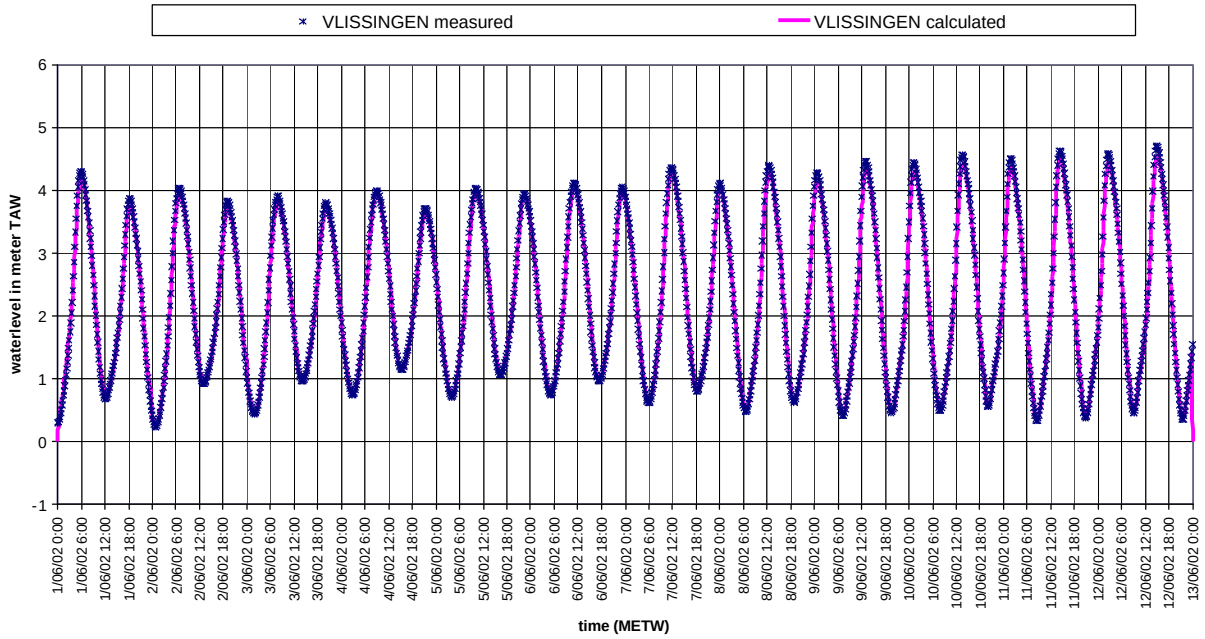

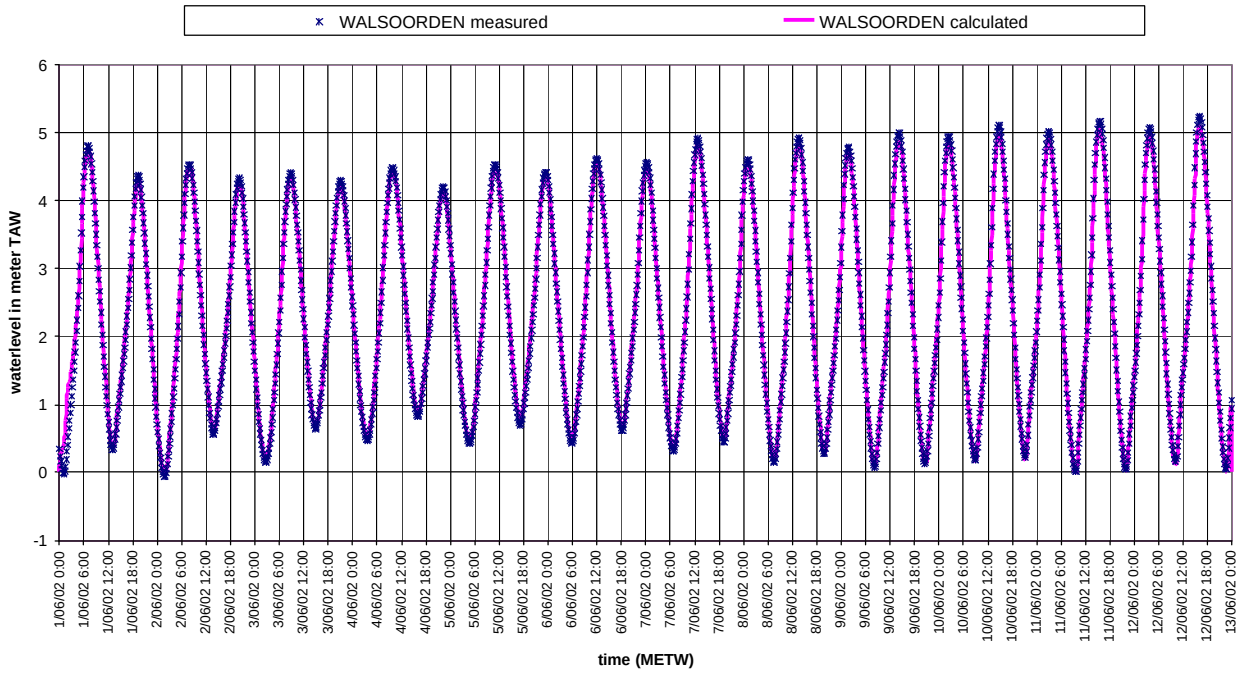

Alternative dumping strategy **Results of physical and numerical modelling**	Validation results of the modified SCALWEST model (June 1st – June 13th 2002 boundary conditions) Locations Vlissingen and Walsoorden

MINISTERIE VAN DE VLAAMSE GEMEENSCHAP **AFDELING WATERBOUWKUNDIG LABORATORIUM EN HYDROLOGISCH ONDERZOEK**	Figure 014	**MODEL 678/1**

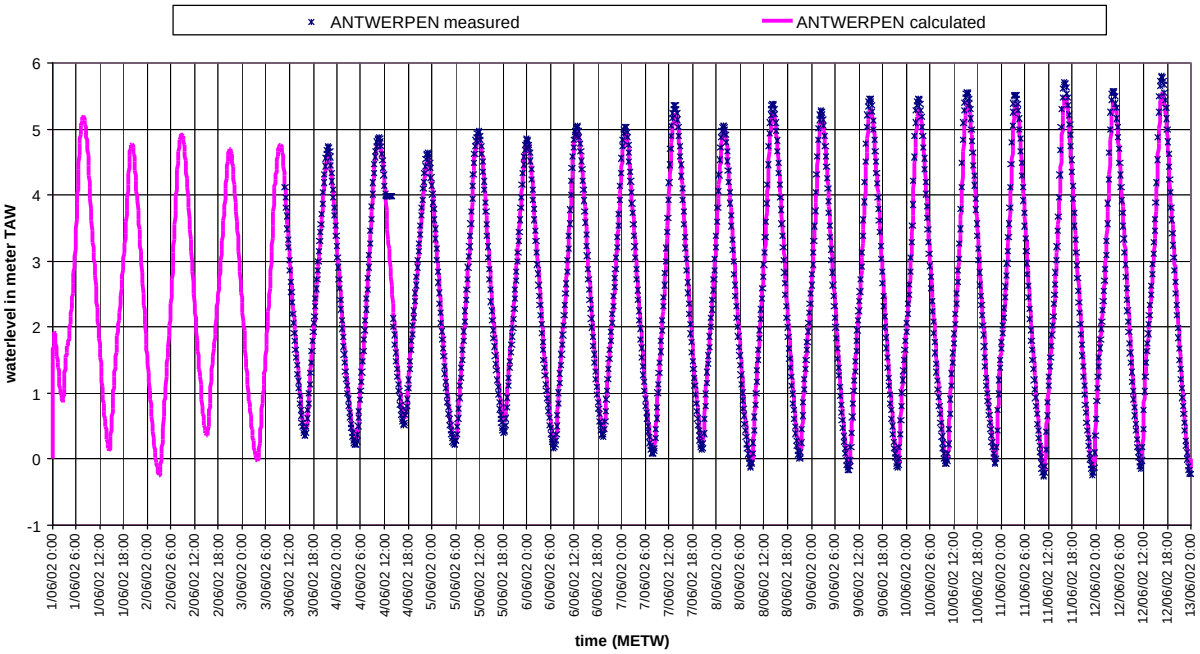

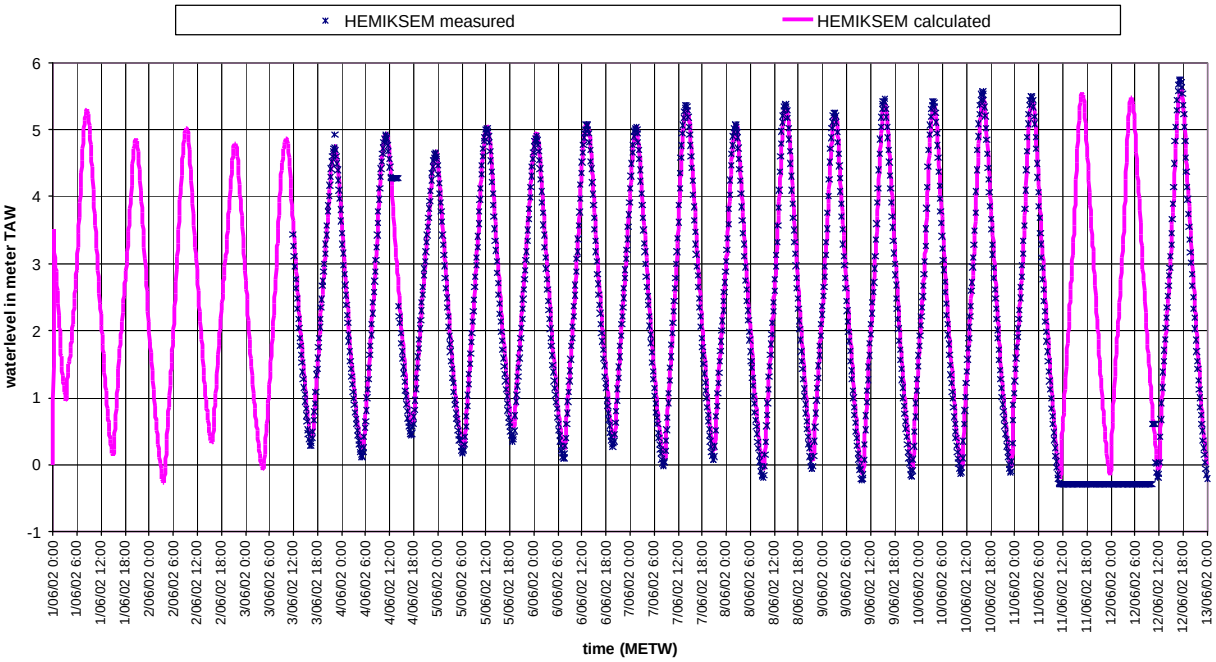

Alternative dumping strategy **Results of physical and numerical modelling**	Validation results of the modified SCALWEST model (June 1st – June 13th 2002 boundary conditions) Locations Antwerpen and Hemiksem

MINISTERIE VAN DE VLAAMSE GEMEENSCHAP **AFDELING WATERBOUWKUNDIG LABORATORIUM EN HYDROLOGISCH ONDERZOEK**	Figure 015	**MODEL 678/1**

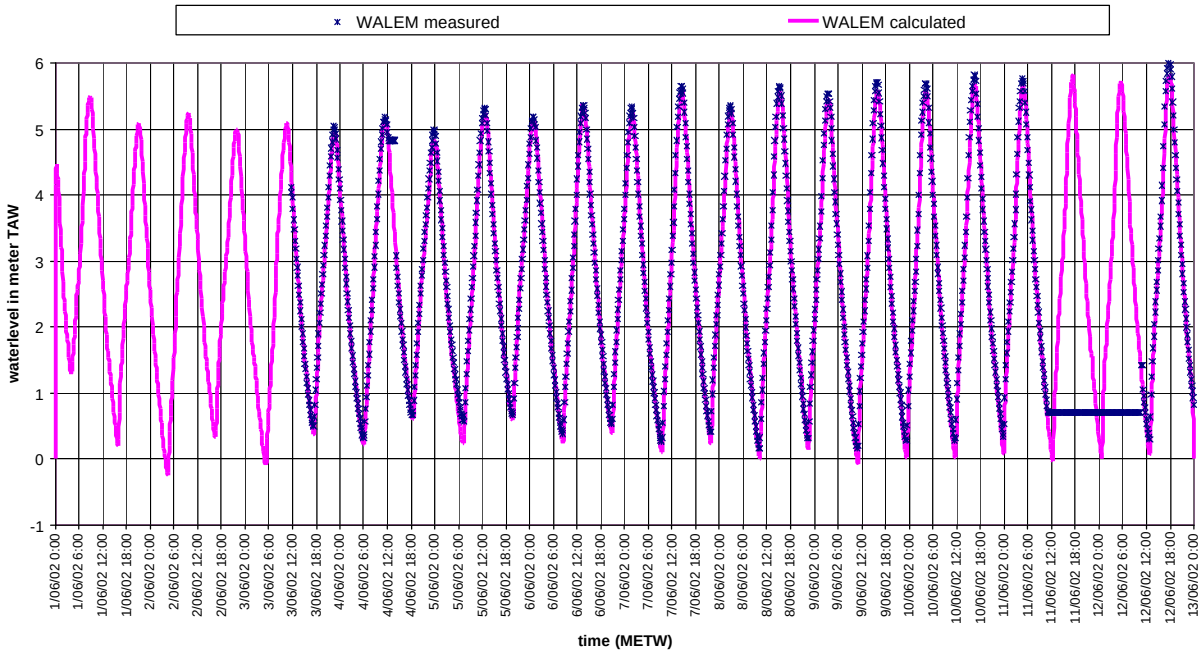

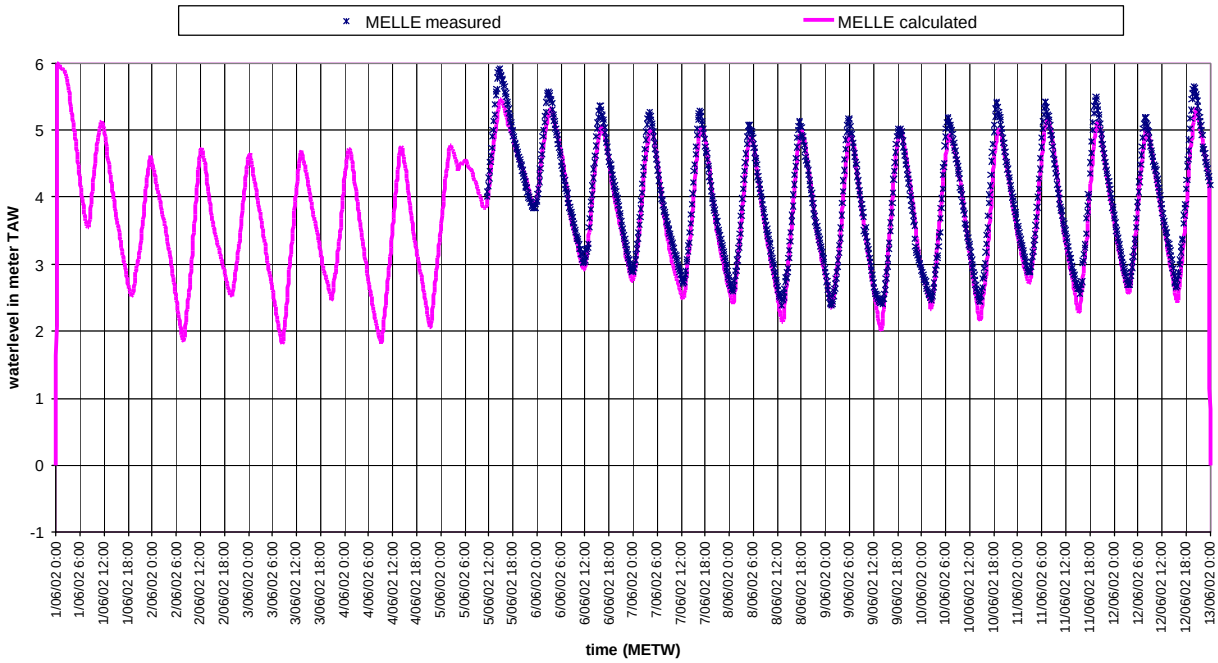

Alternative dumping strategy **Results of physical and numerical modelling**	Validation results of the modified SCALWEST model (June 1st – June 13th 2002 boundary conditions) Locations Walem and Melle

MINISTERIE VAN DE VLAAMSE GEMEENSCHAP **AFDELING WATERBOUWKUNDIG LABORATORIUM EN HYDROLOGISCH ONDERZOEK**	Figure 016	**MODEL 678/1**

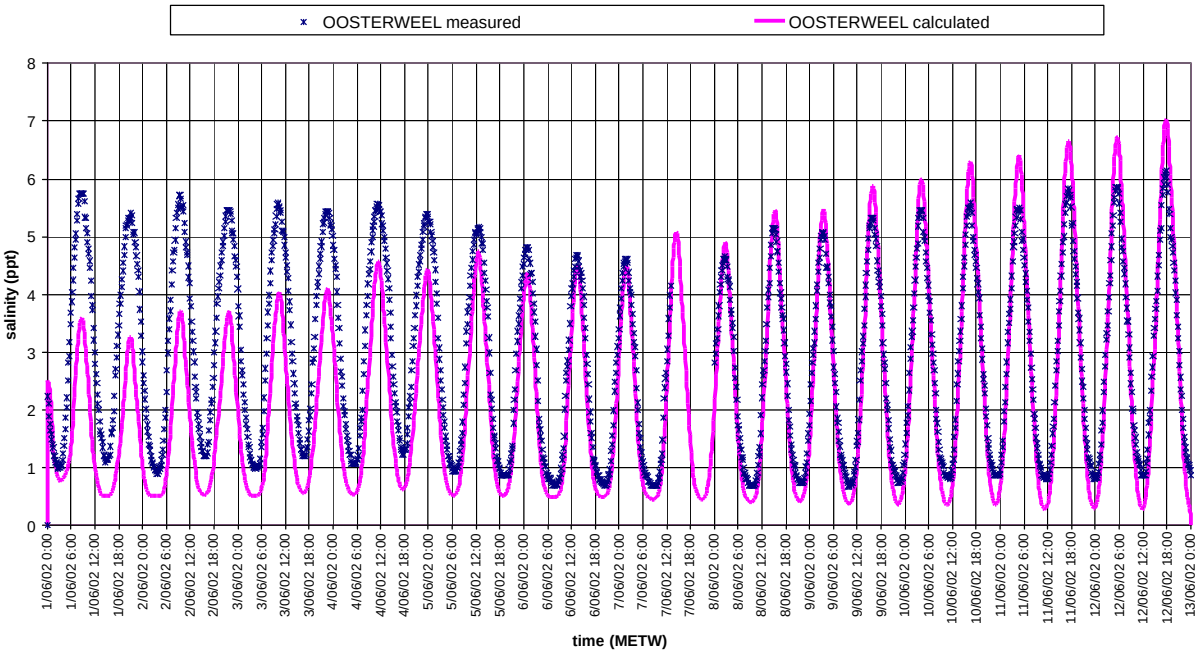

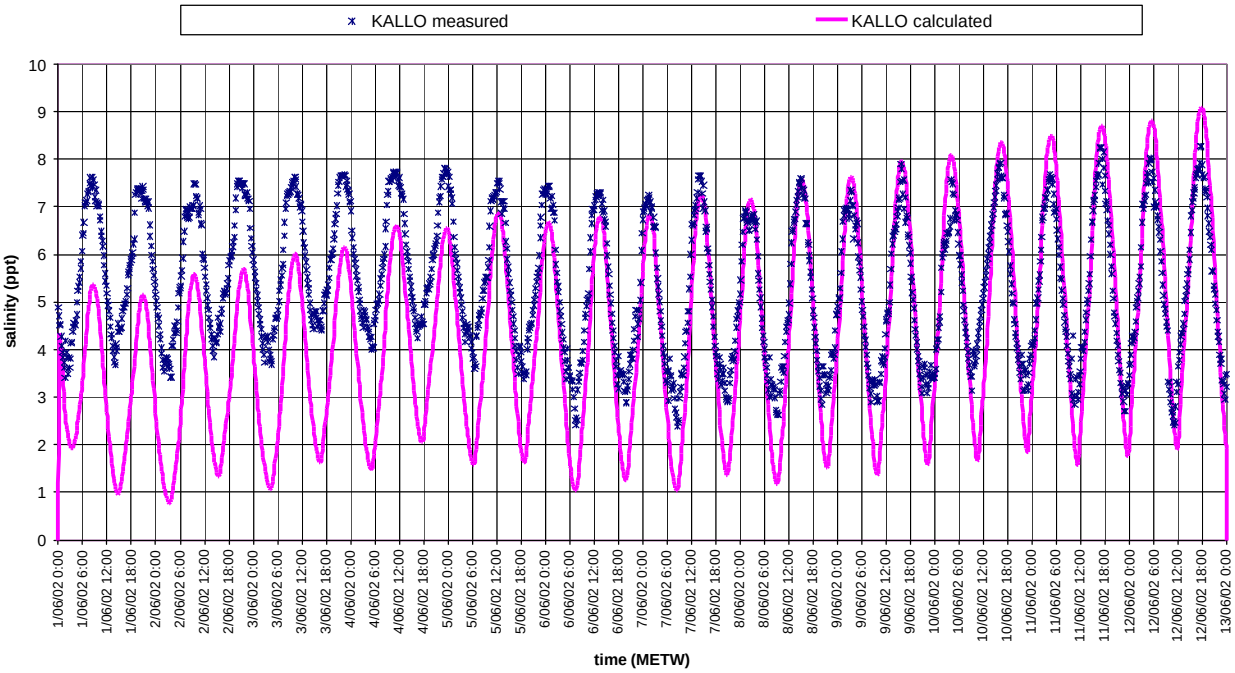

Alternative dumping strategy **Results of physical and numerical modelling**	Validation results of the modified SCALWEST model Calculated depth averaged salinity compared with measured point salinity (15 % – 25 % below the watersurface)

MINISTERIE VAN DE VLAAMSE GEMEENSCHAP **AFDELING WATERBOUWKUNDIG LABORATORIUM EN HYDROLOGISCH ONDERZOEK**	Figure 017	**MODEL 678/1**

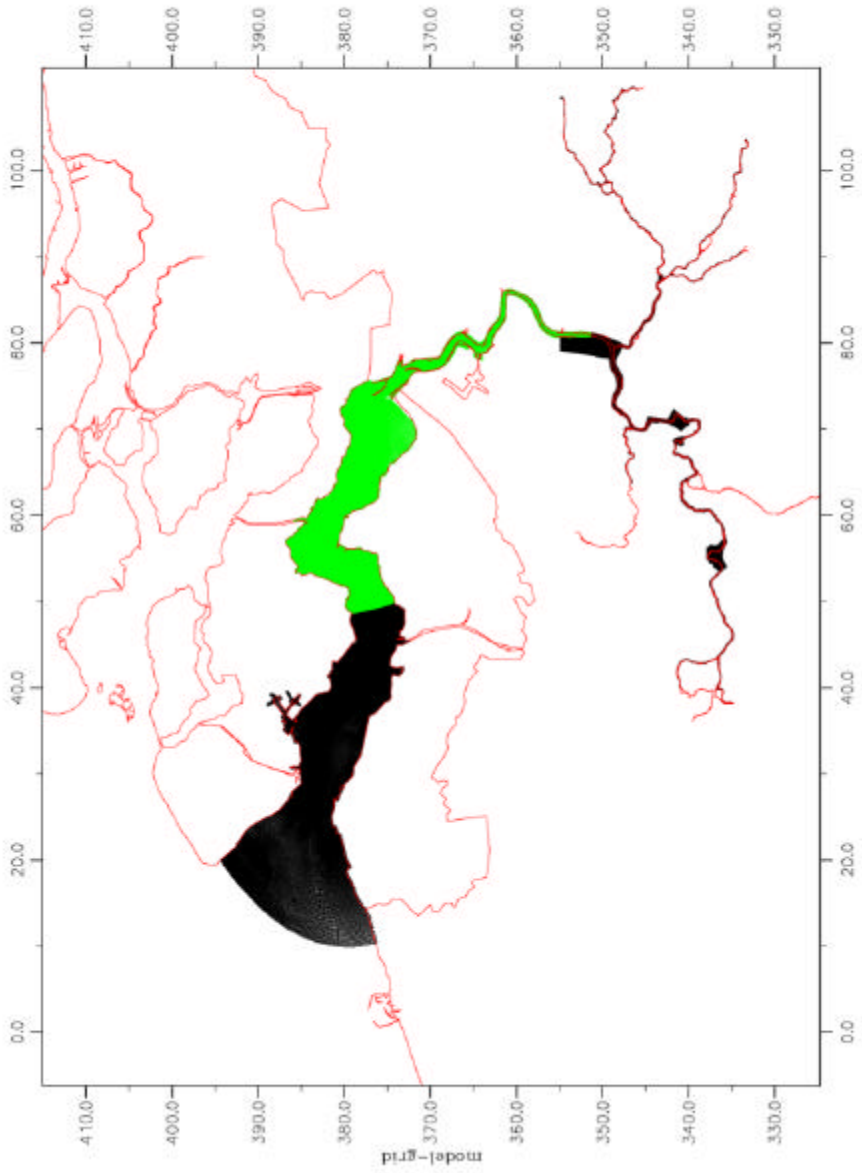

Alternative dumping strategy
Results of physical and numerical modelling

Nesting of the detailed Walsoorden numerical grid into the modified numerical grid of the SCALWEST model (for 2D and 3D modelling)

MINISTERIE VAN DE VLAAMSE GEMEENSCHAP

AFDELING WATERBOUWKUNDIG LABORATORIUM EN HYDROLOGISCH ONDERZOEK

Figure 018

MODEL 678/1

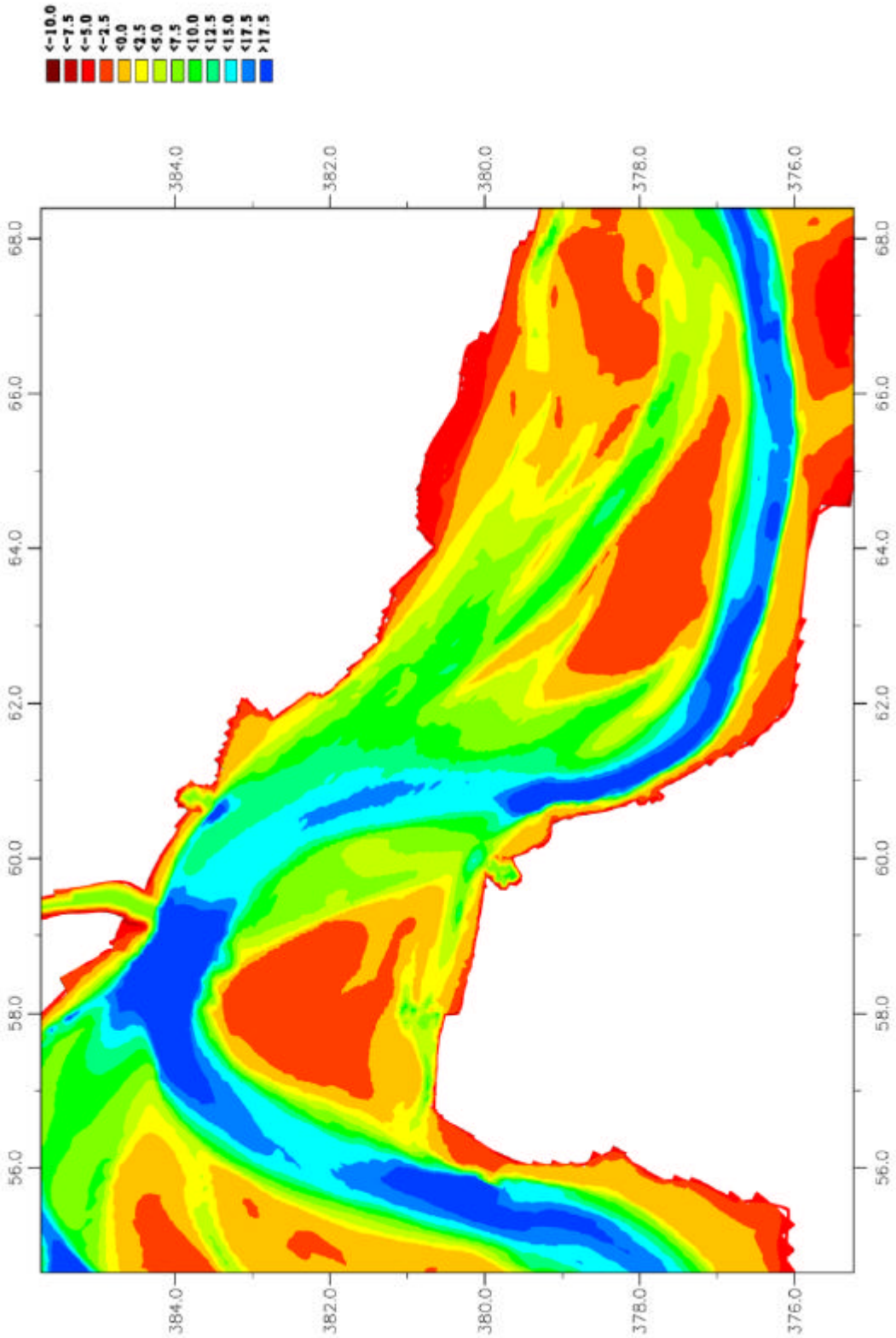

Alternative dumping strategy **Results of physical and numerical modelling**	Bathymetry of the SCALWEST model and basic 3D model (based on surveys of 2000-2001).

MINISTERIE VAN DE VLAAMSE GEMEENSCHAP **AFDELING WATERBOUWKUNDIG LABORATORIUM EN HYDROLOGISCH ONDERZOEK**	Figure 019	**MODEL 678/1**

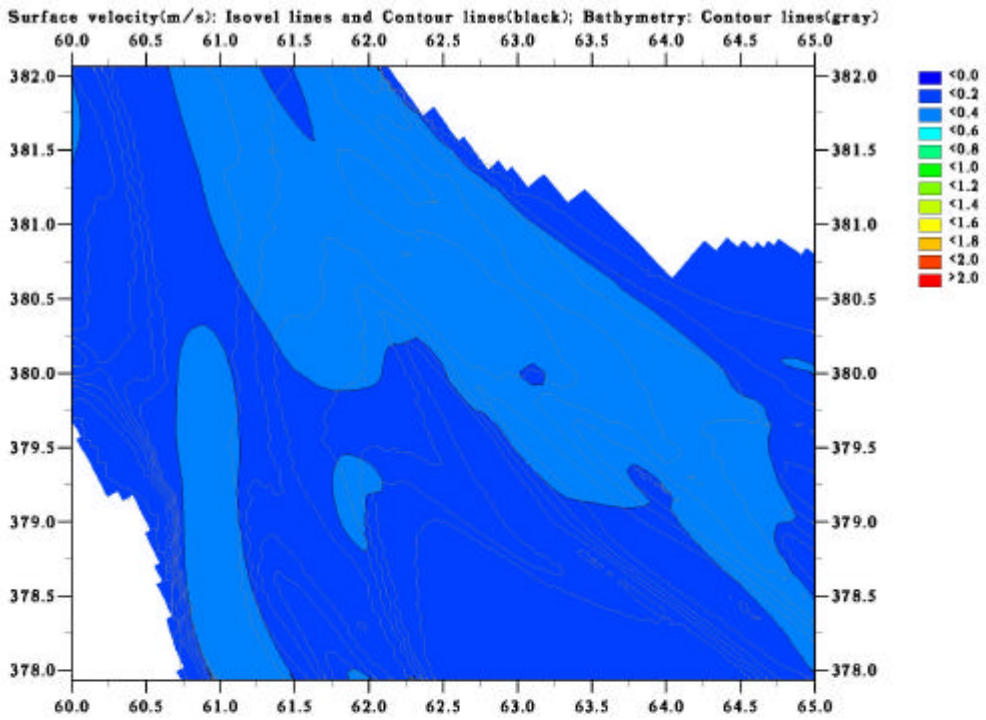

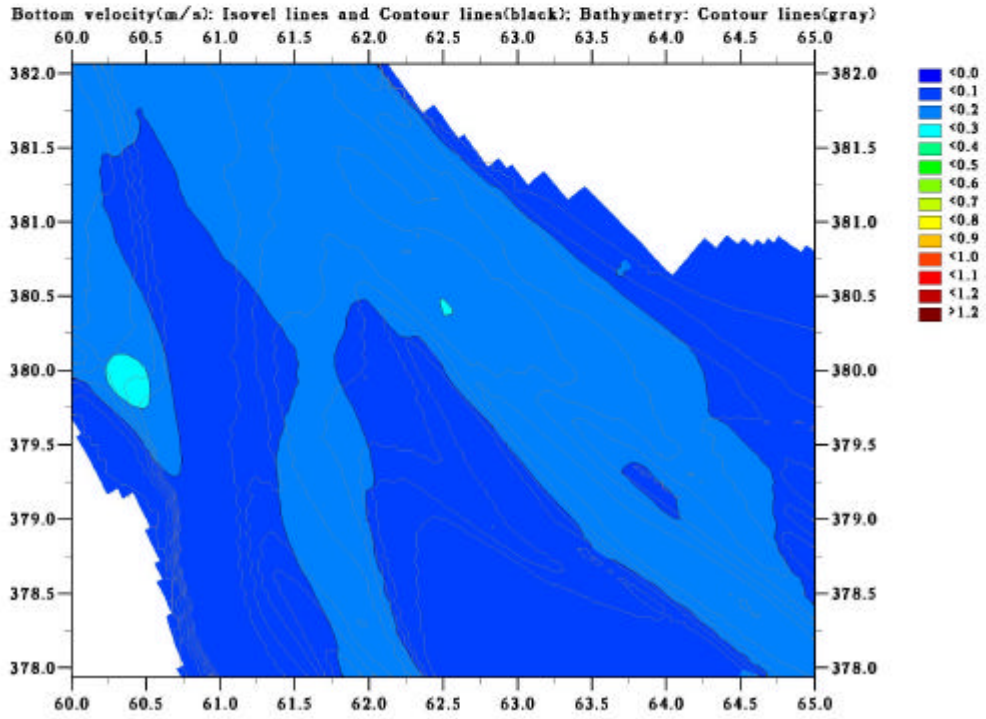

Alternative dumping strategy **Results of physical and numerical modelling**	Isovel lines for surface and bottom velocity at HW-5h Numerical model: 3D model, no refinement, 10 layers, horizontal eddy viscosity 10 m²/s

MINISTERIE VAN DE VLAAMSE GEMEENSCHAP **AFDELING WATERBOUWKUNDIG LABORATORIUM EN HYDROLOGISCH ONDERZOEK**	Figure 020	**MODEL 678/1**

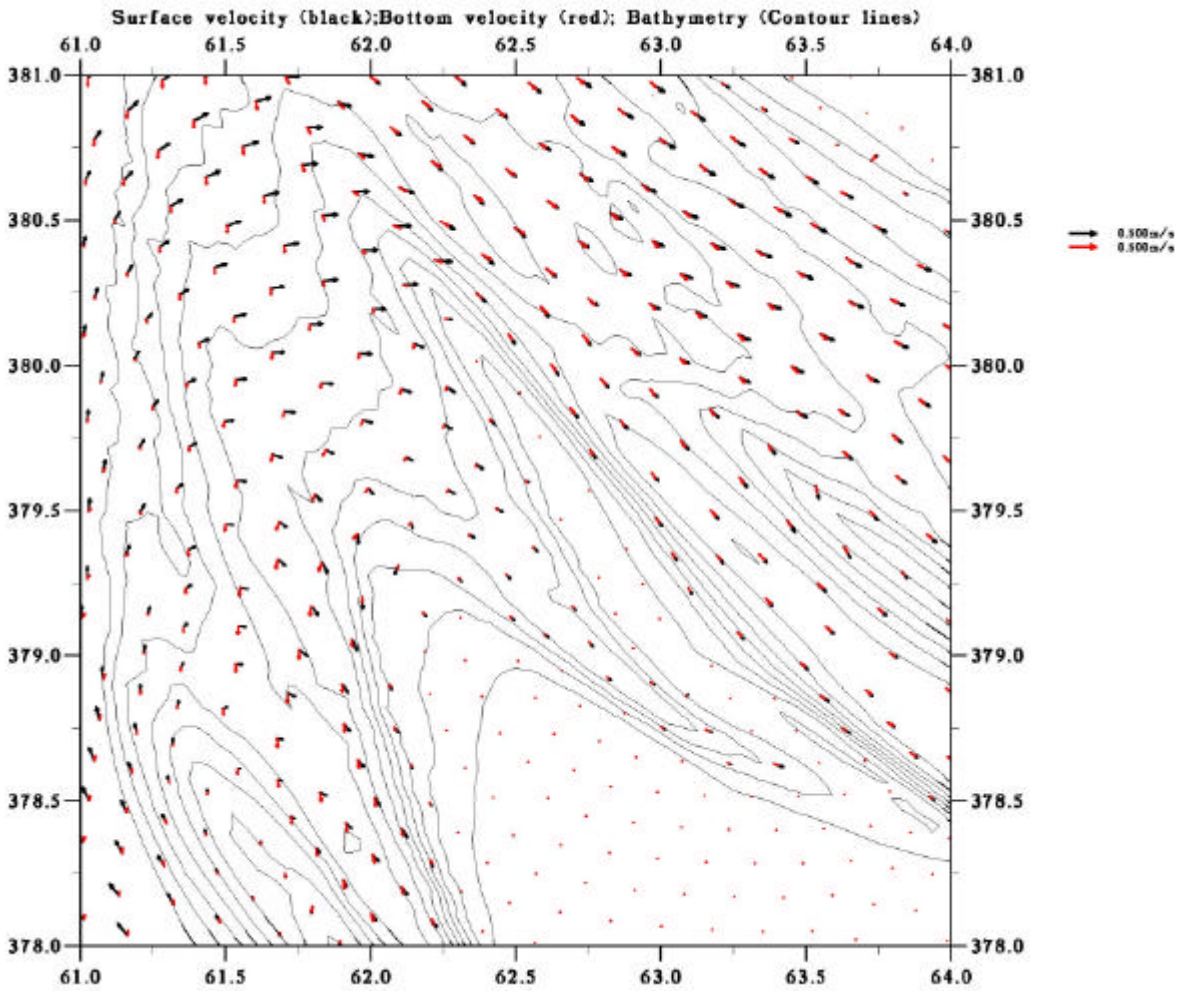

Alternative dumping strategy
Results of physical and numerical modelling

Current pattern computed with the numerical model at HW-5h
Numerical model: 3D model, no refinement, 10 layers, horizontal eddy viscosity 10m²/s

MINISTERIE VAN DE VLAAMSE GEMEENSCHAP

AFDELING WATERBOUWKUNDIG LABORATORIUM EN HYDROLOGISCH ONDERZOEK

Figure 021

MODEL 678/1